FORMATION MODEL OF THE ULUTAŞ SKARN SYSTEM (ERZURUM, NORTHEASTERN ANATOLIA)

A THESIS SUBMITTED TO
THE GRADUATE SCHOOL OF NATURAL AND APPLIED SCIENCES
OF
MIDDLE EAST TECHNICAL UNIVERSITY

BY

ISMAIL BATUHAN KESIM

IN PARTIAL FULFILLMENT OF THE REQUIREMENTS
FOR
THE DEGREE OF MASTER OF SCIENCE
IN
GEOLOGICAL ENGINEERING

APRIL 2023

Approval of the thesis

FORMATION MODEL OF THE ULUTAŞ SKARN SYSTEM (ERZURUM, NORTHEASTERN ANATOLIA)

submitted by **İSMAİL BATUHAN KESİM** in partial fulfillment of the requirements for the degree of **Master of Science** i**n Geological Engineering, Middle East Technical University** by,

Prof. Dr. Halil Kalıpçılar
Dean, Graduate School of **Natural and Applied Sciences** _____

Prof. Dr. Erdin Bozkurt
Head of the Department, **Geological Engineering** _____

Assist. Prof. Dr. Ali İmer
Supervisor, **Geological Engineering, METU** _____

Examining Committee Members:

Prof. Dr. Yurdal Genç
Geological Engineering, Hacettepe University _____

Assist. Prof. Dr. Ali İmer
Geological Engineering, METU _____

Assoc. Prof. Dr. Fatma Toksoy Köksal
Geological Engineering, METU _____

Assoc. Prof. Dr. Kaan Sayıt
Geological Engineering, METU _____

Assoc. Prof. Dr. Sinan Akıska
Geological Engineering Ankara University _____

Date: 26.04.2023

I hereby declare that all information in this document has been obtained and presented in accordance with academic rules and ethical conduct. I also declare that, as required by these rules and conduct, I have fully cited and referenced all material and results that are not original to this work.

Name Last name : İsmail Batuhan Kesim

Signature :

ABSTRACT

FORMATION MODEL OF THE ULUTAŞ SKARN SYSTEM (ERZURUM, NORTHEASTERN ANATOLIA)

Kesim, İsmail Batuhan
Master of Science, Geological Engineering
Supervisor : Assist Prof. Dr. Ali İmer

April 2023, 139 pages

The Ulutaş skarn deposit lies within the Eastern Pontides magmatic belt. The study area consists of a Paleozoic metamorphic basement cross-cut and overlain by volcanic, volcano-sedimentary, and plutonic lithologies of the Jurassic to Eocene age. The metasedimentary package mainly comprises schist, gneiss, amphibolite, and lenses of marble. A large batholithic complex of granitic and granodioritic coarse-grained intrusive rocks have been emplaced into the metasedimentary basement during the Cretaceous. Various mineralized zones, including a Cu-Mo porphyry and Cu-Zn skarn systems were developed within or peripheral to these granitoids. The Skarn zone that this study focuses on was formed as a result of the replacement of calcareous country rocks by prograde calc-silicate assemblage comprising garnet, pyroxene, and wollastonite. Retrograde epidote-chlorite-sericite-tremolite/actinolite-carbonate-hematite developed as an overprint to the calc-silicate assemblage. The main Cu-Zn mineralization at Ulutaş Skarn zone is associated with this later retrograde stage characterized by abundant chalcopyrite and sphalerite accompanied by pyrite.

Keywords: Skarn, copper, zinc, Ulutaş, İspir, Eastern Pontides

ÖZ

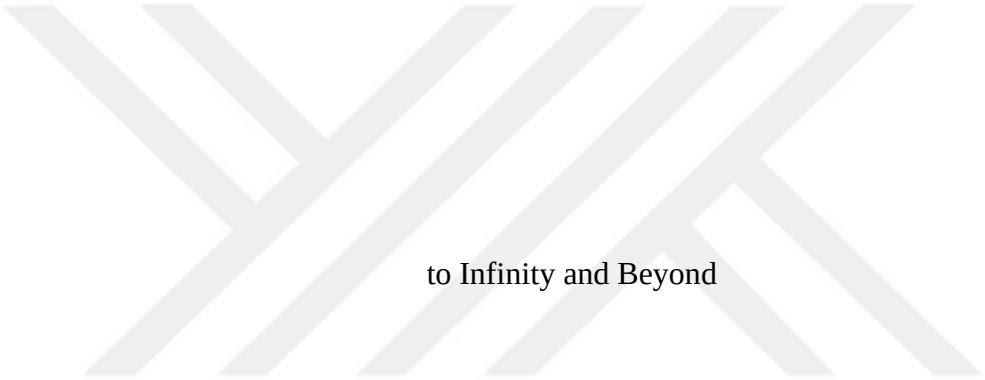
ULUTAŞ SKARN SİSTEMİNİN OLUŞUM MODELİ (ERZURUM, KUZEYDOĞU ANADOLU)

Kesim, İsmail Batuhan
Yüksek Lisans, Jeoloji Mühendisliği
Tez Yöneticisi: Dr. Öğr. Üyesi Ali İmer

Nisan 2023, 139 sayfa

Ulutaş skarn sistemi Doğu Pontidler magmatic kuşağının içerisinde yer almaktadır. Çalışma sahasında Paleozoyik yaşlı taban metamorfikleri Jurasik–Eosen yaşlı volkanik, volkanosedimanter ve plütonik birimler tarafından kesilmiş ve örtülmüştür. Taban metamorfiklerini ağırlıklı olarak şist, gnays, amfibolit ve lens halindeki mermerler oluşturmaktadır. Bunları kesen ve geniş bir alanı kaplayan Kretase yaşlı batolitik kompleks ise iri taneli granitik ve granodiyoritik kayaçlarla temsil edilmektedir. Granitoyid kayaçların içerisinde ve çevresinde bir adet porfiri Cu-Mo ve Cu-Zn skarn sistemi bulunmaktadır. Bu çalışmanın konusu olan Cu-Zn skarn zonunda karbonatlı yankayaçlar prograd evrede kalk-silikat mineralleri tarafından ornatılmıştır. Kalk-silikat mineral topluluğu grosüler granat, diyopsidik piroksen ve vollastonitten oluşmaktadır. Bunların üzerine retrograd evrede epidot-klorit-serizit-tremolit/aktinolit-karbonat-hematit gelişmiştir. Ulutaş Skarn zonundaki ana Cu-Zn cevherleşmesi retrograd aşamayla ilişkili kalkopirit, sfalerit ve bunlara eşlik eden pirit ile karakterizedir.

Anahtar Kelimeler: Skarn, bakır, çinko, Ulutaş, İspir, Doğu Pontidler



to Infinity and Beyond

ACKNOWLEDGMENTS

Firstly, I would like to express my special gratitude to my advisor, Assist. Prof. Dr. Ali İmer for his guidance, support, advice, criticism, encouragement, and insight during the thesis study.

Secondly, I would like to express my appreciation to Demir Export Company for permission for the project, and to Ramazan Yön, General Manager, İsmail Cihan, head of the exploration department, İsmet Cengiz, chief exploration geologist, Dr. Ercan Kuşçu, chief exploration geologist, Serdar Onur Avcı, exploration superintendent, Gökhan Kanaat, database and GIS superintendent, and Demir Export Exploration Team, for all of their support.

I thank my friends and/or colleagues who are Akın Çil, Davuthan Korkmaz, Can Aydoğan and Şevkican Seferoğlu for their help during the thin section examination, field studies, ore domaining and GIS works.

My special appreciation goes to Bengüsu Gürçay Kesim, my best friend and wife. Her endless support, belief, endurance and pure love kept me working on this thesis. This thesis would not be finished without her support and love.

Finally, I would like to express my deepest gratitude, for the support, and love of my family. My mother Gülay Kesim, my father Abdulkadir Kesim, and my little sister Aybike Kesim were always with me and help me to walk this way from beginning to end.

TABLE OF CONTENTS

ABSTRACT v

ÖZ vi

ACKNOWLEDGMENTS viii

TABLE OF CONTENTS ix

LIST OF TABLES xii

LIST OF FIGURES xiii

CHAPTERS

1 INTRODUCTION 1

1.1 Purpose and Scope 1

1.2 Methodology 3

1.3 Location and Setting 4

1.4 Previous Studies 4

2 SKARN DEPOSITS: A REVIEW 9

2.1 Skarn Deposits 10

2.2 Skarn Zonation 15

2.3 Tectonic Settings of Skarn Deposits 18

2.4 Types of Skarn Deposits 19

3 REGIONAL SETTING, GEOLOGY, AND METALLOGENY OF EASTERN PONTIDES 21

3.1 Tectonic Setting of Eastern Pontides 21

3.1.1 Geodynamic Evolution of Eastern Pontides 23

3.2 Geology of Eastern Pontides 31
3.3 Metallogeny of the Eastern Pontides 33
3.3.1 Epithermal Deposits 33
3.3.2 Volcanic-hosted Massive Sulfide (VHMS) Deposits 35
3.3.3 Porphyry Cu-Mo Deposits 37
3.3.4 Skarn Deposits 39
4 GEOLOGY OF ULUTAŞ SKARN CU-ZN DEPOSIT 41
4.1 Lithological Units 45
4.1.1 Pre-Jurassic Metamorphic Basement 45
4.1.2 Cretaceous Volcanics and Igneous Rocks 50
4.1.3 Eocene Volcanic Sequence 63
4.1.4 Pleistocene to Quaternary Cover Deposits 65
5 ALTERATION AND ORE MINERALOGY OF ULUTAŞ SKARN CU-ZN DEPOSIT 67
5.1 Skarn Alteration 67
5.1.1 Stage I - Potassic & Calc-Silicate Alteration (Prograde Stage) 69
5.1.2 Stage II - Retrograde alteration 83
5.2 Zn-Cu Mineralization 88
5.3 Supergene Oxidation and Weathering 105
5.4 Metal Associations/Correlations 106
6 DISCUSSIONS AND CONCLUSIONS 121
6.1 Discussions 121
6.1.1 Geodynamic Evolution of Ulutaş Cu–Zn Skarn Type Deposit 121

6.1.2 Nature of Alteration and Mineralization at Ulutaş Cu–Zn Skarn Type Deposit 123

6.1.3 Regional Significance of the Ulutaş Cu-Zn Skarn Deposit 124

6.1.4 Global Significance of Ulutaş Cu-Zn Skarn Type Deposit 127

6.2 Conclusions 128

REFERENCES 131

LIST OF TABLES

TABLES

Table 2-1. Common Alteration Minerals of Skarn Systems (Meinert et al., 2005) 14
Table 2-2. Different skarn types with their differences in terms of a dominant ore mineral, plutons and skarn mineralogy (Meinert et al., 2005) 20
Table 3-1. Radiometric age of main VHMS deposits in the Eastern Pontides (Revan, 2020). 36
Table 5-1. Descriptive statistical parameters for the upper skarn domain as calculated from assay data (lithogeochemical data courtesy of Demir Export) 107
Table 5-2. Descriptive statistical parameters for the lower skarn domain as calculated from assay data (lithogeochemical data courtesy of Demir Export) 108
Table 5-3. Correlation coefficients for Cu, Zn, Ag, Au, Mo, and Pb for both Upper and Lower Skarn domains at Ulutaş (assay data courtesy of Demir Export)..... 112
Table 5-4. Total tonnage and metal grade values estimated for various skarn domains at the Ulutaş deposit as calculated from assay data of Demir Export..... 119
Table 5-5. Raw samples grade vs. numerical model grade comparison 120
Table 6-1. Summary characteristics of Cretaceous skarn deposits in the Eastern Pontides Abbreviations: grt=garnet, px= pyroxene, wol=wollastonite, ep=epidote, chl=chlorite, cal=calcite, qtz=quartz, tr=tremolite, act=actinolite, mag=magnetite, hem=hematite, cpy=chalcopyrite, py=pyrite, sph=sphalerite, mo=molybdenite, po=pyrrhotite 125

LIST OF FIGURES

FIGURES

Figure 1-1. Location of the study area (retrieved from Google Earth). 4
Figure 2-1. Types of skarn formation A. Isochemical metamorphism B. Reaction skarn C. Skarnoid D. Fluid-controlled metasomatic skarn (Meinert, 1982). 12
Figure 2-2. The stages of intrusion-related skarn deposits showing three sequential stages of formation. (a) Prograde stages, and (b) retrograde stage (Robb, 2005)... 13
Figure 2-3. Schematic illustration of the propagation of multiple reaction fronts during progressive fluid flow (Meinert et al., 2005). 16
Figure 2-4. General models of skarn zonation: A) copper skarn (after Atkinson and Einaudi, 1978); B) zinc skarns (Meinert, 1987). 17
Figure 2-5. Generalized tectonic setting models for skarn formation (Meinert et al., 2005). 18
Figure 3-1.Tectonic division of Anatolia and its neighboring regions located on the Tethyan orogenic belt, showing major structures, sutures, and continental blocks including the Rhodope-Strandja Zone, İstanbul Zone, and Sakarya Zone of the Pontides Domain (Okay and Tüysüz, 1999). 23
Figure 3-2. Paleogeography of the southern hemisphere for the Early Ordovician showing possible locations of the Pontic terranes. MOIS (Moesia, Istanbul, and part of Scythian Platform), ISC (Strandja, Sakarya, and Caucasus), and AHAT (Apulia, Hellenides, Anatolide-Tauride) (Okay and Nikishin, 2015). 24
Figure 3-3. Late Cretaceous to Eocene tectonic evolution model of the Eastern Pontides (Kandemir et al., 2019). 25
Figure 3-4. Cartoon showing geodynamic evolution of Eastern Pontides during the Paleotethys closure and progressive development of the Neotethys ocean together with major magmatic episodes and associated metallic ore deposits (Delibaş et al., 2016; references for geochronological data are shown on the figure). 28
Figure 3-5. Schematic description of Eocene magmatism in Eastern Pontides; Eurasian Plate (EP), Tauride-Anatolide Platform (TAP). A) lithospheric thickening

because of continental collision between Eurasia (Pontides) and Tauride-Anatolide Platform B) post-collisional stage (Kaygusuz and Öztürk, 2015). 30
Figure 3-6. Simplified regional geologic map of the Eastern Pontide magmatic belt. Also shown are the locations of the major ore deposits (Delibaş et al., 2019; after MTA, 2002). Inset shows major tectonic units of Anatolia (simplified after Ketin, 1966). 31
Figure 3-7. Generalized columnar section of the Eastern Pontides (compiled from Güven, 1993; Konak et al., 2001; Kandemir et al., 2019; Revan, 2020) 32
Figure 3-8. Distribution of epithermal-type deposits and prospects in Eastern Pontides (Yiğit, 2009) 35
Figure 3-9. Distribution of the VHMS deposits/prospects of Eastern Pontides (Revan, 2020). 36
Figure 3-10. Distribution of the porphyry deposits and prospects of Turkey (Yiğit, 2009) 37
Figure 3-11. Radiometric ages of porphyry Cu-Mo mineralization and ore-forming events in Eastern Pontides (Delibaş et.al, 2019) 38
Figure 3-12. Distribution of the skarn deposits and prospects of Eastern Pontide (modified from Delibaş et al., 2019; after MTA, 2002 and Kuşcu, 2019). 40
Figure 4-1. Geological map of the study area showing the major lithological units (modified from Giles, 1973; Revan et al., 2017; Delibaş et al., 2019). 42
Figure 4-2. General views of the Ulutaş-İspir district. a) View of skarn mineralization from the İspir porphyry zone, looking southwest. Porphyry-altered exposures in the foreground show quartz-white mica alteration, b) View of Skarn II orebody from Skarn I zone (looking north). Porphyry domain is also visible in the background, to the northeast. 43
Figure 4-3. Discovery outcrop of the Ulutaş Zn-Cu deposit showing oxidized skarn assemblages (660211 E, 4493331 N, 2.302 m a.s.l., UTM Zone 37). 44
Figure 4-4. Gneiss with strong metamorphic fabric in the study area (drill hole EU-027, 108.50 m). 46

Figure 4-5. Hand specimen and microphotographs of gneiss sample a) drill core photograph of gneiss (drill hole EU-038, 108.40 m), b) microphotograph (PPL, TL image) of chlorite altered gneiss (drill hole EU-038, 108.40 m), c) microphotograph (XPL, TL image) of chlorite altered, light colored silicate banded and dark colored biotite banded gneiss (drill hole EU-038, 108.40 m). Abbreviations: K-felds = K-feldspar, bio = biotite, qtz = quartz, chl = chlorite, TL = transmitted light, XPL= cross-polarized light, PPL = plane-polarized light. 47
Figure 4-6. Schist unit with strong foliation intersected by quartz-feldspar porphyry in the study area (drill hole EU-046, 153.60 m.). 48
Figure 4-7. Microphotograph (XPL, TL image) of carbonate altered schist and andesite poprhyry contact (drill hole EU-046, 90.80 m). Abbreviations: qtz = quartz, carb = carbonate, TL = transmitted light, XPL= cross-polarized light. 48
Figure 4-8. Field and drill core views of marble lenses that are part of the Pre-Jurassic metamorphic sequence in the study area. a) A marble lens exposed in the central part of the study area (660610 E, 4494009 N, 2.333 m a.s.l., UTM Zone 37), b) drill core interval of laminated marble (drill hole EU-071, 151.00 m). 49
Figure 4-9. Lower Volcanic-Sedimentary Sequence in the study area. a) rhyolitic lapilli tuff (661218 E, 4494552 E, 2374 m a.s.l., UTM Zone 37) b) coarsely pebbly sandstone/conglomerate (661485 E, 4495767 N, 2658 m a.s.l., UTM Zone 37). .. 50
Figure 4-10. Outcrop view of equigranular granodiorite (660621 E, 4493406 N, 2119 m a.sl., UTM Zone 37)..... 51
Figure 4-11. Drill core sample of Early Cretaceous granodiorite in Ulutaş porphyry mineralization area (drill hole EU-309, 222.50 m). 52
Figure 4-12. Drill core sample of altered porphyritic granodiorite with biotite, quartz, and feldspar phenocrysts from Ulutaş porphyry prospect (drill hole EU-009, 271.4 m.). Abbreviations: qtz = quartz, pl = plagioclase, bio = biotite. 52
Figure 4-13. Andesite porphyry in the study area (drill hole EU-094, 181.30 m). Abbreviations: qtz = quartz, pl = plagioclase. 53
Figure 4-14. a) Microphotograph (XPL, TL image) showing a relatively fresh, twinned plagioclase surrounded by fine-grained groundmass (drill hole EU-094,

181.70 m), b) microphotograph (XPL, TL image) of coarse grained quartz cross cut by carbonate vein (drill hole EU-094, 171.70 m). Abbreviations: pl=plagioclase, qtz=quartz, TL=transmitted light, XPL=cross polarized light, PPL= plane polarized light.....55
Figure 4-15. a) Microphotograph (PPL, TL image) sericitized and K-feldspar altered plagioclase with chloritized hornblende (drill hole EU-094, 160.70 m), b) Microphotograph (XPL, TL image) sericitized and K-feldspar altered plagioclase with chlorite and hornblende (drill hole EU-094, 160.70 m). Abbreviations: pl=plagioclase, chl=chlorite, hb= hornblende TL=transmitted light, XPL=cross polarized light, PPL= plane polarized light.....56
Figure 4-16. Zr/Ti vs. Nb/Y diagram plot (Pearce, 1996) of andesite porphyry unit as based on drill hole assays of the Ulutaş Cu-Zn skarn (lithogeochemical data courtesy of Demir Export).....57
Figure 4-17. Drill core sample of a basaltic dike from the study area (drill hole EU-094, 179.70 m).....58
Figure 4-18. Zr/Ti vs. Nb/Y diagram (Pearce, 1996) of basaltic dike intervals from Ulutaş Cu-Zn skarn deposit (lithogeochemical data courtesy of Demir Export).....59
Figure 4-19. Drill core interval of andesite porphyry (left) cross-cut by a basaltic dike (drill hole EU-071, 50.70 m). Andesite porphyry shows intense carbonate-chlorite-sericite alteration, whereas the basaltic dike experienced intense chloritization as indicated by its distinct green color.....60
Figure 4-20. Drill core interval with a basaltic dike cross-cutting the andesite porphyry (drill hole EU-102, 159.80 m).....60
Figure 4-21. Outcrop image showing a basaltic dike cross-cutting the Cretaceous granodiorite (660621 E, 4493406 N, 2.119 m a.s.l., UTM Zone 37).....61
Figure 4-22. a) Microphotograph (XPL, TL image) of chlorite-sericite-altered basaltic dike (drill hole EU-094, 179.70 m), b) microphotograph (XPL, TL image) of euhedral pyrite within basaltic dike (drill hole EU-094, 179.70 m) Abbreviations: chl=chlorite,ser=sericite, py=pyrite, TL=transmitted light, XPL=cross polarized light.....62

Figure 4-23. Polymict andesitic breccia within Eocene Volcanic Sequence..... 63
Figure 4-24. Eocene andesite porphyry andesite in the study area (662816 E, 4494629 N, 2538 m a.s.l., UTM Zone 37)..... 64
Figure 4-25. Fossiliferous sandstone with abundant bivalves and nummulites within the Eocene Volcanic Sequence (662657 E, 4493415 N, 2328 m a.s.l., UTM Zone 37)..... 64
Figure 4-26. Drill core image of Pleistocene glacial till (drill hole EU-55, 44.00-47.80-meter interval)..... 65
Figure 5-1. Drill core images of porphyry-style alteration in the Ulutaş porphyry area. a) potassic alteration characterized by secondary K-felspar on porphyritic monzonite with minor sericitic overprint along quartz-pyrite veinlets (drill hole EU-040, 312.70 m), b) potassic alteration with secondary K-feldspar on porphyritic diorite with minor sericitic overprint along quartz-pyrite veinlets (drill hole EU040, 294.00 m), c) intensely quartz-sericite-pyrite (phyllic) altered granitoid rock cross-cut by stockworking quartz-pyrite veins (drill hole EU-019, 77.50 m)..... 68
Figure 5-2. Yellowish brown colored garnet with greenish colored pyroxene skarn in the study area (drill hole EU051, 83.00 m)..... 69
Figure 5-3. a) Drill core image showing early potassic alteration, which is represented by abundant secondary K-feldspar. Altered quartz-feldspar porphyry has been cut by actinolite veins (drill hole EU-051, 111.00 m). b) Microphotograph (XPL, TL image) showing secondary K-feldspar replacing plagioclase in quartz-feldspar porphyry. Fine flakes of sericite have later overgrown K-feldspar (drill hole EU-051, 111.00 m). Abbreviations: qtz = quartz, K-feld = K-feldspar, XPL= cross-polarized light..... 71
Figure 5-4. Drill core image showing the sharp contact between marble and garnet-dominant garnet-pyroxene skarn. Garnet-pyroxene skarn is replacive towards marble, which has been cut by calcite veins. Late tremolite-actinolite replaces garnet-pyroxene skarn (drill hole EU-094, 108.50 m)..... 73
Figure 5-5. Drill core image showing progressive transition from garnet-rich skarn to wollastonite at the marble front. Hematite developed after garnet imparting a

reddish color to the sample. Carbonate and sphalerite developed during retrograde overprint (drill hole EU-094, 88.20 m). Abbreviations: grt = garnet, sph = sphalerite, wol = wollastonite. 73
Figure 5-6. Reddish-brown colored garnet skarn in sharp contact with foliated marble (drill hole EU051, 35.40 m). 74
Figure 5-7. Drill core photograph showing the transitional contact between non-skarn andesite porphyry and endoskarn (drill hole EU-094, 160.70 m). Red-green coloring is due to late hematite-chlorite replacement of garnet. 74
Figure 5-8. a) Drill core image of yellowish brown-colored garnet-rich prograde skarn, intensely overprinted by a late carbonate vein from Ulutaş area (drill hole EU-046, 124.80 m), b) Microphotograph (XPL, TL image) showing compositionally zoned garnets cross-cut and partly replaced by late stage carbonate (drill hole EU-046, 101.30 m). Abbreviations: grt=garnet, cal=calcite TL=transmitted light, XPL=cross polarized light. 76
Figure 5-9. Drill core image and microphotographs of retrograde overprinting of garnet-rich calc-silicate alteration. a) Coarse-grained garnet retrograded into hematite (reddish core) and chlorite (green rims). Sample is fractured and brecciated by fluids that are rich in carbonate. Specularite is also present as a late phase (drill hole EU-046, 101.30 m), b) microphotograph (XPL, TL image) showing sector-zoned garnet crystals fractured and cut by late stage carbonate (drill hole EU-046, 101.30 m), c) microphotograph (PPL, TL image) showing chlorite and carbonate overprinting of garnet (drill hole EU-046, 101.30 m). Abbreviations: grt=garnet, chl=chlorite, spe=specularite, cal=calcite, TL=transmitted light, XPL=cross polarized light, PPL= plane polarized light. 77
Figure 5-10. Drill core image and microphotographs of early garnet-pyroxene overprinted by late retrograde assemblages. a) drill core image of brown garnet and pale green-beige pyroxene cut and overprinted by carbonate alongside chlorite (drill hole EU-051, 78.90 m), b) microphotograph (XPL, TL image) showing intense carbonate veining after zoned garnet (drill hole EU-051, 78.90 m) c) microphotograph (XPL, TL image) showing partial replacement of garnet by late

carbonate (drill hole EU-046, 101.30 m). Abbreviations: grt = garnet, cal = calcite, TL = transmitted light, XPL = cross-polarized light..... 78
Figure 5-11. a, b) Drill core images showing hematite (red) and carbonate (white) pseudomorphing of early coarse-grained, zoned garnet. Sphalerite (dark gray) is intergrown with carbonate (drill hole EU-038, 86.00 and 85.00 meters, respectively). Abbreviations: grt=garnet, sph=sphalerite. 79
Figure 5-12. a) Marble – garnet-pyroxene skarn contact (drill hole EU-094, 108.50 m). b) microphotograph (XPL, TL image) py which shows high relief and high birefringence color (drill hole EU-094, 108.50 m), c) microphotograph (XPL, TL image) wollastonite show fibrous texture (drill hole EU-094, 108.50 m) Abbreviations: px=pyroxene, wol=wollastonite, carb=carbonate, TL=transmitted light, XPL=cross polarized light. 81
Figure 5-13. Hand specimen and microphotographs of wollastonite-bearing samples. a) drill core photograph of wollastonite showing fibrous texture (drill hole EU-081, 125.00 m), b) microphotograph (XPL, TL image) of wollastonite showing fibrous texture alongside carbonate (drill hole EU-081, 125.00 m) Abbreviations: wol=wollastonite, TL=transmitted light, XPL=cross polarized light. 82
Figure 5-14. Hand specimen and microphotographs of chlorite-epidote skarn sample a) drill core photograph of banded chlorite-epidote skarn (drill hole EU-051, 81.80 m), b) microphotograph (XPL, TL image) of chlorite-epidote skarn (drill hole EU-051, 81.80 m), c) microphotograph (PPL, TL image) of chlorite-epidote skarn (drill hole EU-051, 81.80 m). Abbreviations: chl = chlorite, cal = calcite, ep = epidote, TL = transmitted light, XPL= cross-polarized light, PPL = plane-polarized light. 83
Figure 5-15. a) Microphotograph (PPL, TL image) of actinolite replaces andesite porphyry (drill hole EU-071, 52.70 m), c) microphotograph (XPL, TL image) carbonate altered plagioclase from retrograde altered andesite poprhyry (drill hole EU-071, 52.70 m). Abbreviations: act = actinolite, car = carbonate, TL = transmitted light, XPL= cross-polarized light, PPL = plane-polarized light. 84

Figure 5-16. Cross-sectional view (looking SE) showing main lithological units and their cross-cutting relationships at the Ulutaş Cu-Zn skarn type deposit. Upper and lower marble units largely localized development of exoskarn. A steeply-dipping fault separates the domains to the northeast and southwest. 86
Figure 5-17. Skarn zonation pattern with andesite porphyry (AP) and basaltic dikes (BD) in Ulutaş Cu-Zn skarn type deposit.....87
Figure 5-18. Paragenetic sequence of the Ulutaş Cu-Zn skarn type deposit as obtained from petrographic observations of altered and mineralized samples. 89
Figure 5-19. a) Drill core sample shows the massive pyrite mineralization in the study area (drill hole EU-071, 126.00 m). b) drill core samples show disseminated sphalerite, pyrite and chalcopyrite mineralization (drill hole EU0102, 111.5-112.00 m). Abbreviations: sph = sphalerite, cpy = chalcopyrite, py = pyrite. 90
Figure 5-20. Drill core samples shows disseminated sphalerite and specularite mineralization on marble (drill hole EU-081, 83.30 m.) Abbreviations: sph = sphalerite, spe = specularite.....91
Figure 5-21. Microphotograph (XPL, RL image) of magnetite replaced by acicular specularite (drill hole EU-081, 91.70 m) Abbreviations: mag = magnetite, spe = specularite, hem = hematite RL= reflected light, XPL = cross-polarized light.....92
Figure 5-22. Hand specimen and microphotographs showing specularite-pyrite assemblages. a) drill core photograph of retrograde skarn with disseminated acicular specularite and pyrite (drill hole EU-051, 31.10 m), b) microphotograph (XPL, RL image) of fibrous specularite (drill hole EU-051, 31.10 m), c) microphotograph (XPL, RL image) of specularite and pyrite (drill hole EU-051, 31.10 m), Abbreviations: py=pyrite, spe=specularite, RL=reflected light, XPL=cross polarized light.....93
Figure 5-23. Microphotograph (XPL, RL image) of magnetite occurs rims on sphalerite with chalcopyrite and py (drill hole EU-051, 90.00 m), Abbreviations: cpy = chalcopyrite, hem = hematite, py = pyrite, mag = magnetite, RL = reflected light, XPL = cross-polarized light. 94

Figure 5-24. Microphotograph (XPL, RL image) showing chalcopyrite (yellow) replacement of sphalerite (gray, center). Sphalerite is rimmed by acicular specularite (gray, right) (drill hole EU-081, 91.70 m), Abbreviations: spe=specularite, sph=sphalerite, RL=reflected light, XPL=cross polarized light .. 94
Figure 5-25. Hand specimen and microphotographs of sphalerite mineralized samples a) microphotograph (XPL, RL image) of sphalerite with chalcopyrite disease texture cross-cut by calcite (drill hole EU-046, 102.00 m), b) microphotograph (XPL, RL image) of sphalerite with chalcopyrite disease texture cross-cut by calcite (drill hole EU-046, 102.40 m), c) microphotograph (PL, TL image) of brownish colored sphalerite cross-cut by calcite with opaque minerals (possible pyrite) (drill hole EU-046, 102.40 m), d) microphotograph (PL, TL image) of reddish brown colored sphalerite cross-cut by calcite (drill hole EU-081, 82.80 m), e) drill core photograph of massive and disseminated sphalerite (drill hole EU-046, 102.40 m) Abbreviations: cpy = chalcopyrite, sph = sphalerite, RL = reflected light, TL = transmitted light, PPL = plane-polarized light, XPL= cross-polarized light. 97
Figure 5-26. Hand specimen and microphotographs of sphalerite and chalcopyrite mineralized samples. a) drill core photograph of retrograde skarn with disseminated sphalerite and chalcopyrite (drill hole EU-081, 85.00 m), b) microphotograph (XPL, RL image) of sphalerite showing chalcopyrite disease texture (sample EU81-8150, drill hole EU-081, 81.50 m), Abbreviations: cpy = chalcopyrite, sph = sphalerite, RL = reflected light, XPL = cross-polarized light..... 98
Figure 5-27. Microphotograph (XPL, RL image) microphotograph (XPL, RL image) of pyrrhotite replacement of sphalerite showing chalcopyrite disease texture (drill hole EU-094, 86.60 m), Abbreviations: pyr = pyrrhotite, sph = sphalerite, cpy = chalcopyrite, RL=reflected light, XPL = cross-polarized light. 99
Figure 5-28. a) Microphotograph (XPL, RL image) of euhedral pyrite with chalcopyrite (drill hole EU-046, 115.00 m), b) microphotograph (XPL, RL image) of sphalerite I (chalcopyrite disease) which is intersected by pyrite (drill hole EU-

046, 112.00 m), Abbreviations: py = pyrite, sph = sphalerite, cpy = chalcopyrite, RL = reflected light, XPL = cross-polarized light. 100
Figure 5-29. Microphotograph (XPL, RL image) showing early euhedral pyrite surrounded by coarse-grained chalcopyrite, which in turn is cross-cut by sphalerite II (drill hole EU-038, 90.40 m). Abbreviations: py = pyrite, sph = sphalerite, cpy=chalcopyrite, RL = reflected light, XPL = cross-polarized light. 101
Figure 5-30. Microphotograph (XPL, RL image) showing early coarse-grained chalcopyrite surrounded and partly replaced by sphalerite II, which was later replaced by fine-grained chalcopyrite (chalcopyrite II; drill hole EU-046, 116.10 m). Abbreviations: py = pyrite, sph = sphalerite, cpy = chalcopyrite, hem = hematite, RL = reflected light, XPL = cross-polarized light. 101
Figure 5-31. a) Microphotograph (XPL, RL image) showing coarse-grained sphalerite I with chalcopyrite disease and disseminations of tabular molybdenite crystals (drill hole EU-081, 125.00 m). b) Microphotograph (XPL, RL image) showing coarse-grained sphalerite, which is cross-cut and replaced by chalcopyrite, alongside tabular molybdenite crystals (drill hole EU-081, 125.00 m). c) Microphotograph (XPL, RL image) showing a cluster of medium-grained, tabular molybdenite (drill hole EU-081, 125.00 m). d) Microphotograph (XPL, RL image) showing medium-grained, tabular molybdenite with hematite (drill hole EU-046, 116.10 m). Abbreviations: mol = molybdenite, sph = sphalerite, cpy = chalcopyrite, hem = hematite, RL = reflected light, XPL = cross-polarized light. 102
Figure 5-32. a) Microphotograph (XPL, RL image) of anhedral marcasite replaces the euhedral, cataclastic pyrite with chalcopyrite and sphalerite I (drill hole EU-046, 112.00 m), b) microphotograph (XPL, RL image) of tetrahedrite marcasite replaces sphalerite (drill hole EU-038, 90.40 m), c) microphotograph (XPL, RL image) of marcasite replaces py with cpy (drill hole EU-046, 116.10 m), b) microphotograph (XPL, RL image) of tetrahedrite marcasite accompanied with pyrite and chalcopyrite replaces sphalerite I (drill hole EU-046, 116.10 m). Abbreviations: mrc = marcasite, py = pyrite, sph = sphalerite, cpy = chalcopyrite, ttr = tetrahedrite, RL = reflected light, XPL = cross-polarized light. 103

Figure 5-33. a) Microphotograph (XPL, RL image) of covellite replaces the chalcopyrite (drill hole EU-046, 73.00 m), b) microphotograph (XPL, RL image) of bornite replaces covellite with pyrite and chalcopyrite (drill hole EU-046, 73.00 m). Abbreviations: cov = covellite, py = pyrite, bn = bornite, cpy = chalcopyrite, RL = reflected light, XPL = cross-polarized light. 104
Figure 5-34. Strongly-weathered mineralized skarn (drill hole EU-051, 47-53 meters)..... 105
Figure 5-35. Moderately-weathered garnet skarn (drill hole EU-051, 26- 30 meters)..... 106
Figure 5-36. Drill core image showing weathered skarn samples represented by limonite and malachite (drill hole EU-038, 50.00 m). 106
Figure 5-37. Bivariate correlation diagrams for selected metals of Cu, Zn, Ag, Au, Mo, and Pb for the upper skarn domain at Ulutaş (assay data courtesy of Demir Export). 110
Figure 5-38. Bivariate correlation diagrams for selected metals of Cu, Zn, Ag, Au, Mo, and Pb for the lower skarn domain at Ulutaş (assay data courtesy of Demir Export). 111
Figure 5-39. Log histogram of Zn assays of the Ulutaş skarn deposit..... 113
Figure 5-40. Log histogram of Cu assays of the Ulutaş skarn deposit. 114
Figure 5-41. General view of ore domains in the Ulutaş skarn deposit (red traces represent the drill holes)..... 114
Figure 5-42. Histogram of sample lengths. 115
Figure 5-43. a) Plan view, and b) Cross-sectional view showing spatial distribution of Cu- and Zn-rich domains at the Ulutaş Zn-Cu skarn deposit as based on drill hole data of Demir Exports. 117
Figure 5-44. Spatial distribution of a) Cu and b) Zn grade shells at Ulutaş as projected on to surface (assay data courtesy of Demir Export). 118
Figure 5-45. Cross-sectional views of a) Cu and b) Zn grade shells at the Ulutaş Cu-Zn skarn deposit (assay data courtesy of Demir Export). 119
Figure 5-46. Swath plot of Cu grades for raw data vs. numerical model. 120

Figure 5-47. Swath plot of Zn grades for raw data vs. numerical model. 120

CHAPTER 1

INTRODUCTION

1.1 Purpose and Scope

Eastern Pontides, which is located in northeastern Turkey, forms a segment of the collisional tectonic belt that developed after the episodic opening and closure of the Tethys oceanic basins, which were once located between the continental fragments derived from Laurasia and Gondwana (Şengör and Yılmaz, 1981; Okay and Tüysüz, 1999). The geodynamic and tectonic evolution of the Eastern Pontides are directly related to the northward subduction of the northern branch of the Neotethys in the Mesozoic and Late Cretaceous to early Cenozoic collision to post-collisional process that followed ocean closure (Şengör & Yılmaz, 1981; Okay & Şahintürk, 1997; Okay, 2008; Kandemir et al., 2019).

Due to its geodynamic evolution, including oceanic and Andean-type subduction to later collision, the Mesozoic–Cenozoic Eastern Pontide magmatic belt presents an important potential for formation of various types of metallic ore deposits. Such tectonic settings are particularly suitable for development of magmatic-hydrothermal deposit types including porphyry Cu±Mo±Au, epithermal Au±Ag±Cu±Pb±Zn, and skarn deposits (e.g., Sillitoe, 1972; Hedenquist and Lowenstern, 1994; Richards, 2011). A large number of such magmatic-hydrothermal systems have already been discovered in this region, particularly in close spatial and temporal association with Late Cretaceous to Eocene magmatic systems (e.g., Yiğit, 2009; Richards, 2015; Kuşcu et al., 2019; Revan, 2020; Rabayrol et al., 2022). In addition to various porphyry-, epithermal- and skarn-type mineralizations, Late Cretaceous island arc magmatic rocks of the belt also host numerous Kuroko-type volcanic-hosted massive sulfide deposits, including some of the most regionally-significant deposits of the

Tethyan Belt such as Murgul and Çayeli (Yiğit, 2009; Çiftçi, 2019; Kandemir et al., 2019; Revan, 2020).

Despite its significant potential for magmatic-hydrothermal mineralization, economic skarn systems (and similarly porphyry-type deposits) are rare in the Eastern Pontides. Known skarn systems are generally small-sized, sub-economic Fe±Cu skarn mineralizations that formed during the Late Cretaceous–Eocene magmatic activity. These include the Kartiba Fe skarn system in Rize, the Eğrikar and Karabörk Fe±Cu skarns in Gümüşhane, Kotana and Çatak Fe skarn systems in Giresun, and Çambaşı, and Fundacık Fe skarn systems in Ordu (Yigit, 2009; Çiftçi, 2011; Sipahi et al., 2017; Kuşcu et al., 2019).

This study focuses on the Ulutaş skarn deposit, which is located near the town of İspir, in Erzurum Province in northeastern Türkiye. Ulutaş is the only developed skarn project with economic Zn and Cu mineralization. The district also contains the İspir porphyry Mo-Cu prospect of Demir Export. Both the Ulutaş Zn-Cu skarn deposit and the neighboring İspir porphyry Mo±Cu prospect are part of a large batholith that was dated at 133–131 Ma (Delibaş et al., 2016). According to preliminary geochronological data of Delibaş et al. (2016), Ulutaş-İspir district seems to be associated with a period of magmatic activity that pre-dates almost all other ore-related igneous centers in the Eastern Pontides. This, and the fact that there are no other known Zn-Cu skarn mineralizations in this region makes Ulutaş a metallogenically important ore system. Taking these into consideration, this thesis research aims to answer several scientific questions. These are:

- What are the general geological features of the Ulutaş skarn system?
- What are the general mineralization characteristics (alteration and mineralization styles, mineralogical and elemental zonation, mineral paragenesis) at Ulutaş?
- What is the spatiotemporal relationship between Zn- and Cu-rich domains at Ulutaş?

- How Ulutaş is distinguished from other skarn systems in the Eastern Pontides?

Ultimately, the findings pertaining to the formation of the Ulutaş Zn-Cu deposit will be compared and correlated with other regional skarn systems of the Eastern Pontide magmatic belt.

1.2 Methodology

This thesis project includes both field and laboratory studies conducted between early 2019 and late 2022. Frequent site visits were held together with Demir Export personnel during 2018–2021, where outcrop mapping at the scale of 1:25.000, drill hole logging, sampling, and geological-mineralization modelling was carried out.

Main field work was carried out in June 2021, which aimed at general observation of deposit geology, quick logging of drill cores and also at drill core sampling. For this purpose, a total of 7 diamond drill holes, representing various geological and ore domains of the Ulutaş skarn system were investigated. A total of 90 core samples were collected from these diamond drill holes. Brief mesoscopic scale definitions of all samples were recorded and samples were photographed on site.

All samples were later prepared into thin sections and/or polished blocks at the Minerals Research and Exploration Institute of Turkey (MTA). Prepared sections were investigated for identification of their primary and secondary (ore and gangue) minerals, alteration styles, textural characteristics, and finally for mineral parageneses at the Middle East Technical University, using a Nikon brand polarizing microscope with transmitted and reflected light capabilities. Microphotographs were also acquired during petrographic studies.

Geological and numerical modeling of the Ulutaş Zn-Cu deposit was undertaken with an aim to understand distribution of different ore domains (Zn-rich versus Cu-rich), alteration types as well as for highlighting elemental zonation within the skarn

system. For this purpose, a drill hole database containing log and assay data from a total of 244 drill holes from Ulutaş were used. Modeling studies were conducted by using Leapfrog Geo 2021.1.1 Version software.

1.3 Location and Setting

The Ulutaş Zn-Cu deposit is located in İspir District in the north of Erzurum province in the Pontic mountains that border the northern margin of the Anatolian plateau. Ulutaş is located at 40°53'31.53"E 40°34'22.33"N (Figure 1-1), at elevations of 2,000 m to 2,400 m a.s.l. The nearby İspir district has a population of about 15,000, mostly living in İspir town, the local administrative and business center. İspir lies along the main course of the valley associated with the Çoruh river at an elevation of 1,200 m a.s.l.



Figure 1-1. Location of the study area (retrieved from Google Earth).

1.4 Previous Studies

The tenement of the Ulutaş deposit is owned by Demir Export A.Ş and the deposit area was previously explored by the General Directorate of Mineral Research and

Exploration Institute of Turkey (MTA). Demir Export later completed a reconnaissance exploration program through stream, soil, and rock sampling combined with geophysical surveys. Initial drilling by Demir Export commenced in 2012 and continued until 2020. The mining activities by Demir Export at Ulutaş Zn-Cu skarn type deposit is started in 2022.

The Ulutaş Deposit was explored by the General Directorate of Mineral Research and Exploration (MTA) as part of a United Nations Development Programme (UNDP) from 1971 to 1974 (Giles, 1974). Cu-Mo porphyry mineralization was identified in 1971 by a follow-up study of regional reconnaissance stream-sediment sampling campaign that highlighted significant copper and molybdenum anomalism (Giles, 1974). This was then followed up with rock-chip sampling, soil sampling (grid and ridge-and-spur), and mapping. An area of significant copper-molybdenum anomaly was defined and porphyry-style alteration and mineralized vein stockworks were confirmed.

Giles (1974) also identified skarn alteration consisting of garnet, epidote, and pyroxene at contacts between quartz monzonite intrusions and marble lenses, but no further exploration was conducted on the skarn prospect. MTA undertook a limited diamond drilling on the porphyry target and completed a total of 3,040 meters of drilling in 14 diamond drill holes. On this basis, a low-grade “resource” was estimated to total 73.6 million tonnes (Mt) at 0.31% Cu and 0.022% Mo (Yiğit, 2009), and based on these estimates the prospect was considered to be uneconomic.

Taylor and Fryer (1980) studied hydrothermal alteration at the Bakırçay and Ulutaş prospects. They concluded that differences were observed in the two prospects in terms of hydrothermal alteration (in particular, alteration overprinting), igneous textures, the abundance of xenoliths, extent of brecciation, and style and intensity of fracturing may relate to different levels of exposure within a conceptual model of a porphyry system. According to this study, Bakırçay represents the deep root zone of a porphyry system, whereas Ulutaş formed at a much higher level, close to the apex

of the porphyry system, or these prospects reflect different levels of magma emplacement (Taylor and Fryer, 1980).

Soylu (1999) conducted a regional study of the porphyry Cu-Mo systems of the Eastern Pontide belt, including the area where İspir Cu-Mo porphyry and Ulutaş skarn mineralizations are located. This study was concerned with the geology, alteration, and mineralization features, and also with the economic potential of these porphyry mineralizations. Soylu (1999) concluded that the Ulutaş prospect still has the potential for being an economic porphyry copper deposit.

Later, Oğuz (2010) re-evaluated exploration carried out during the 1971–1974 period based on recent conditions and proposed that the alteration relationships at Ulutaş had not been emphasized in sufficient detail in the previous studies. Within the scope of his study, it was investigated whether the Ulutaş Cu-Mo porphyry prospect, which is thought to be uneconomical, is in fact economically feasible and there is potential for porphyry mineralization to contain gold.

Delibaş et al. (2016) focused on the geological setting of porphyry mineralizations in the Eastern Pontides. To understand the relationship between magmatism and the geodynamic evolution of Eastern Pontides which is poorly understood, they gathered geochemical and geochronological data from Ulutaş Cu-Mo, Güzelyayla Cu-Mo, Emeksen Mo, and Elbeyli Mo-Cu porphyry systems. Based on laser ablation-inductively coupled plasma-mass spectrometry (LA-ICP-MS) U-Pb zircon ages, this study concluded that the İspir–Ulutaş Cu-Mo porphyry mineralization is hosted within a highly sericitized 131.1±0.9 Ma-old quartz-porphyry that intruded into a 132.9 ± 0.6 Ma-old granitic porphyry (Delibaş et al., 2016).

Delibaş et al. (2019) further investigated the time relationships of the Elbeyli, Güzelyayla, Emeksen, and Ulutaş porphyry systems concerning the geodynamic and magmatic evolution of the Eastern Pontides by using Re-Os molybdenite geochronology. Molybdenite from the İspir-Ulutaş¸ deposit yielded a Re-Os age of 131.0±0.7 Ma, which is consistent with the previously published LA-ICP-MS U-Pb zircon ages of local calc-alkaline intrusions. This demonstrated that the Eastern

Pontides porphyry mineralizations were already formed during the Early Cretaceous subduction of the Northern Neotethys Ocean along the Eastern Pontides and that they can be correlated with porphyry Cu events in the adjacent Lesser Caucasus (Delibaş et at., 2019).

CHAPTER 2

SKARN DEPOSITS: A REVIEW

Skarn deposits are one of the world's most abundant metallic ore deposit types. The term "skarn" refers to a rock type defined by its mineralogy, and which includes calc-silicate minerals such as garnet and pyroxene (Meinert, 1992). Skarn systems occur on all continents of various ages (Meinert et al., 2005).

Although most skarn deposits occur in lithologies containing carbonated rocks, they also can develop in various other rock types including shales, sandstone, granite, basalts, and komatiite (Meinert et al., 2005). Skarns can form through regional or contact metamorphism and from metasomatic processes by fluids originating from magmatic, metamorphic or meteoric sources (Meinert et al., 2005). Metasomatic skarn alteration can affect wide areas, often resulting in a zoned alteration mineralogy that can sometimes be mappable. Recognition of such zoned patterns is important for the exploration of these deposits (Chang and Meinert, 2008).

Skarns can be classified by based on the precursor rock they replace or by their metal contents (Meinert, 1992). The terms "endoskarn" and "exoskarn" are used to refer to zones of replacement of parental intrusive rocks and sedimentary rocks, respectively (Meinert et al., 2005). Exoskarns are further classified into two as calcic exoskarns and magnesian exoskarns. Magnesian exoskarns contain Mg-bearing silicates such as forsterite, diopside, and phlogopite, and are formed from precursor dolostones (Meinert et al., 2005). Calcic exoskarns replace calcium carbonate-rich country rocks and contain Ca-bearing minerals mainly including andradite, hedenbergite, johannsenite (Einaudi and Burt, 1982).

Economic skarns can be subdivided based on the dominant metal content like Sn, W, Fe, Au, Cu, Zn, Pb, and Mo. (Meinert et al., 2005).

Skarn zonation can occur from the microscopic scale to even kilometer scales (Meinert et al., 2005). This zonation pattern is a function of fluid flow, wall-rock characteristics, formation depth, and oxidation state (Chang and Meinert, 2008). The general trend of the zonation is proximal garnet towards distal pyroxene, and finally to vesuvianite, wollastonite, massive sulfides, and/or oxides at the marble front (Meinert, 1997, Meinert et al.,2005). Generally, the garnet:pyroxene ratio is high close to the plutonic center and it becomes lower towards distal zones (Meinert, 1987).

The colors and mineral chemistries of calc-silicate assemblages also may show systematic variations with respect to the position of the parental magma body. Garnet color is expected to become lighter towards distal zones from the igneous source, whereas pyroxene color becomes darker, and the pyroxene abundance as well as Fe and/or Mn increase towards the marble front (Meinert et al., 2005).

2.1 Skarn Deposits

The formation of a skarn deposit can be considered as a dynamic process. Generally, most skarn deposit shows the transition from early metamorphism resulting in hornfels, reaction skarn, and skarnoid to later metasomatism which results coarse-grained ore-bearing skarn (Meinert, 1992) (Figure 2-1).

Pluton-related skarn deposits are formed in a relationship between the sequence of emplacement, mineralization, alteration, and cooling of the pluton which relationship with the metamorphism, metasomatism, and retrograde alteration in the adjacent rock (Robb, 2005; Figure 2-2). Within the first stage, the pluton intrudes into country rock and contact metamorphism occurred (Meinert, 1992). Contact metamorphism produces marble from limestone, hornfels from shale, and quartzite from sandstone (Meinert et al., 2005; Figure 2-1). Also, reaction skarns occurred along the lithological boundary and prograde skarns started to form (Meinert, 1992). The second stage is the multiple stages of metasomatism (Meinert et al., 2005).

Magmatic fluid exsolution occurs from the pluton to from endoskarn and exoskarn. Although magnetite and scheelite precipitation occurs in W skarn, sulfide mineralization does not form in this stage (Meinert, 1992). The third and last stage of skarn formation is the retrograde alteration stage (Robb, 2005). Magmatic-hydrothermal fluids undergo cooling. The cooling system allows the meteoric water to enter the intrusion-skarn system (Robb, 2005). While meteoric water dominated, retrograde alteration is classified by epidote, chlorite, plagioclase, calcite, quartz, tremolite-actinolite, talc, serpentine, and olivine overprint the prograde skarn (Robb, 2005). Also, sulfide and base metal precipitation occur within the third stage of skarn formation (Meinert et al., 2005). Sulfide ore minerals occur as disseminated ore minerals or veins that cut the prograde alteration assemblages (Robb, 2005). Metal precipitation within the skarn system is related to the temperature decreasing of the ore fluids, fluid mixing, or neutralization of the fluid by reaction with the carbonate lithology (Robb, 2005). Also, mixing the magmatic fluid with meteoric fluid, and due to the mixing changes in the redox condition controls the metal precipitation (Meinert et al., 2005).

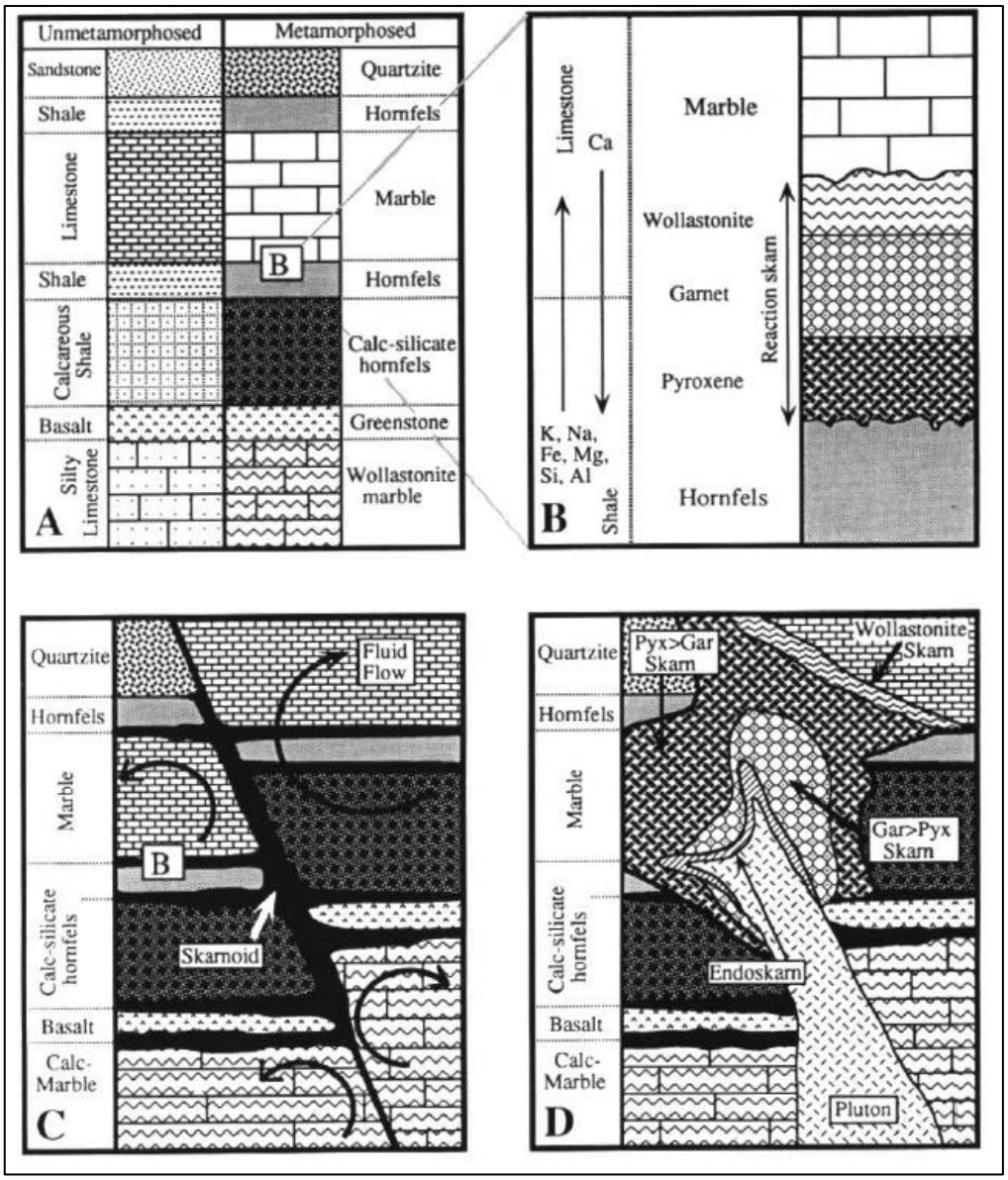


Figure 2-1. Types of skarn formation A. Isochemical metamorphism B. Reaction skarn C. Skarnoid D. Fluid-controlled metasomatic skarn (Meinert, 1982).

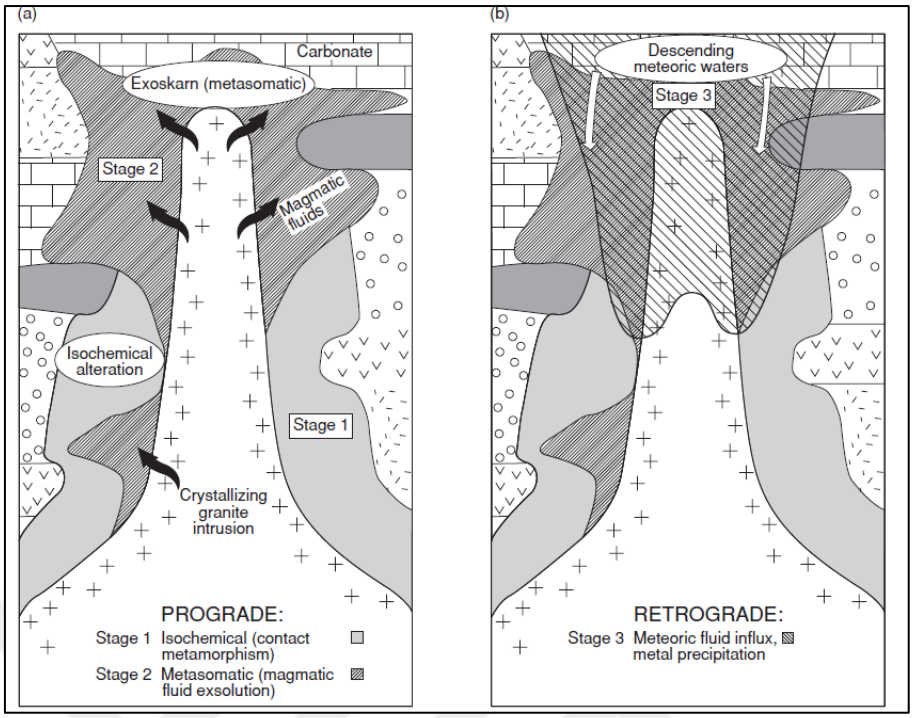


Figure 2-2. The stages of intrusion-related skarn deposits showing three sequential stages of formation. (a) Prograde stages, and (b) retrograde stage (Robb, 2005).

The mineralogy of skarn deposits is important for the classification and identification of skarn deposits. Also, understanding the mineral compositional variations is important for understanding skarn formation. Table 2-1 shows the most common skarn minerals observed in various skarn deposits (Meinert et al., 2005).

Table 2-1. Common Alteration Minerals of Skarn Systems (Meinert et al., 2005)

General group	End members	Abbreviation	Composition	Related names
Garnet	Grossularite	Gr	$Ca_3Al_2Si_3O_{12}$	Grandite
	Andradite	Ad	$Ca_3Fe_2Si_3O_{12}$	
	Spessartine	Sp	$Mn_3Al_2Si_3O_{12}$	Subcalcic garnet
	Almandine	Al	$Fe_3Al_2Si_3O_{12}$	
	Pyrope	Py	$Mg_3Al_2Si_3O_{12}$	
Pyroxene	Diopside	Di	$CaMgSi_2O_6$	Salite
	Hedenbergite	Hd	$CaFeSi_2O_6$	
	Johannsenite	Jo	$CaMnSi_2O_6$	
	Fassaite	Fas	$Ca(Mg,Fe,Al)(Si,Al)_2O_6$	
Olivine	Forsterite	Fo	Mg_2SiO_4	Monticellite
	Fayalite	Fa	Fe_2SiO_4	Knebelite
	Tephroite	Tp	Mn_2SiO_4	Glaucochroite
	Monticellite	Mc	$CaSiO_4$	
Pyroxenoid	Ferrosilite	Fs	$FeSiO_3$	Pyroxmangite
	Rhodonite	Rd	$MnSiO_3$	Bustamite
	Wollastonite	Wo	$CaSiO_3$	
Amphibole	Tremolite	Tr	$Ca_2Mg_5Si_8O_{22}(OH)_2$	Actinolite
	Ferroactinolite	Ft	$Ca_2Fe_5Si_8O_{22}(OH)_2$	
	Manganese actinolite	Ma	$Ca_2Mn_5Si_8O_{22}(OH)_2$	
	Hornblende	Hb	$Ca_2Mg_4Al_2Si_7O_{22}(OH)_2$	
	Pargasite	Pg	$NaCa_2Mg_4Al_3Si_6O_{22}(OH)_2$	Hastingsite
	Ferrohastingsite	Fh	$NaCa_2Fe_4Al_3Si_6O_{22}(OH)_2$	
	Cummingtonite	Cm	$Mg_5Fe_2Si_8O_{22}(OH)_2$	
	Dannemorite	Dm	$Mn_5Fe_2Si_8O_{22}(OH)_2$	Subcalcic amphibole
	Grunerite	Gru	$Fe_7Si_8O_{22}(OH)_2$	
Epidote	Piemontite	Pm	$Ca_2MnAl_2Si_3O_{12}(OH)$	
	Allanite	All	$(Ca,REE)_2FeAl_2Si_3O_{12}(OH)$	
	Epidote	Ep	$Ca_2FeAl_2Si_3O_{12}(OH)$	
	Pistacite	Ps	$Ca_2Fe_3Si_3O_{12}(OH)$	
	Clinozoisite	Cz	$Ca_2Al_3Si_3O_{12}(OH)$	
Plagioclase	Anorthite	An	$CaAl_2Si_2O_8$	
Scapolite	Meionite	Me	$Ca_4Al_6Si_6O_{24}(CO_3,OH,Cl,SO_4)$	
Other	Vesuvianite (idocrase)	Vs	$Ca_{19}(Mg,Fe,Mn)_3Al_4Si_9O_{34}(OH, Cl, F)_4$	
	Prehnite	Pr	$Ca_2Al_2Si_3O_{10}(OH)_2$	
	Axinite	Ax	$(Ca,Mn,Fe)_3Al_2BO_3Si_4O_{12}(OH)$	

2.2 Skarn Zonation

According to Meinert (1997), in most skarns, a general zonation pattern is observed. This zonation is indicated by proximal garnet, distal pyroxene, and vesuvianite or pyroxenoid such as wollastonite, bustamite, or rhodonite (Figure 2-3).

Skarn minerals such as garnet and pyroxene may also show deposit- to district-scale zonation in terms of color and compositional. Generally, the color of the garnet is dark-red brown in proximal occurrences and it becomes lighter in more distal occurrences and the garnet can be observed as pale green near the marble front (Atkinson and Einaudi, 1978). Also, pyroxene becomes darker away from the fluid conduits. Moreover, in the Cu, Mo, and Fe skarn, amphiboles are more iron-rich in the tremolite-actinolite series, and amphiboles in the Zn skarn are Mn-rich (Meinert, 1992). Retrograde alteration minerals which are the epidote, amphibole, chlorite, and other hydrous minerals are structurally controlled and this retrograde alteration overprints the prograde alteration minerals like garnet and pyroxene (Meinert et al.,2005). In shallower skarn deposits, retrograde alteration is more intense and outspread. The extensive retrograde alteration may completely overprint the prograde alteration assemblages (Robb, 2005). Since the zonation pattern can occur on a kilometer-to-meter scale, it is important for the exploration of skarn deposits.

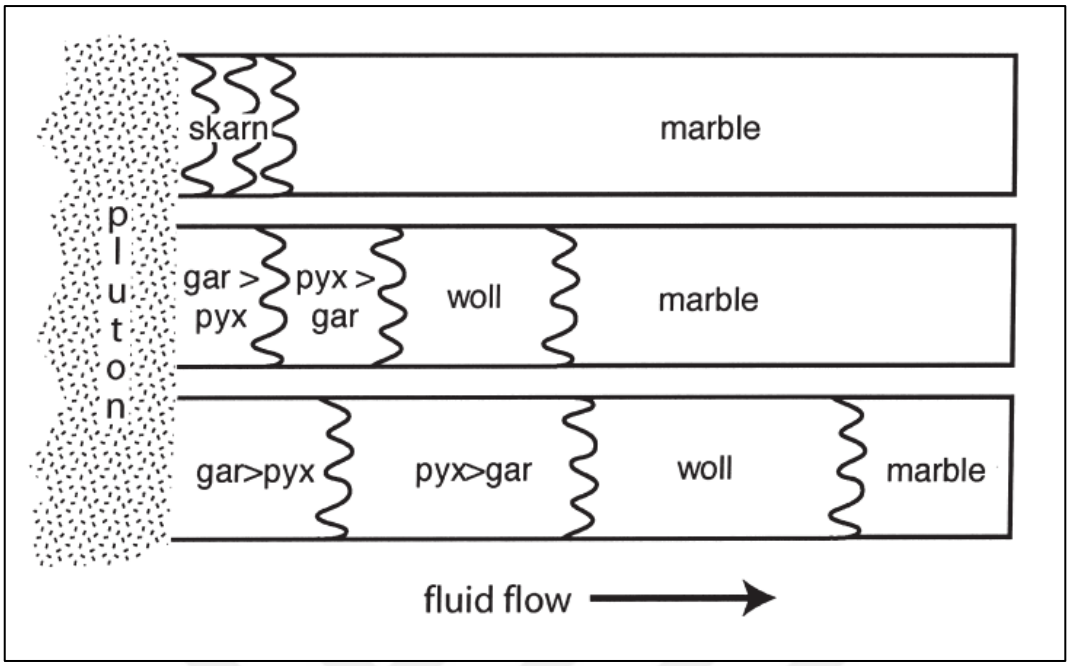
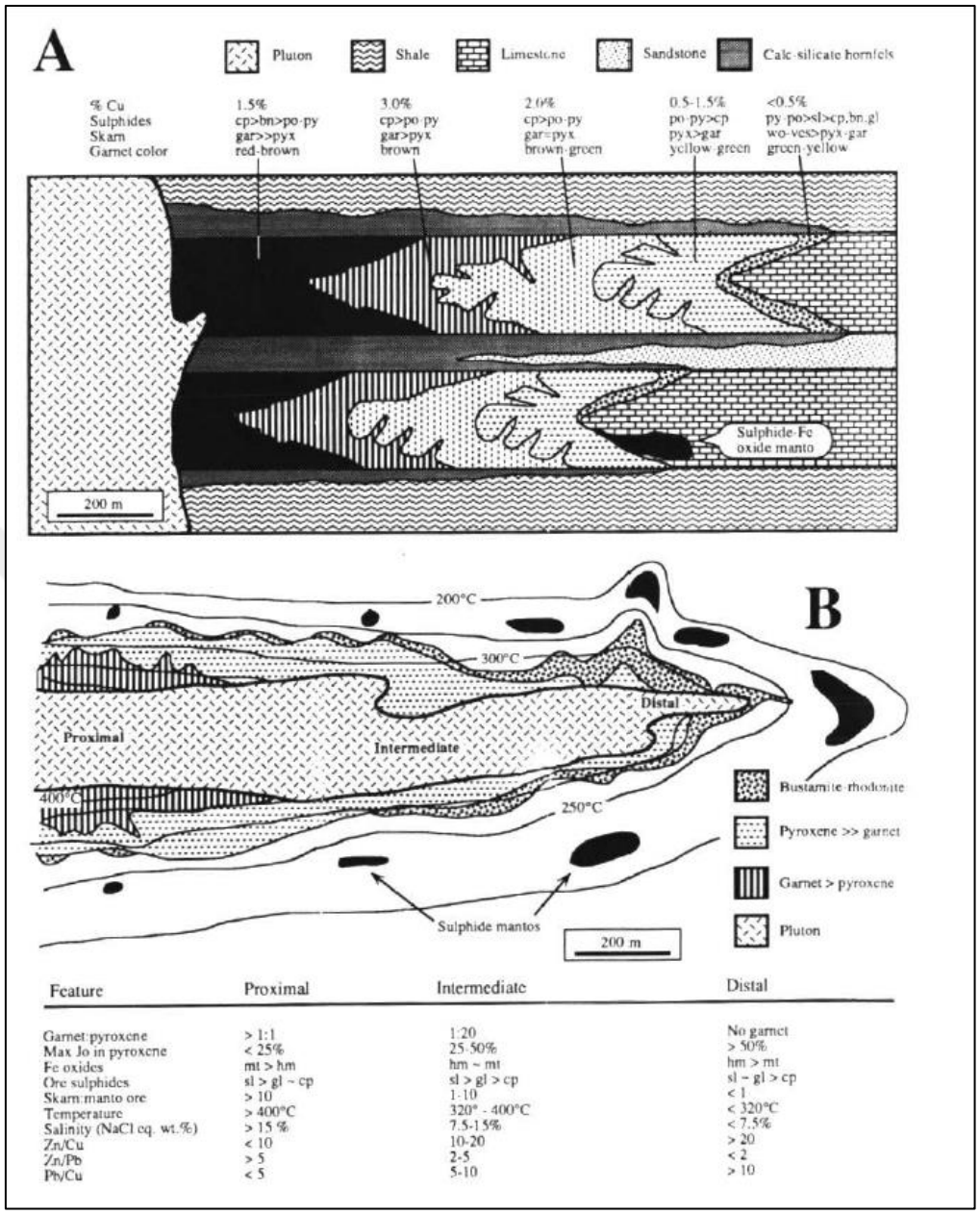


Figure 2-3. Schematic illustration of the propagation of multiple reaction fronts during progressive fluid flow (Meinert et al., 2005).

There are some common zonation patterns observed in different skarn types (Figure 2-4.) These variations show different tectonic settings, geological conditions, and geochemistry of the skarn environment.



Feature	Proximal	Intermediate	Distal
Garnet:pyroxene	> 1:1	1:20	No garnet
Max Jo in pyroxene	< 25%	25-50%	> 50%
Fe oxides	mt > hm	hm ~ mt	hm > mt
Ore sulphides	sl > gl ~ cp	sl > gl > cp	sl ~ gl > cp
Skarn:manto ore	> 10	1-10	< 1
Temperature	> 400°C	320° - 400°C	< 320°C
Salinity (NaCl eq. wt.%)	> 15 %	7.5-15%	< 7.5%
Zn/Cu	< 10	10-20	> 20
Zn/Pb	> 5	2-5	< 2
Pb/Cu	< 5	5-10	> 10

Figure 2-4. General models of skarn zonation: A) copper skarn (after Atkinson and Einaudi, 1978); B) zinc skarns (Meinert, 1987).

2.3 Tectonic Settings of Skarn Deposits

Figure 2-5 shows the different tectonic setting models for skarn formation (Meinert et al., 2005). Calcic Fe and Cu skarn deposits occur in oceanic island arc terranes. According to Meinert (1992), some economic gold skarn was formed in the back-arc basin which is associated with the oceanic volcanic arc. Most of the skarn deposits are associated with a magmatic arc which is related to continental subduction (Meinert, 1992). Magmatism associated with low-angle subduction is related to the formation of Mo and W-Mo skarn (Meinert et al., 2005). Although most skarns are associated with subduction-related magmatism, some of the skarn formations are not related to this tectonic setting. S-type magmatism which may be associated with rifting causes the formation of Sn skarn (Meinert et al., 2005).

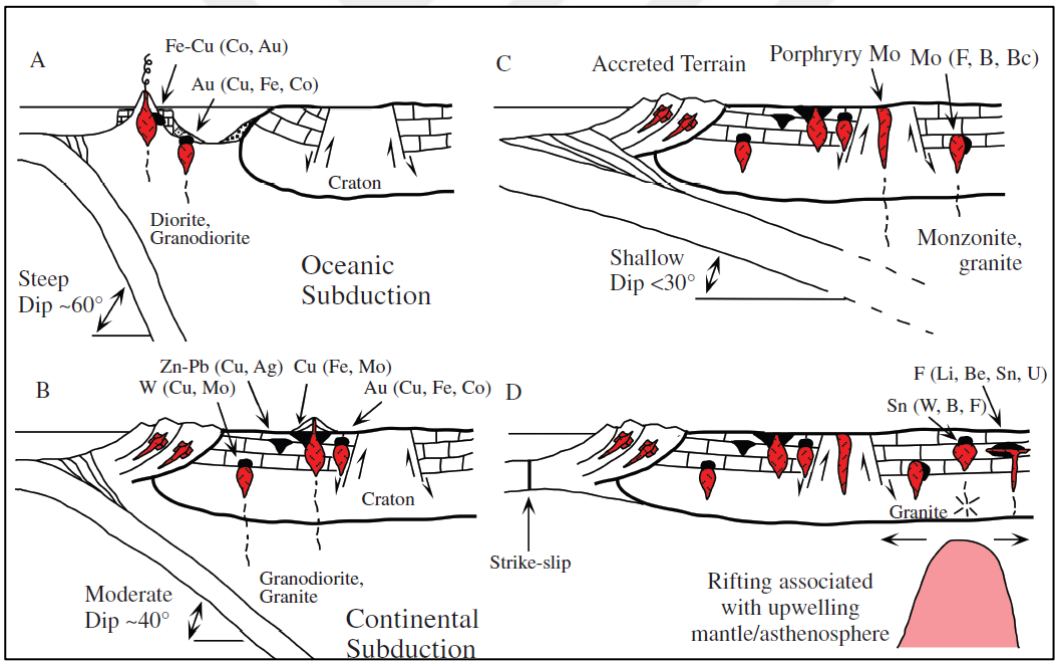


Figure 2-5. Generalized tectonic setting models for skarn formation (Meinert et al., 2005).

2.4 Types of Skarn Deposits

Skarn deposits can be classified by considering their protolith composition, rock type, dominant economic metals, mechanism of fluid movement, the temperature of formation, and extent of magmatic involvement (Meinert, 1992). Also, dominant metal content is important for the classification of skarn deposits. There are seven major skarn types which are the Fe, Au, Cu, W, Zn, Mo, and Sn skarn. Although these are the major skarn types, there are other skarn types like REE and U skarns (Meinert, 1992). Table 2-2 Shows the general differences between the major skarn types which are classified as their dominant economic metals. Since the thesis focuses on the Cu and Zn skarn, these types are explained in more detailed.

Cu skarns are common throughout the world. They generally occur in orogenic zones related to subduction (Meinert, 1992). Cu skarns are related to I-type, magnetite series, calc-alkaline porphyritic plutons (Meinert et al., 2005). Many of these have shallow co-genetic volcanic rocks, zones of stockwork veining, and brecciation. These properties indicate relatively shallower environments of formation. Copper skarns generally develop proximal to the parental intrusions and their mineralogy reflects (e.g., presence of andradite) oxidizing conditions. Other abundant alteration minerals are diopside, vesuvianite, wollastonite, actinolite, and epidote (Meinert, 1992). Magnetite and hematite are also present in many copper skarn deposits (Meinert et al., 2005). According to Einaudi et al. (1981), zonation occurs in the copper skarn as garnet near the pluton (proximal), pyroxene increasing towards the marble (distal), and vesuvianite and/or wollastonite at the marble front. Pyrite and chalcopyrite are the common sulfide minerals that occurs in copper skarns (Meinert, 1992). Moreover, endoskarn alteration is rare in copper skarn deposits (Meinert et al., 2005).

Zn skarns occur in subduction or continental rift settings (Meinert, 1992). These are mined predominantly for zinc with by-product lead and silver (Meinert et al., 2005). Associated igneous rocks range from diorite to granite. They are formed in different geological environments like deep-seated batholiths, shallow dyke – sill complexes,

and surface volcanic extrusions (Meinert, 1992; Meinert et al., 2005). Zinc skarn ores occur distally with respect to their associated igneous rocks. Zn skarns can be divided by considering several criteria like distance from the magmatic source, formation temperature, the relative ratio of skarn and sulfide minerals, and the general shape of the ore body (Meinert et al., 2005). Generally, alteration minerals which are garnet, pyroxene, amphiboles, chlorite, olivine, ilmenite, pyroxenoid, and serpentine in the zinc skarn are enriched in manganese (Meinert, 1992). Also, the pyroxene/garnet ratio and manganese content of skarn minerals may increase along the fluid flow path (Meinert, 1987). This situation can be used to understand the skarn zonation concerning distal and proximal skarn.

Table 2-2. Different skarn types with their differences in terms of a dominant ore mineral, plutons and skarn mineralogy (Meinert et al., 2005)

Types of Skarn	Fe	Cu	Zn-Pb	Au	W	Sn	Mo
Dominant ore	Mgt (endoskarn) Cp, Co-Ni-sulfide (exoskarn)	Chalcopyrite, pyrite, bornite, hematite and magnetite	Sphalerite, Galena, Pyrite, Pyrrhotite	Pyrite, pyrrhotite, arsenopyrite	Mo-rich scheelite, pyrite	Casiterite , minor pyrrhotite, arsenopyrite	Molybdenite, polymetalic including W, Cu, Zn, Pb, Bi, Sn, and U.
Pluton	Mafic plutonic and/or hypabyssal	Calc-alkline, magnetite-series, hypabyssal granodiorite or Qz monzonite	Diorite through high silica granite	Plutonic or hypabyssal, partly ilmenite bearing granodiorite and diorite	Coarse-grained equigranular batholiths (with pegmatite and aplite dikes)	High silica granite	Highly differentiated pluton such as leucoclatic granite, minor pegmatite, and aplite
Skarn mineral	Pyroxene , garnet , epidote, magnetite	Andraditic garnet with diopsidic pyroxene, vesuvianite, wollastonite, actinolite and	garnet, pyroxene, olivine, ilvaite, pyroxenoid, amphibole, chlorite, and serpentine	Fe rich pyroxene, grandite garnet with K-feldspar, scapolite, vesuvianite,	Hedenbergitic pyroxene and lesser grandite garnet with Mo-rich scheelite	Magnesian, calcic, proximal, and distal skarns Proximal Fe-rich Gnt and Cpx, distal cassiterite bearing massive sulfide ore body	Hedenbergitic pyroxene with lesser grandite garnet, wollastonite, amphibole and fluorite

CHAPTER 3

REGIONAL SETTING, GEOLOGY, AND METALLOGENY OF EASTERN PONTIDES

3.1 Tectonic Setting of Eastern Pontides

Turkey consists of three main tectonic blocks with distinct stratigraphic and structural features based on the earlier work by Ketin (1966): (1) the Anatolide-Tauride Block, (2) the Arabian Block, and (3) the Pontides. The latter is further sub-divided into three main tectonic entities as the Rhodope-Strandja, Istanbul, and the Sakarya Zones (Figure 3-1; Ketin, 1966; Şengör and Yılmaz, 1981; Okay and Tüysüz, 1999).

Anatolide-Tauride Block, Pontides, and the Arabian Block are bounded by main oceanic sutures, which are the Izmir-Ankara-Erzincan Suture, Intra-Pontide Suture, Inner-Tauride Suture, and Assyrian-Zagros/Bitlis-Zagros Suture Zones (Figure 3-1; Okay and Tüysüz, 1999). These distinct tectonic blocks have now been juxtaposed against each other, forming a single landmass during the closure of different branches of the intervening Tethyan ocean basins from the Late Mesozoic to Late Cenozoic (Şengör and Yilmaz, 1981; Okay and Tüysüz, 1999; Stampfli, 2000; Bozkurt and Mittwede, 2001; Stampfli and Borel, 2002; Okay, 2008).

The Pontides as a mountain range can be divided into three sectors, which are the Western Pontides, Central Pontides, and Eastern Pontides in respect to their tectonic characteristics (Yılmaz et al., 1997). Eastern Pontides form a mountain chain 500 km-long and 100 km-wide along the eastern Black Sea region and extends into the Lesser Caucasus to the east (Okay, 2008). Eastern Pontides is also the region constituting the eastern part of the Sakarya Block and is bounded by İzmir Ankara Erzincan Suture in the south and by the East Black Sea Basin in the north (Okay and Şahintürk, 1997).

Eastern Pontides in NE Turkey forms part of the collisional tectonic belt that developed after the episodic subduction and opening of the Tethys oceanic basins, which were once located between the continental fragments derived from Laurasia and Gondwana (Şengör and Yılmaz, 1981; Okay and Tüysüz, 1999). Its geological evolution is generally accepted to be related to the northward subduction of Neotethys during the Late Mesozoic, and subsequent ocean closure and collision that occurred in the Late Cretaceous to Early Cenozoic (Şengör and Yılmaz, 1981; Okay and Şahintürk, 1997; Okay, 2008; Kandemir et al., 2019). However, Eyüboğlu et al. (2011) proposed a southward subduction model of the Tethyan oceanic lithosphere for the same geological time interval.

According to Kaygusuz and Öztürk (2015), Eastern Pontides can be divided into northern and southern zones as these domains show different geological affinities. The Northern Zone is dominated by Carboniferous to Eocene volcanic and volcaniclastic rocks, whereas Paleozoic to Eocene plutonic, volcanic, metamorphic, and sedimentary rocks predominate the Southern Zone (Okay and Şahintürk, 1997; Kaygusuz and Öztürk, 2015).

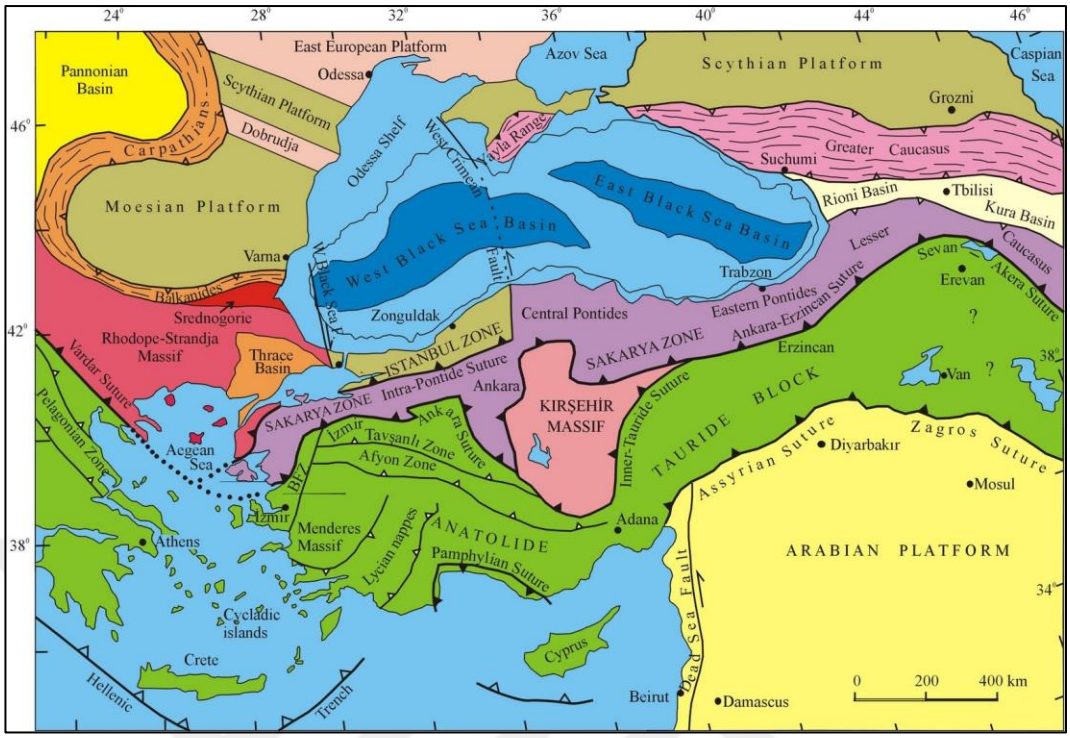


Figure 3-1.Tectonic division of Anatolia and its neighboring regions located on the Tethyan orogenic belt, showing major structures, sutures, and continental blocks including the Rhodope-Strandja Zone, İstanbul Zone, and Sakarya Zone of the Pontides Domain (Okay and Tüysüz, 1999).

3.1.1 Geodynamic Evolution of Eastern Pontides

Geodynamic evolution of NE Anatolia between the Sakarya Zone and Anatolide-Tauride Block shaped the geology of the Eastern Pontides in the relation to the opening and closure of the Paleotethys and Neotethys oceanic basins (Okay and Şahintürk, 1997).

During the Late Ordovician to Early Silurian, the Paleotethys basin opened between the Hun Superterrane and the northern Gondwana margin (Stampfli and Borel, 2002). In this period, Pontides and Taurides were derived from Gondwana in relationship with the initiation of Paleotethys Ocean Basin (Figure 3-2; Okay and Nikishin, 2015). Pangea formation due to the collision of Gondwana and Laurasia and consumption of Paleotethys Ocean in relation to Variscan Orogeny occurred in

the Late Paleozoic (Stampfli and Borel, 2002). The closure of Paleotethys started from the Triassic and continued until the Jurassic with the Cimmerian Orogeny (Stampfli and Borel, 2002).

During the closure of the Paleotethys, Neotethys ocean basin started to open from east to west by rifting of the Cimmerian continents from the northern part of the Gondwana margin in the Permian to the Early Triassic period, and rifting continued until the Early Tertiary (Şengör and Yilmaz, 1981; Robertson and Dixon, 1984; Stampfli et al., 1991; Stampfli and Borel, 2002).

The closure of Paleotethys started the northward subduction of Neotethys along the southern margin of Laurasia in the Jurassic (Şengör and Yilmaz, 1981; Robertson and Dixon, 1984; Okay and Nikishin, 2015). The subduction and suturing started the formation of relatively small but interconnected Vardar, Izmir-Ankara-Erzincan, and Pindos oceanic basins during the Late Cretaceous (Stampfli and Borel, 2004).

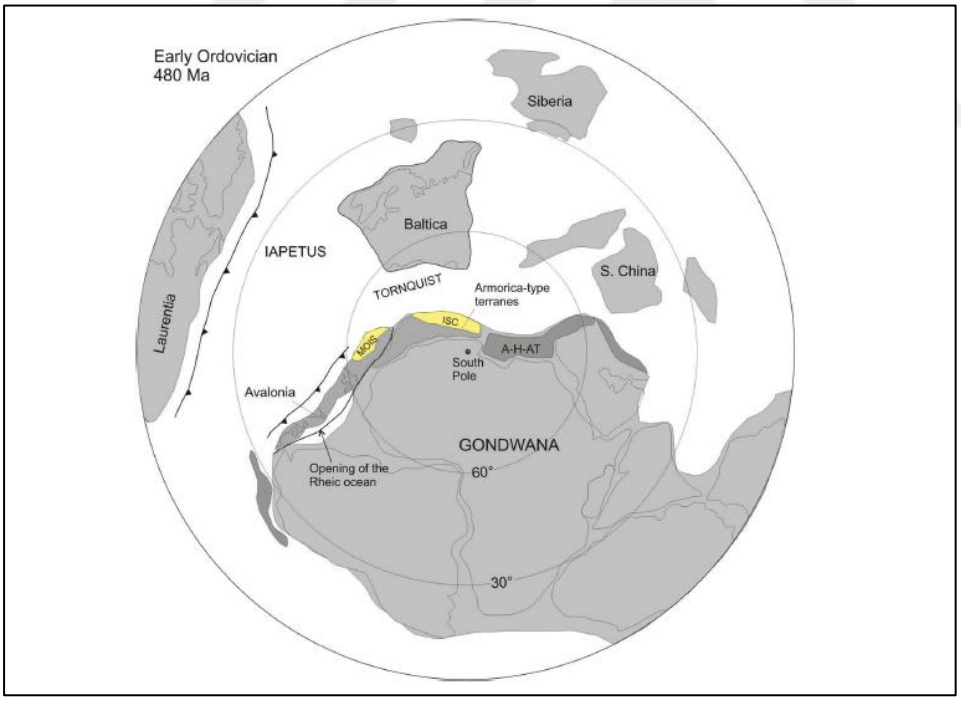


Figure 3-2. Paleogeography of the southern hemisphere for the Early Ordovician showing possible locations of the Pontic terranes. MOIS (Moesia, Istanbul, and part of Scythian Platform), ISC (Strandja, Sakarya, and Caucasus), and AHAT (Apulia, Hellenides, Anatolide-Tauride) (Okay and Nikishin, 2015).

The geodynamic evolution of Eastern Pontides can be examined within two major tectono-magmatic periods, (1) the Late Cretaceous magmatism due to the northward subduction of Neotethys and (2) collision and post-collisional magmatism as a result of the collision of the Anatolide-Tauride Block with the Pontides and closure of the Izmir-Ankara-Erzincan Ocean (Figure 3-3).

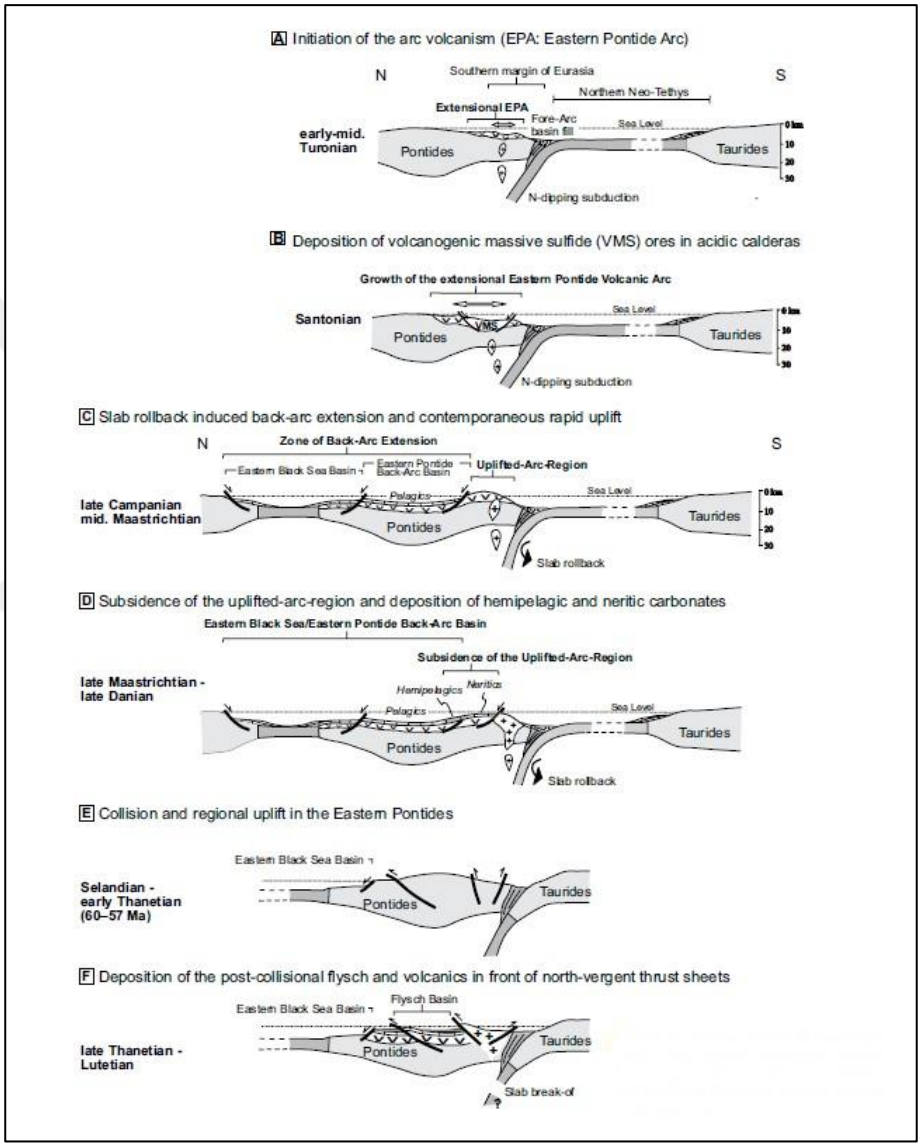


Figure 3-3. Late Cretaceous to Eocene tectonic evolution model of the Eastern Pontides (Kandemir et al., 2019).

3.1.1.1 Pre-Cenozoic Evolution of Eastern Pontides

Subduction and closure of the Paleotethys Ocean during the Permian to Middle Triassic, the opening of the Neotethys Ocean in the Late Permian to Triassic, contemporaneous subduction of Neotethys under the southern margin of Laurasian and the final closure of northern Neotethys in Late Cretaceous are the main tectonic events occurred in the pre-Cenozoic period (Figure 3-4; Okay and Şahintürk, 1997; Kandemir et al., 2019).

According to Okay (2008), the three Pontic terranes which are Strandja, İstanbul and Sakarya were amalgamated into single Pontides in the Middle Cretaceous following the closure of the Intra-Pontide Ocean and opening of Black Sea Basin.

There are two models relating to the vergence and timing of the subduction of the Neotethys during the Mesozoic. Many researchers suggested that the evolution of Eastern Pontides is related to northward subduction of Neotethys during the Late Cretaceous (Şengör and Yılmaz, 1981; Okay and Şahintürk, 1997; Kandemir et al., 2019). However, to some, a southward subduction model is valid, which is responsible from Paleozoic to Eocene magmatism in the Eastern Pontides (Figure 3-4; Bektaş et al., 1999; Eyüboğlu et al., 2011).

In the Late Cretaceous, I-type, high-K calc-alkaline to alkaline magmatism developed due to the northward subduction of Neotethyan oceanic slab underneath the Pontides (Okay and Şahintürk, 1997; Okay and Tüysüz, 1999). Several researchers indicated that Neotethys was subducted under the Pontides in the Early Cretaceous and a magmatic arc was initiated in the Late Cretaceous (Okay and Şahintürk, 1197, Okay et al., 2006, Robinson et al., 1995). However, Early Cretaceous aged calc-alkaline magmatic rocks from the eastern part of the Eastern Pontides (131.1 ± 0.9 Ma and 132.9 ± 0.6 Ma from granodiorite at İspir-Ulutaş, 142 Ma-old Rize pluton; 138.5 ± 2.2 Ma-old Çamlıkaya granitoid) indicate the arc magmatism had already started in Early Cretaceous (Taner, 1977; Giles, 1973; Boztuğ and Harlavan, 2008; Delibaş et al., 2016).

High-K, calc-alkaline to shoshonitic, A-type granitoids were emplaced in the Eastern Pontides from 81 to 74 Ma (Delibaş et al., 2016, Karslı et al., 2012; Kaygusuz et al., 2014). This magmatic activity is suggested to have resulted from a switch to an extensional stress regime, indicating the transition from a compressional to an extensional arc setting attributed to the roll-back of the subducted Neotethyan lithosphere in the Late Campanian (Delibaş et al., 2016, Karslı et al., 2010, Kandemir et al., 2019). Formation of widespread VHMS deposits of the Eastern Pontides corresponds to the development of this extensional environment (Delibaş et al., 2016, Kandemir et al., 2019; Revan, 2020).

All of the regional Kuroko-type volcanic-hosted massive sulfide deposits as well as few porphyry Cu-Mo and Fe-Cu skarn mineralizations were formed in close association with Cretaceous magmatism (Yiğit, 2009; Çiftçi, 2019; Kuşcu 2019; Kuşcu et al., 2019; Revan, 2020).

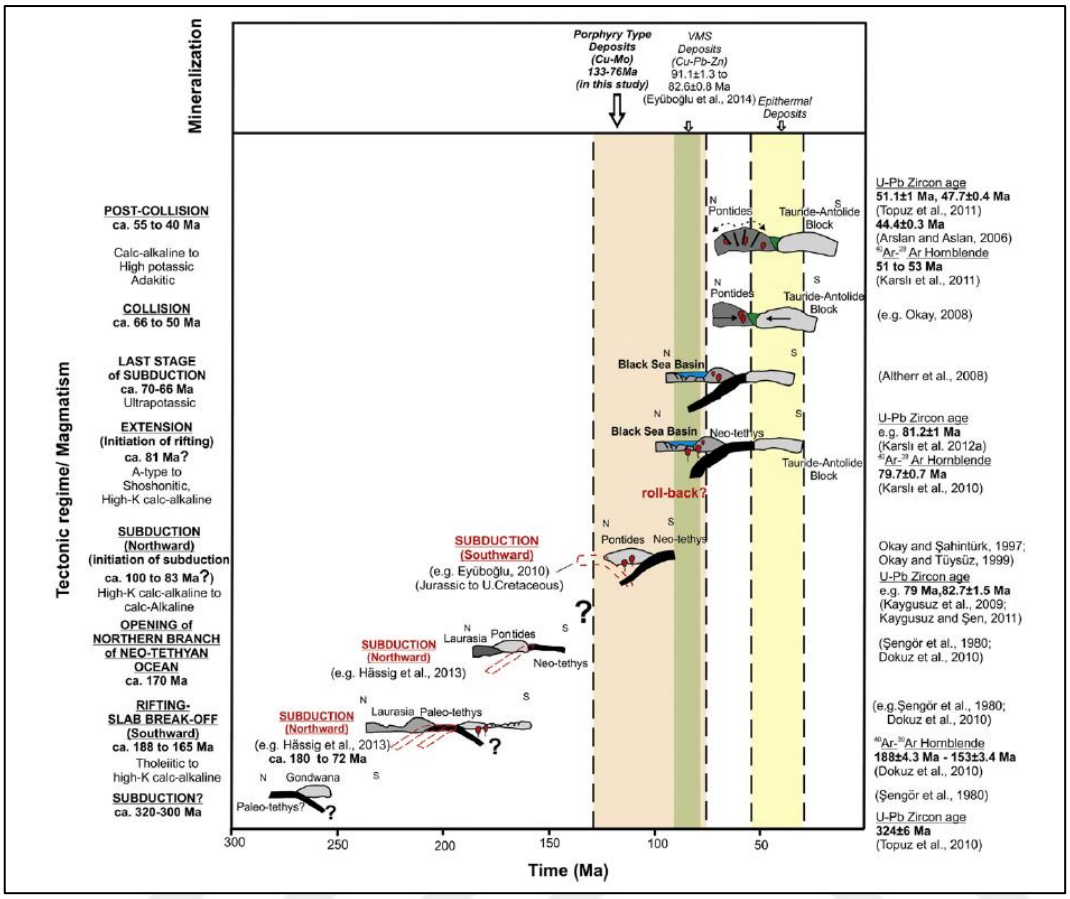


Figure 3-4. Cartoon showing geodynamic evolution of Eastern Pontides during the Paleotethys closure and progressive development of the Neotethys ocean together with major magmatic episodes and associated metallic ore deposits (Delibaş et al., 2016; references for geochronological data are shown on the figure).

3.1.1.2 Cenozoic Evolution of Eastern Pontides

The closure of the Neotethys Ocean caused the collision between Eastern Pontides and the Tauride-Anatolide Platform during the latest Cretaceous–Early Paleogene (Okay and Şahintürk, 1997; Kandemir et al., 2019). This collision triggered widespread collisional to post-collisional magmatism in Eastern Pontides, particularly during the Eocene (Figure 3-4 and Figure 3-5; Topuz et al., 2005; Arslan and Aslan 2006; Kaygusuz and Öztürk, 2015). Eocene magmatic rocks generally occur along an E–W trend within the northern and eastern sectors of the Eastern Pontides (Kaygusuz et al., 2019). Eocene magmatic lithologies are represented by plutonic, sub-volcanic, and volcanic rocks associated with volcano-sedimentary units (Kaygusuz and Öztürk, 2015; Kandemir et al., 2019). Eocene magmatism in Eastern Pontides is of I-type, high-K, calc-alkaline to shoshonitic in composition and exhibits a metaluminous to peraluminous character (Topuz et al., 2005; Kaygusuz et al., 2019; Kuşcu et al., 2019).

Generally, epithermal-type mineralization in the Eastern Pontides is hosted by Eocene volcanic sequences (Figure 3-4; Yiğit, 2009; Oyman, 2019). Some of the base metal skarn and porphyry Cu-Mo mineralization also occurs in relation to Eocene magmatism (Kuşcu, 2019; Kuşcu et al., 2019).

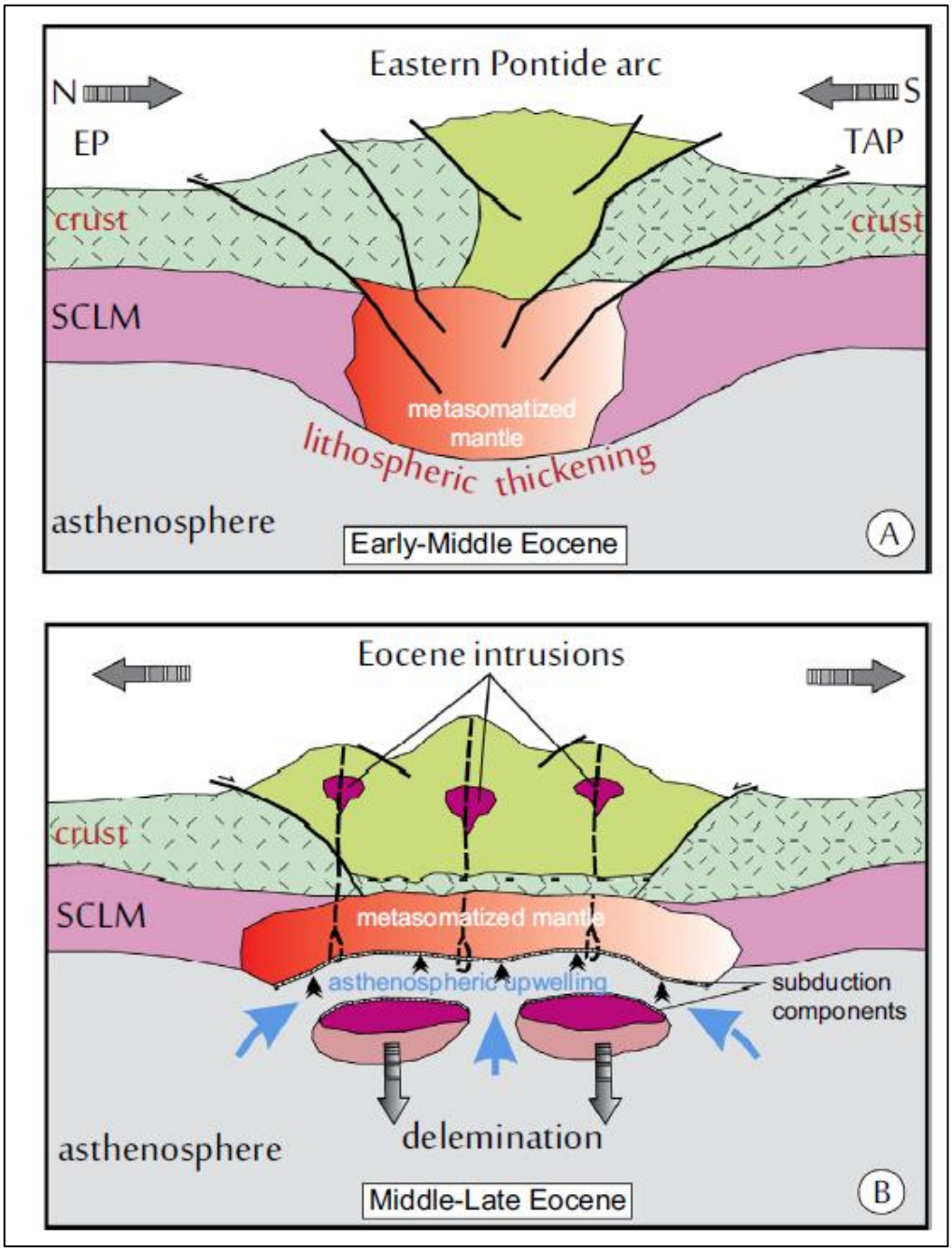


Figure 3-5. Schematic description of Eocene magmatism in Eastern Pontides; Eurasian Plate (EP), Tauride-Anatolide Platform (TAP). A) lithospheric thickening because of continental collision between Eurasia (Pontides) and Tauride-Anatolide Platform B) post-collisional stage (Kaygusuz and Öztürk, 2015).

3.2 Geology of Eastern Pontides

The Eastern Pontide belt can be classified into 4 tectonostratigraphic units including the pre-Jurassic metamorphic basement, Jurassic volcaniclastic rocks, Late Cretaceous arc-related volcano-plutonic rocks, and Eocene collisional/post-collisional magmatic rocks (Yılmaz et al, 1997; Figure 3-6 and Figure 3-7).

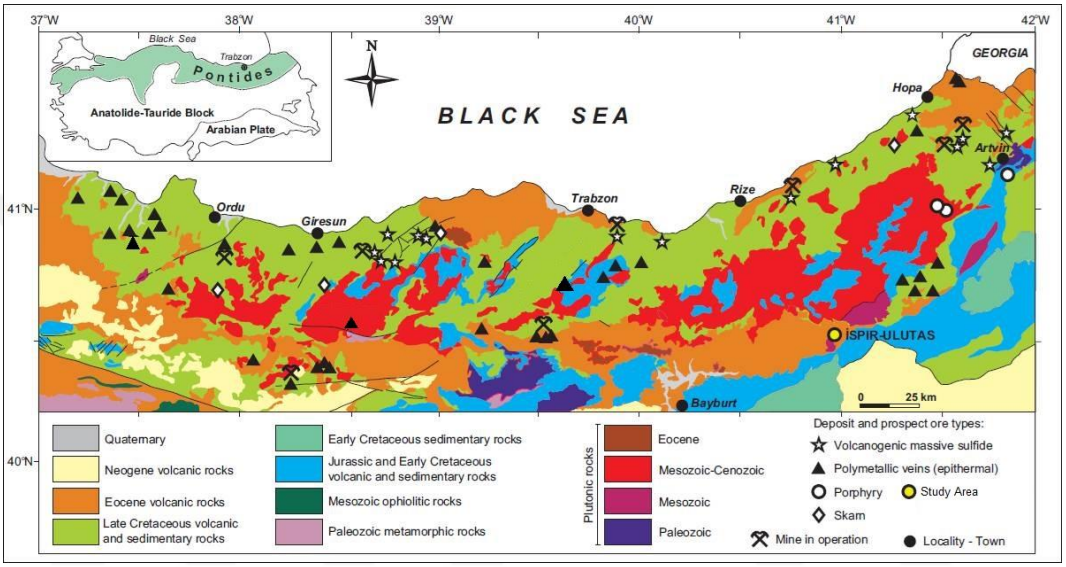


Figure 3-6. Simplified regional geologic map of the Eastern Pontide magmatic belt. Also shown are the locations of the major ore deposits (Delibaş et al., 2019; after MTA, 2002). Inset shows major tectonic units of Anatolia (simplified after Ketin, 1966).

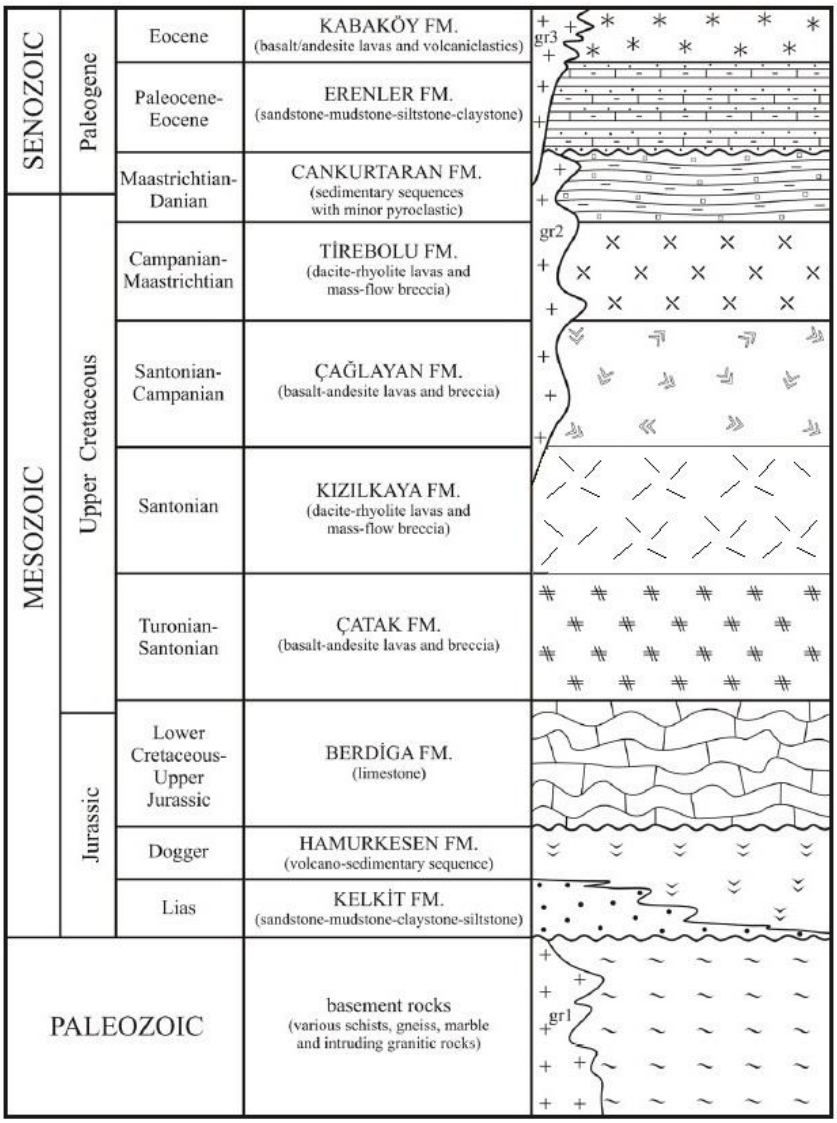


Figure 3-7. Generalized columnar section of the Eastern Pontides (compiled from Güven, 1993; Konak et al., 2001; Kandemir et al., 2019; Revan, 2020)

The pre-Jurassic metamorphic basement consists of Devonian(?) aged high-grade metamorphic rocks, lower Carboniferous granodiorites, dacites, upper Carboniferous-lower Permian sedimentary rocks, and Permo-Triassic metabasite-phyllite-marble units (Okay and Şahintürk, 1997).

Jurassic volcanoclastic rocks unconformably overlie the Pre-Jurassic metamorphic basement. Volcaniclastic rocks consist of basaltic and andesitic lithic tuffs,

volcanogenic sandstone, shale, basaltic and andesitic lavas, and conglomerates (Okay and Şahintürk, 1997).

Late Cretaceous arc-associated volcanic-plutonic rocks were formed in two successive phases; Volcanic and volcanoclastic rocks are called early arc, and intrusive rocks are called late arc. Giles (1974) indicated that Ulutaş Cu-Mo porphyry mineralization formed in relation to Late Cretaceous magmatism.

Eocene collisional/post-collisional volcanic, volcaniclastic rocks and intrusion invaded the Late Cretaceous volcanic-plutonic rocks and pre-Jurassic metamorphic basements (Okay and Şahintürk, 1997).

3.3 Metallogeny of the Eastern Pontides

Eastern Pontides domain comprises on of the richest concentration of metallic ore deposits in the Western Tethyan Metallogenic Belt. The region comprises the most important volcanic-hosted massive sulfide (VHMS) deposits in Turkey and also contains significant epithermal Au-Ag-Pb-Zn and skarn deposits as well as some sub-economic porphyry Cu/Cu-Mo occurrences (Yiğit, 2009; Kuşcu et al., 2019). Almost all of these ore systems are associated with Late Cretaceous to Eocene magmatism (Soylu, 1999; Yiğit, 2009; Kuşcu, 2019; Kuşcu et al., 2019; Rabayrol et al., 2022).

3.3.1 Epithermal Deposits

Syn- to post-collisional Eocene magmatism was key for development of epithermal-style mineralization in the Eastern Pontides, mainly in the Southern Zone (Yiğit, 2009; Figure 3-8). Host rocks are commonly andesitic to dacitic volcanic and volcanosedimentary lithologies (Tüysüz et al., 1995; Oyman, 2019; Rabayrol et al., 2022). There is limited epithermal-type mineralization that has been recognized in

Late Cretaceous-Paleocene volcanic rock which is related to arc-type magmatism during the Late Mesozoic to Early Cenozoic (Oyman, 2019).

Most common mineralization types include intermediate-sulfidation (IS) epithermal mineralization, whereas high- (HS) and low-sulfidation (LS) epithermal deposits are less common and are generally associated with Late Cretaceous arc-related andesitic volcanic and volcanosedimentary rocks (Bilir, 2015; Rabayrol et al., 2022).

According to Oyman (2019), Bilir (2015), and Yiğit (2009), several epithermal deposits and prospects in the Eastern Pontides are listed below:

- Related with Eocene magmatism: Mastra (IS type (?)), Hasandağ (HS type), Arzular (LS type), etc.
- Related with Late Cretaceous Magmatism: Taç (IS type), Çorak (IS type), Altıntepe (LS type), etc.

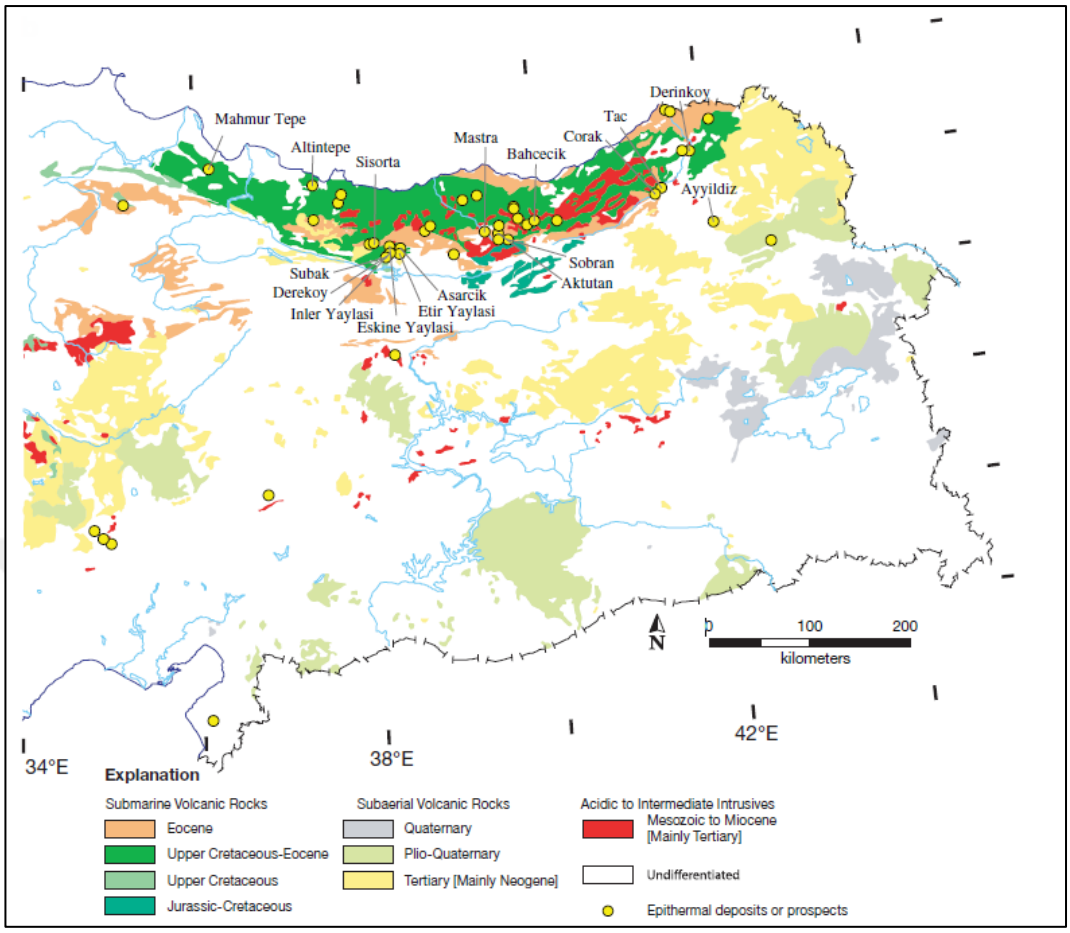


Figure 3-8. Distribution of epithermal-type deposits and prospects in Eastern Pontides (Yiğit, 2009)

3.3.2 Volcanic-hosted Massive Sulfide (VHMS) Deposits

VHMS deposits of Eastern Pontides are mainly classified as typical Kuroko-type deposits (Yiğit, 2009; Çiftçi, 2019, Revan, 2020). In a few of these systems (e.g., Cerattepe), there is also evidence of late silicification and clay alteration overprint alongside gold introduction, suggesting presence of hybrid Kuroko and high-sulfidation epithermal mineralization (Uçurum et al., 2021). The Eastern Pontide VHMS deposits, which are important producers of Cu, Pb, and Zn, are associated with Late Cretaceous felsic volcanic rocks of the Northern Zone, including dacitic and rhyolitic lavas of the Kızılkaya Formation (Revan, 2020; Figure 3-9).

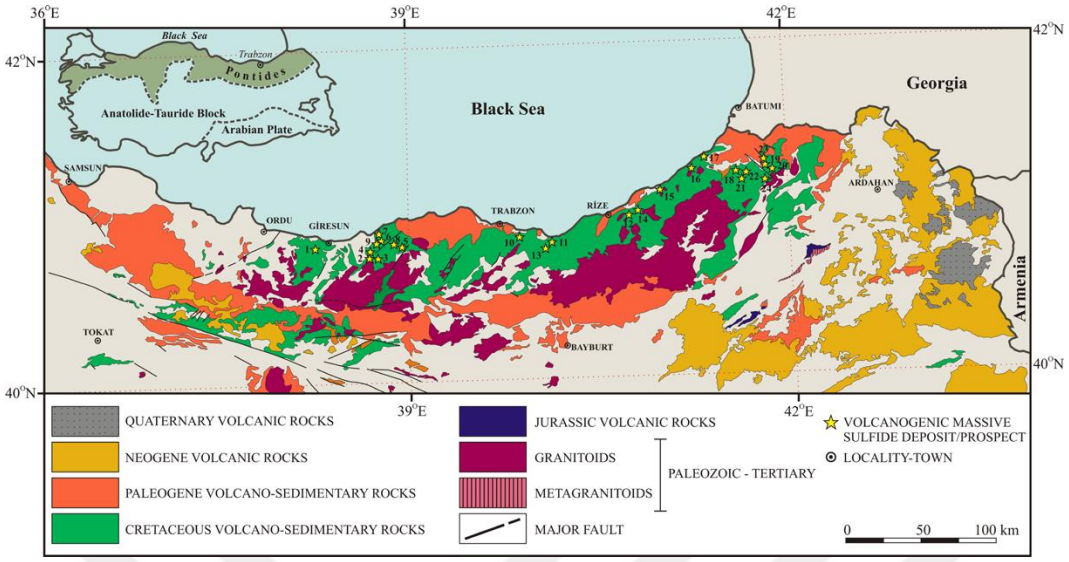


Figure 3-9. Distribution of the VHMS deposits/prospects of Eastern Pontides (Revan, 2020).

According to Revan (2020), VHMS systems of Eastern Pontides were likely formed in an extensional tectonic regime during the northward subduction of the Northern Neotethys oceanic lithosphere in the Late Cretaceous by considering the trace element geochemical signatures of the host rocks. The age determinations also indicate that VHMS deposits in this region have a restricted formation time between 91.1 and 82 Ma (Revan, 2020; Table 3-1).

Table 3-1. Radiometric age of main VHMS deposits in the Eastern Pontides (Revan, 2020).

No.	Location	Rock type	Method	Dating minerals	Age (Ma)	Reference
1	Murgul mine	Sulfide ore from massive ore	Pb-Pb	Galena	89.0	Çiftçi (2004)
2	Lahanos mine	Sulfide ore from massive ore	Pb-Pb	Galena	89.0	[2]
3	Köprübaşı mine	Sulfide ore from massive ore	Pb-Pb	Galena	89.0	[2]
5	Çayeli southeast	Dacite -Tirebolu Fm	$^{40}Ar/^{39}Ar$	Dacite groundmass	83.2 ± 1.0	Alan et al. (2019)
4	Murgul south	Dacite – Kızılkaya Fm	$^{40}Ar/^{39}Ar$	Dacite groundmass	88.8 ± 0.9	Kandemir et al. (2019)
6	Tunca prospect	Dacite - Kızılkaya Fm	K-Ar	Sericite	82.0 ± 1.8	JICA (2005)
7	Tunca prospect	Dacite - Kızılkaya Fm	K-Ar	Sericite	83.1 ± 2.1	[2]
8	Tunca prospect	Dacite - Kızılkaya Fm	U-Pb (LA-ICP-MS)	Zircon	88.1 ± 1.2	Revan et al. (2017)
9	İsraildere prospect	Dacite/Rhyolite -Kızılkaya Fm	U-Pb (SHRIMP)	Zircon	91.1 ± 1.3	Eyuboglu et al. (2014)
10	Köprübaşı mine	Dacite/Rhyolite -Tirebolu Fm	U-Pb (SHRIMP)	Zircon	82.6 ± 1.0	[2]
11	Köprübaşı mine	Dacite/Rhyolite-Tirebolu Fm	U-Pb (SHRIMP)	Zircon	86.6 ± 0.8	[2]
12	Çanakçı prospect	Quartz porphyry – Kızılkaya Fm	U-Pb (SHRIMP)	Zircon	88.6 ± 1.4	Aydın et al. (2016)
13	Çanakçı prospect	Dacite/Rhyolite – Kızılkaya Fm	U-Pb (SHRIMP)	Zircon	85.0 ± 1.2	[2]
14	Artvin	Rhyolite – Kızılkaya Fm	U-Pb (SHRIMP)	Zircon	86.5 ± 0.7	[2]

3.3.3 Porphyry Cu-Mo Deposits

Porphyry Cu-Mo deposits in the Eastern Pontide magmatic belt are associated with the Late Cretaceous arc to Eocene syn- to post-collisional magmatism (Soylu, 1999, Yiğit, 2009; Kuşcu et al., 2019; Figure 3-10). Host rocks are typical I-type, calc-alkaline granodioritic, monzonitic, and granitic intrusives (Soylu, 1999; Yiğit, 2009; Kuşcu et al., 2019). However, Delibaş et al. (2019) demonstrate that porphyry Cu-Mo ore formation in Eastern Pontides commenced much earlier, in the Early Cretaceous (Figure 3-11), which is based on a Re-Os molybdenite age of 131.0 ± 0.7 Ma from the İspir porphyry Cu-Mo system.

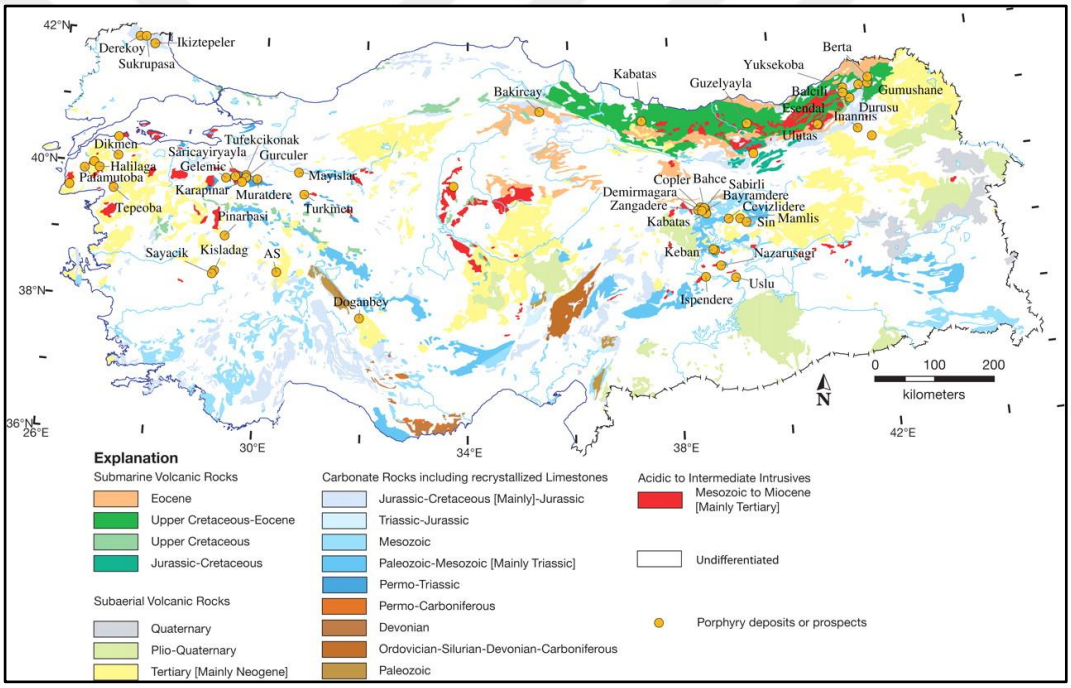


Figure 3-10. Distribution of the porphyry deposits and prospects of Turkey (Yiğit, 2009)

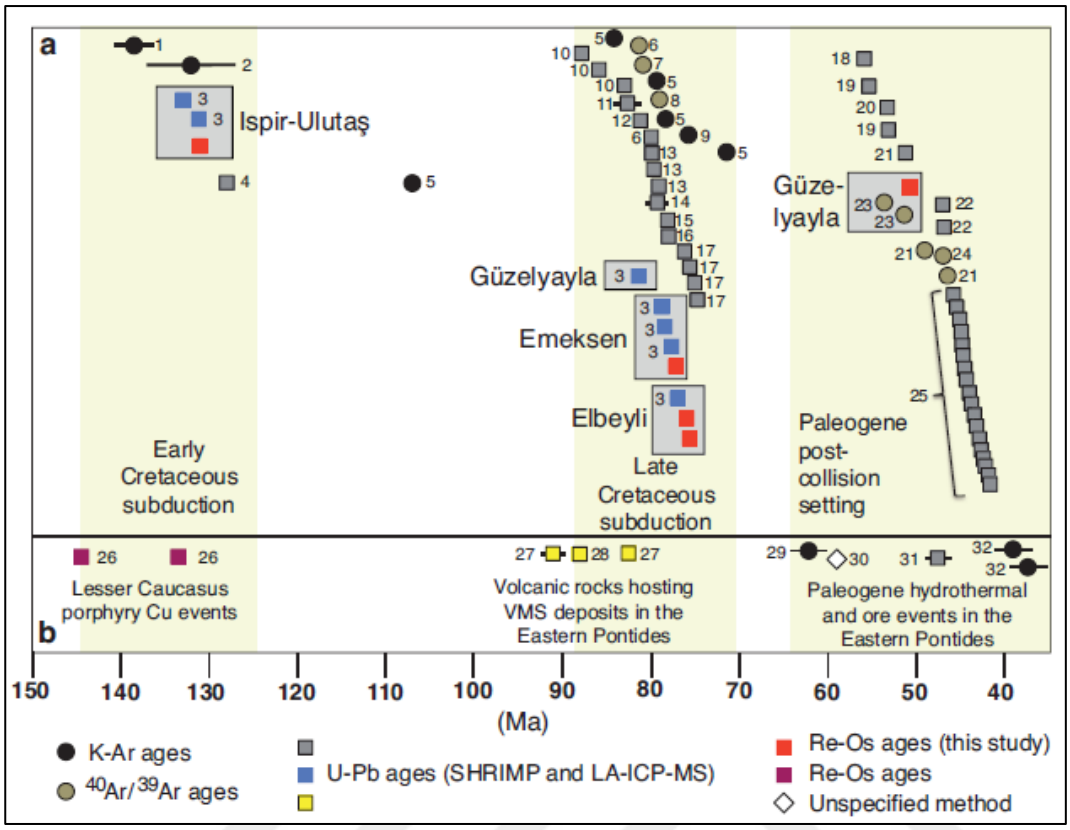


Figure 3-11. Radiometric ages of porphyry Cu-Mo mineralization and ore-forming events in Eastern Pontides (Delibaş et.al, 2019)

Some of the porphyry Cu-Mo deposit examples are listed below:

- Güzelyayla Cu-Mo Porphyry in Trabzon, 186.2 Mt @ 0.3% Cu_{eq} (Yiğit, 2009)
- Balcılı Cu-Mo Porphyry in Artvin, 145 Mt @ 0.25% Cu_{eq} (Soylu, 1999)
- Ulutaş Cu-Mo Poprhyry in Erzurum, 73.6 Mt @ 0.31% Cu + 0.022% Mo (Giles, 1974)
- Gümüşhane (Ardala) Cu-Au-Mo Porphyry in Artvin, 30 Mt @ 0.3 g/t Au, 0.3 %Cu (Yiğit, 2009).

3.3.4 Skarn Deposits

Skarn deposits within the Eastern Pontides are associated with the Late Cretaceous or Eocene intrusive rocks that intruded the Jurassic-Cretaceous calcic-carbonate rocks or Late Cretaceous volcanic-volcanoclastic rocks (Kuşcu, 2019). Major types of skarn mineralization are Fe skarns, but Fe-Cu and Cu skarns are occasionally observed, without any significant Zn-Pb credits (Yiğit, 2009; Kuşcu, 2019). In general, Fe, Fe-Cu, and Cu skarns are typical calcic skarns (Kuşcu, 2019).

The main skarn-producing event in the Eastern Pontides is related to the geo-evolution of Neotethys in the Late Cretaceous. The northward subduction in the Late Cretaceous of oceanic crust at colliding plate boundaries resulted in the formation of a series of magmatic arcs in Eastern Pontide. This collision results in the formation of significant skarn and porphyry mineralization at the Eastern Pontide (Kuşcu, 2019).

The known skarn deposits in Eastern Pontides are listed below (Figure 3-12):

- Fe Skarns: Kartiba (Rize), Akkaya (Rize), Kotana (Giresun), Catak (Giresun), Kurtulmus (Giresun), Karabork, Arnastal, Camibogazi, (Gumushane), and Cambasi-Fundacik (Ordu) (Kuşcu, 2019)
- Fe-Cu Skarns: Armutlu, Deregözü (Görele, Giresun), Özdil, Tuzlak mezra (Araklı, Trabzon), Dağbaşı, Köprübaşı, Gezge, Ayman (Araklı, Trabzon), Kıranmaden (Kürtün), Egrikar (Torul) (Kuşcu, 2019).

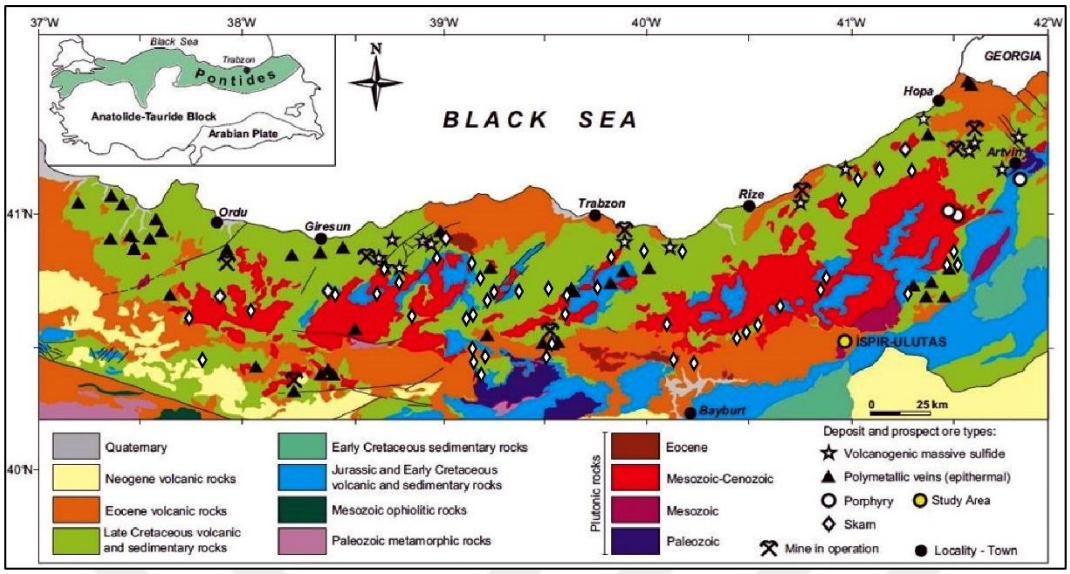


Figure 3-12. Distribution of the skarn deposits and prospects of Eastern Pontide (modified from Delibaş et al., 2019; after MTA, 2002 and Kuşcu, 2019).

CHAPTER 4

GEOLOGY OF ULUTAŞ SKARN CU-ZN DEPOSIT

The Ulutaş Deposit is located in the İspir District, along the northern limits of the Erzurum Province. This area is a part of the vast Pontide mountain range that borders the northern margin of the Anatolian plateau. Ulutaş Cu-Zn skarn deposit is located at coordinates of 40°53'31.53"E and 40°34'22.33"N (Figure 1-1). Ulutaş area is characterized by steep mountainous topography with an elevation ranging between 2,000 m to 2,600 m above sea level.

Ulutaş Cu-Zn skarn and the nearby İspir Cu-Mo porphyry systems are located in the southeastern part of the Eastern Pontides, which predominantly consists of Mesozoic plutonic rocks and Eocene volcanics (Figure 3-6). The main lithological units of the Ulutaş area are Jurassic–Eocene volcanic and sedimentary rock assemblages and their associated intrusions. These collectively cut and overlie a basement sequence of Paleozoic metamorphic rocks (Figure 4-1).

In the study area, both Cu-Zn skarn and porphyry Cu-Mo mineralizations occur within 2 km of each other (Figure 4-2). The main skarn zone (named Skarn I) that this study focuses on was formed as a result of metasomatic alteration and replacement of calcareous country rocks at the intrusion contacts. Both prograde calc-silicate assemblages comprising grossular garnet, diopsidic pyroxene, and wollastonite, and later retrograde phases of epidote-chlorite-sericite-actinolite/tremolite-carbonate-hematite/specularite occur in this skarn mineralized zone. Outcrops showing metasomatic alteration are scarce (Figure 4-3) due to widespread cover of the Pleistocene glacial till. Immediately to the north of this skarn body, another skarn zone (named Skarn II) that is much smaller than to the Skarn I mineralization is also present.

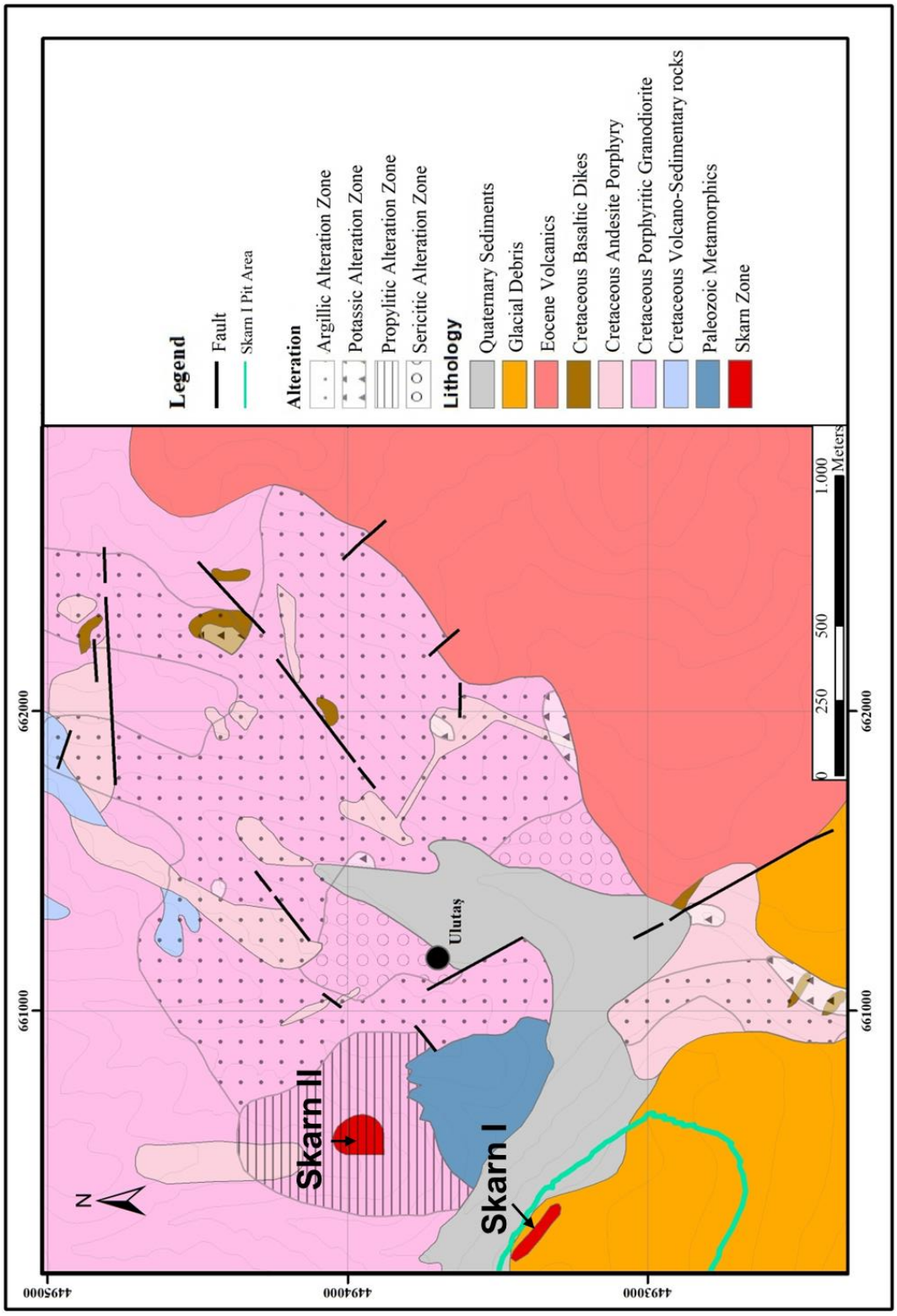


Figure 4-1. Geological map of the study area showing the major lithological units (modified from Giles, 1973; Revan et al., 2017; Delibaş et al., 2019).



Figure 4-2. General views of the Ulutaş-İspir district. a) View of skarn mineralization from the İspir porphyry zone, looking southwest. Porphyry-altered exposures in the foreground show quartz-white mica alteration, b) View of Skarn II orebody from Skarn I zone (looking north). Porphyry domain is also visible in the background, to the northeast.



Figure 4-3. Discovery outcrop of the Ulutaş Zn-Cu deposit showing oxidized skarn assemblages (660211 E, 4493331 N, 2.302 m a.s.l., UTM Zone 37).

4.1 Lithological Units

The study area consists of a pre-Jurassic metamorphic basement that has been cross-cut and overlain by volcanic, volcano-sedimentary, and plutonic rocks of Jurassic to Eocene age (Figure 4-1). The metamorphic basement mainly comprises a sequence of alternating schist, gneiss, amphibolite with lenses of marble. The coarse-grained phaneritic and porphyritic, granitic to granodioritic intrusive rocks of the İspir batholithic complex have been mainly emplaced into these units. Pleistocene glacial till overlies much of the southern part of the study area (Figure 4-1).

4.1.1 Pre-Jurassic Metamorphic Basement

The oldest rocks in the study area are pre-Jurassic metamorphics, which constitute a sequence of schist, and augen gneiss with intercalating amphibolite and marble lenses (Giles, 1974). Schist, and gneiss units have commonly been intersected during drilling (Figure 4-4 and Figure 4-6). Marble lenses, which are a part of the pre-Jurassic basement, are the predominant host lithologies of the Ulutaş Cu-Zn skarn, localizing much of the replacement-type mineralization. According to Giles (1974), this metamorphic sequence belongs to the albite-epidote-amphibolite facies.

Gneiss is readily identified in the drill core by alternating dark-colored bands mainly consisting of biotite and light-colored bands of silicate minerals represented mainly by quartz, K-feldspar, and lesser plagioclase (Figure 4-5). In the least-altered drill core intervals, this unit shows weak chlorite-sericite alteration, and is cut by thin carbonate veinlets. Schist units within the mineralized system are generally more strongly altered, and main metamorphic minerals have been partially to completely replaced by alteration minerals. Where preserved, schist units have a mineral assemblage of biotite (partly chloritized) and quartz with secondary carbonates (Figure 4-7).

Marble crops out at the surface in the central part of the study area and have been intersected in drilling extensively (Figure 4-8). Lensoid- to irregularly-shaped coarse-grained, laminated to massive, crystalline marble blocks occur within enveloping schist and gneiss. These marble lenses vary in thickness from ~1 m to a maximum of up to 25 meters.

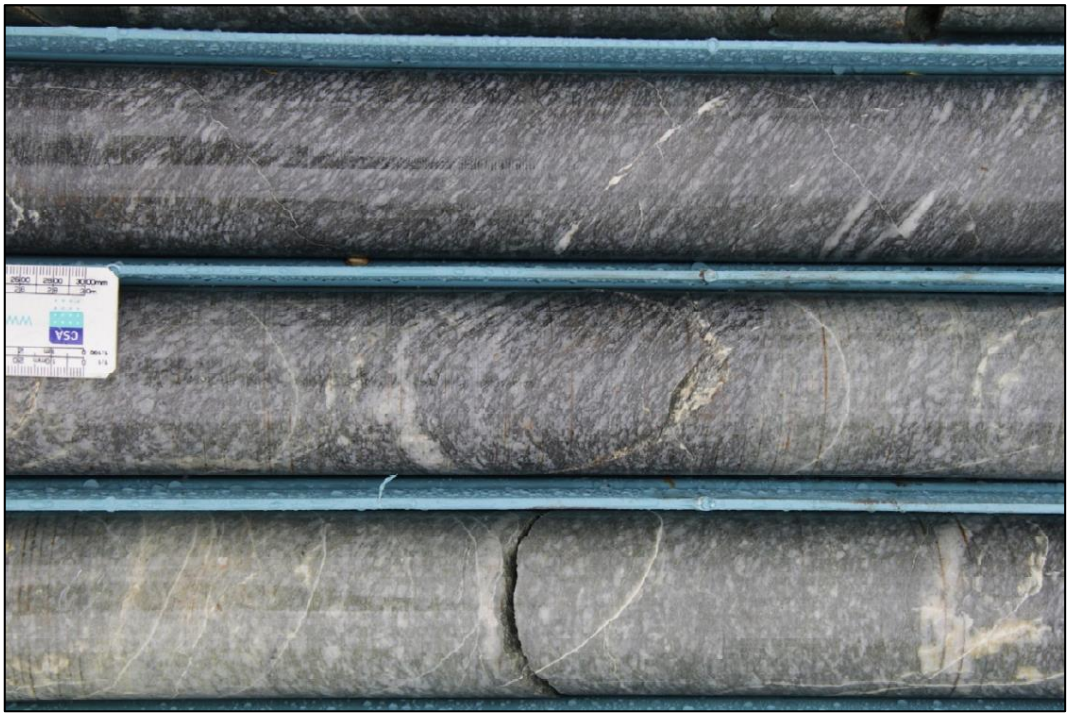


Figure 4-4. Gneiss with strong metamorphic fabric in the study area (drill hole EU-027, 108.50 m).

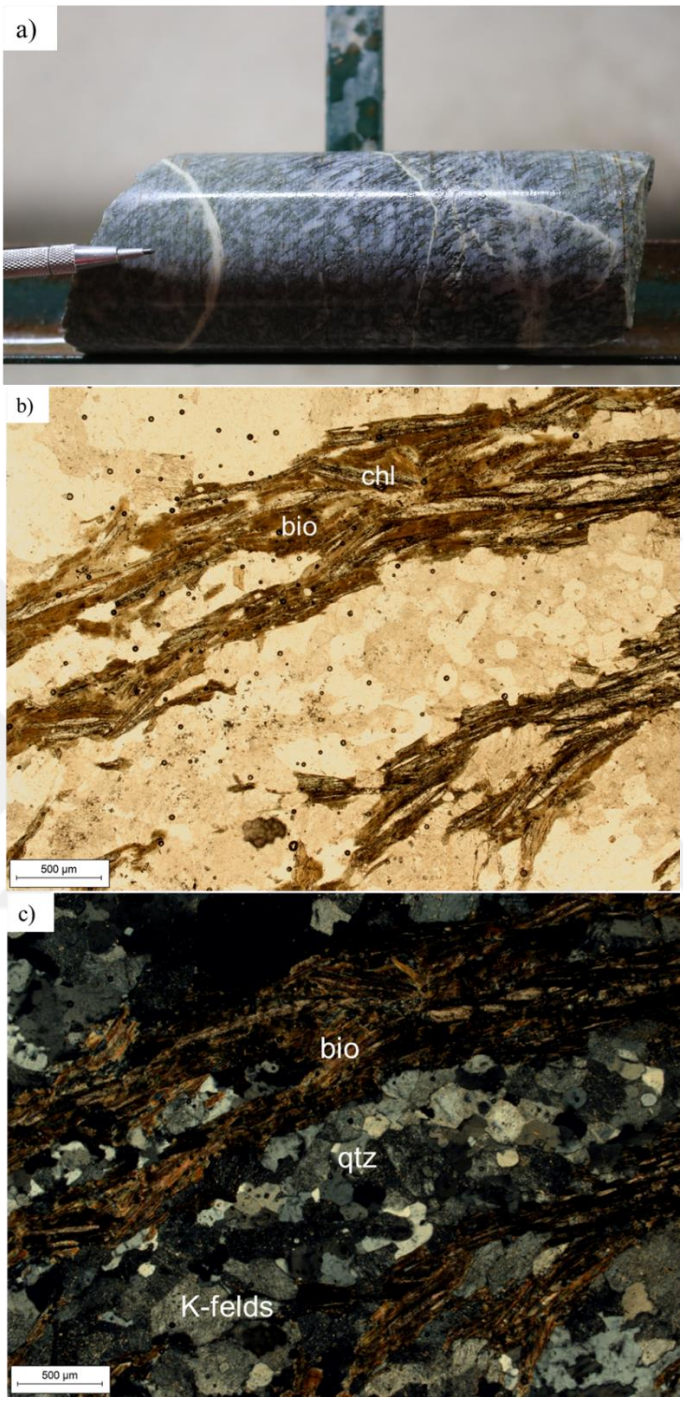


Figure 4-5. Hand specimen and microphotographs of gneiss sample a) drill core photograph of gneiss (drill hole EU-038, 108.40 m), b) microphotograph (PPL, TL image) of chlorite altered gneiss (drill hole EU-038, 108.40 m), c) microphotograph (XPL, TL image) of chlorite altered, light colored silicate banded and dark colored biotite banded gneiss (drill hole EU-038, 108.40 m). Abbreviations: K-felds = K-

feldspar, bio = biotite, qtz = quartz, chl = chlorite, TL = transmitted light, XPL= cross-polarized light, PPL = plane-polarized light.

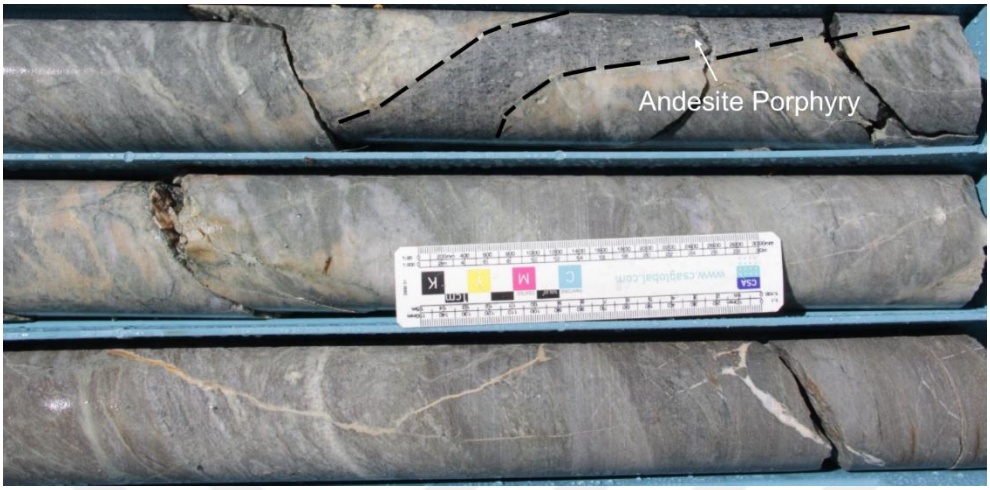


Figure 4-6. Schist unit with strong foliation intersected by quartz-feldspar porphyry in the study area (drill hole EU-046, 153.60 m.).

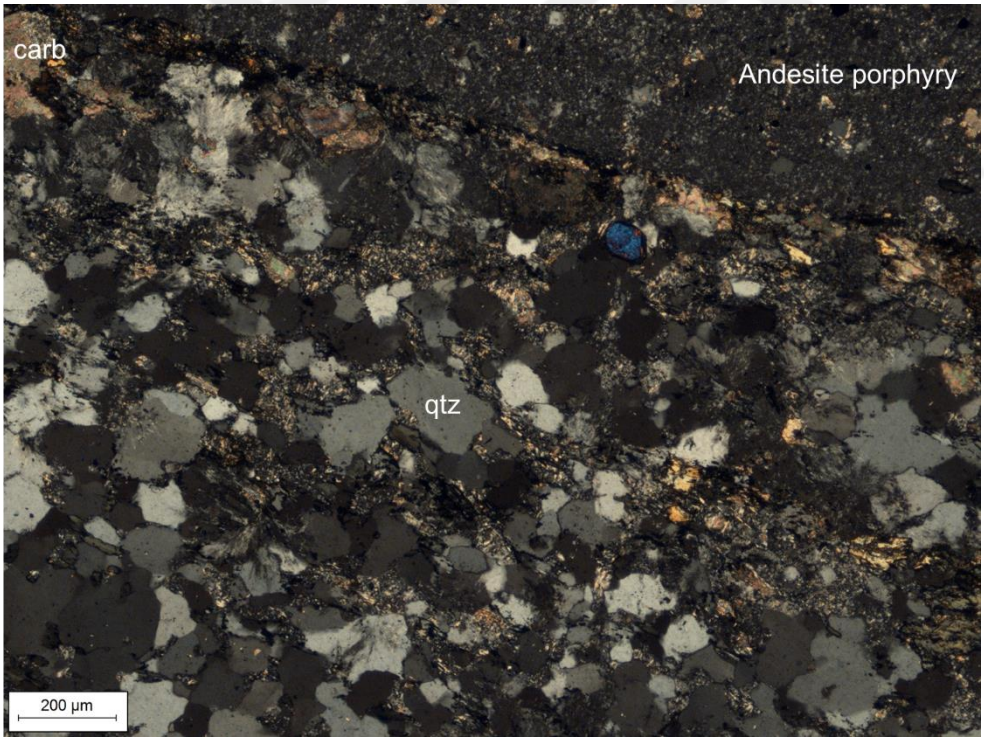


Figure 4-7. Microphotograph (XPL, TL image) of carbonate altered schist and andesite poprhyry contact (drill hole EU-046, 90.80 m). Abbreviations: qtz = quartz, carb = carbonate, TL = transmitted light, XPL= cross-polarized light.

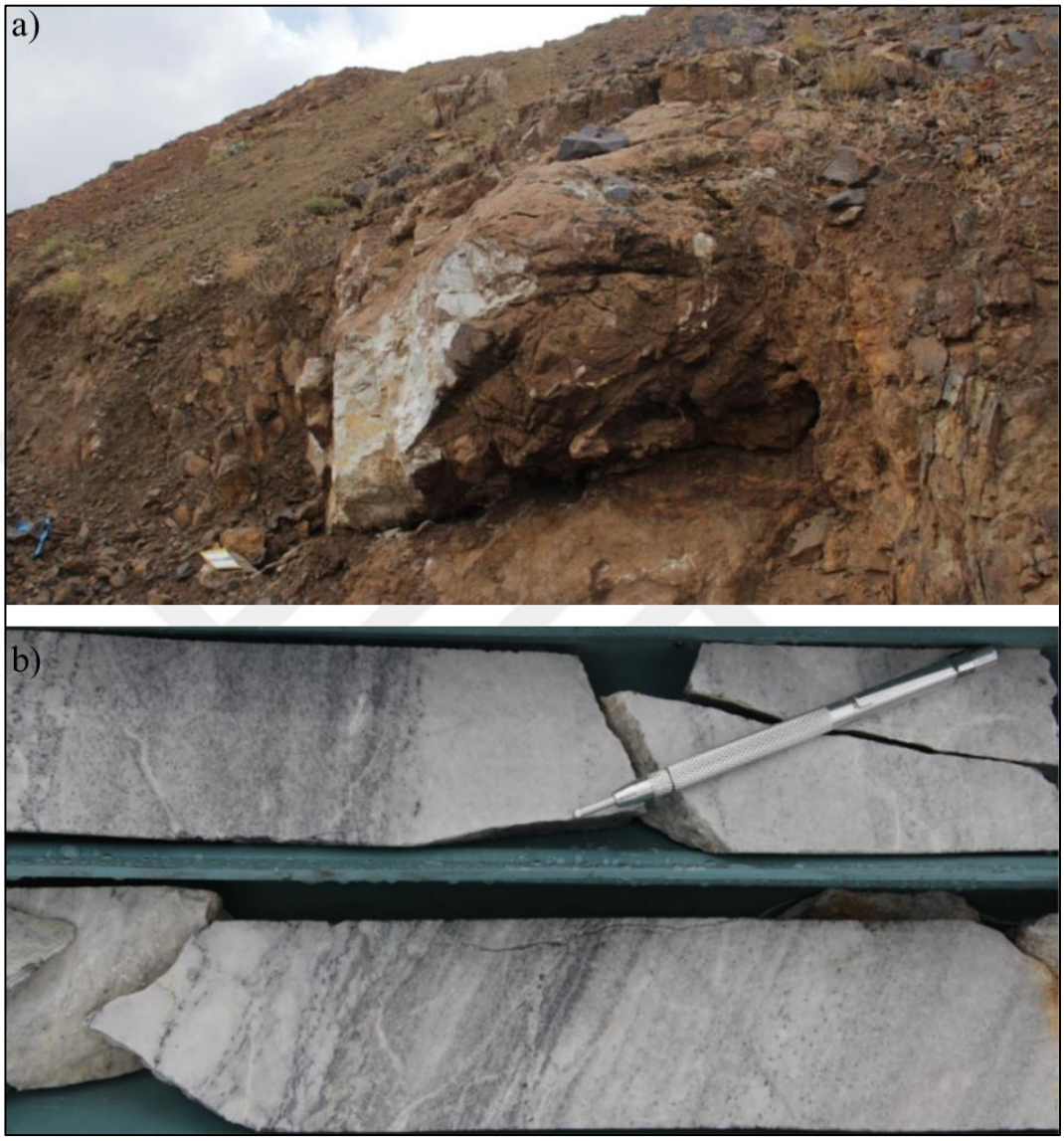


Figure 4-8. Field and drill core views of marble lenses that are part of the Pre-Jurassic metamorphic sequence in the study area. a) A marble lens exposed in the central part of the study area (660610 E, 4494009 N, 2.333 m a.s.l., UTM Zone 37), b) drill core interval of laminated marble (drill hole EU-071, 151.00 m).

4.1.2 Cretaceous Volcanics and Igneous Rocks

4.1.2.1 Lower Volcanic-Sedimentary Sequence

The lower volcanic-sedimentary sequence consists of dacitic to rhyolitic flows and pyroclastics with intercalated laminated mudstone, silty shale, and intraformational conglomerates (Giles,1974; Figure 4-9). The stratigraphic position of the sequence is not well constrained as its lower contact could not be observed in the outcrop and also in drill holes. This unit has been encountered as in contact with Cretaceous porphyritic rhyolite, which is also known as Ulutaş Stock in the north of the study area (Giles, 1974; Figure 4-1).



Figure 4-9. Lower Volcanic-Sedimentary Sequence in the study area. a) rhyolitic lapilli tuff (661218 E, 4494552 E, 2374 m a.s.l., UTM Zone 37) b) coarsely pebbly sandstone/conglomerate (661485 E, 4495767 N, 2658 m a.s.l., UTM Zone 37).

4.1.2.2 Cretaceous Granodiorite Porphyry

The pre-Jurassic metamorphic sequence has been extensively cross-cut by a multi-phase, intermediate composition intrusive suite. This suite is predominantly made up of equigranular granodiorite and porphyritic granodiorite, collectively named as the İspir batholith (Taylor and Fryer, 1980; Giles, 1974; Figure 4-10). The İspir batholith is defined as a composite stock made up of medium-grained equigranular biotite-hornblende granodiorite and biotite-feldspar granodiorite porphyry (Giles, 1974, Figure 4-11 and Figure 4-12). Early K-Ar radiometric dating of biotite from the granodiorite yielded an age of 132 ± 5 Ma (Giles, 1974). Later, Delibaş et al. (2016) dated the same unit through LA-ICP-MS U-Pb zircon geochronology and obtained an age of 132.9 ± 0.9 Ma. This latter age correlates well with the age data of Giles (1974) but is considered to be more accurate.



Figure 4-10. Outcrop view of equigranular granodiorite (660621 E, 4493406 N, 2119 m a.sl., UTM Zone 37).

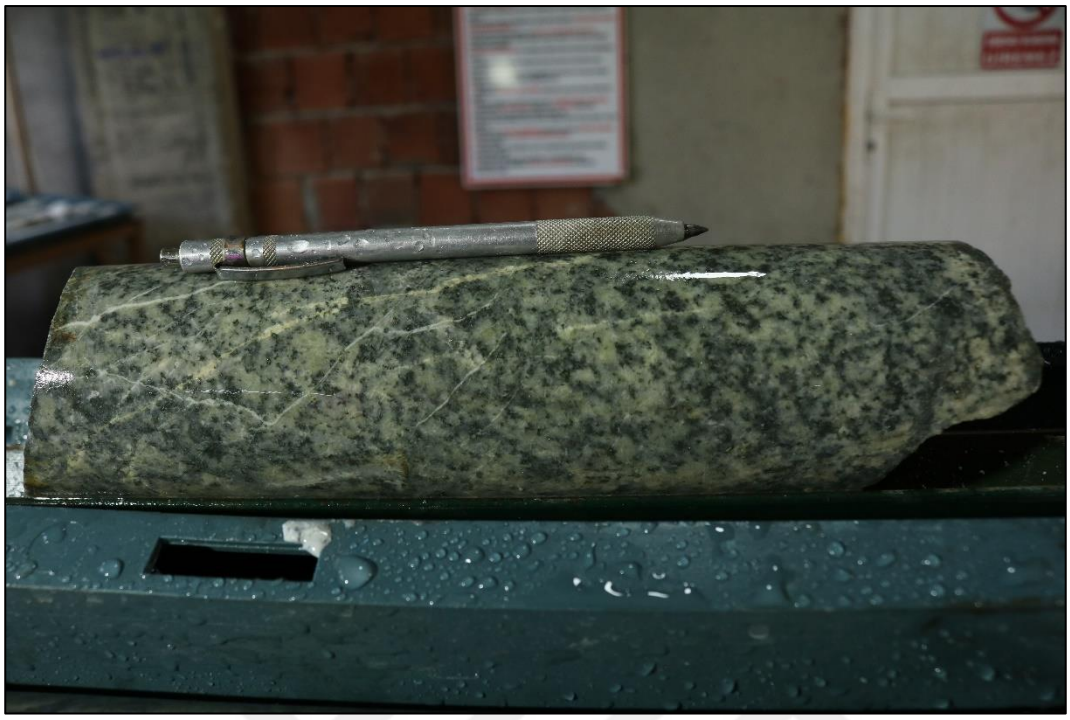


Figure 4-11. Drill core sample of Early Cretaceous granodiorite in Ulutaş porphyry mineralization area (drill hole EU-309, 222.50 m).

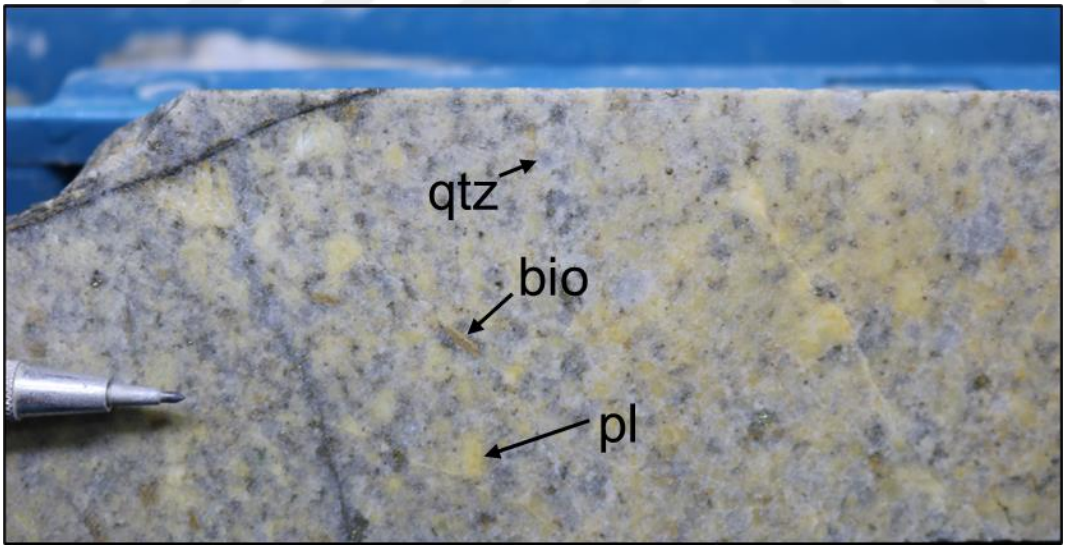


Figure 4-12. Drill core sample of altered porphyritic granodiorite with biotite, quartz, and feldspar phenocrysts from Ulutaş porphyry prospect (drill hole EU-009, 271.4 m.). Abbreviations: qtz = quartz, pl = plagioclase, bio = biotite.

4.1.2.3 Andesite Porphyry (Cretaceous)

The principal mineralized unit at Ulutaş is a Cretaceous porphyritic andesite, which is termed as the Ulutaş Stock. This unit is elongated in north-northeast direction in the study area and covers a surface area of approximately 2 km x 5 km (Giles, 1974; Figure 4-13). The stock is overlain by post-intrusive Eocene volcanic rocks in the east of the study area.

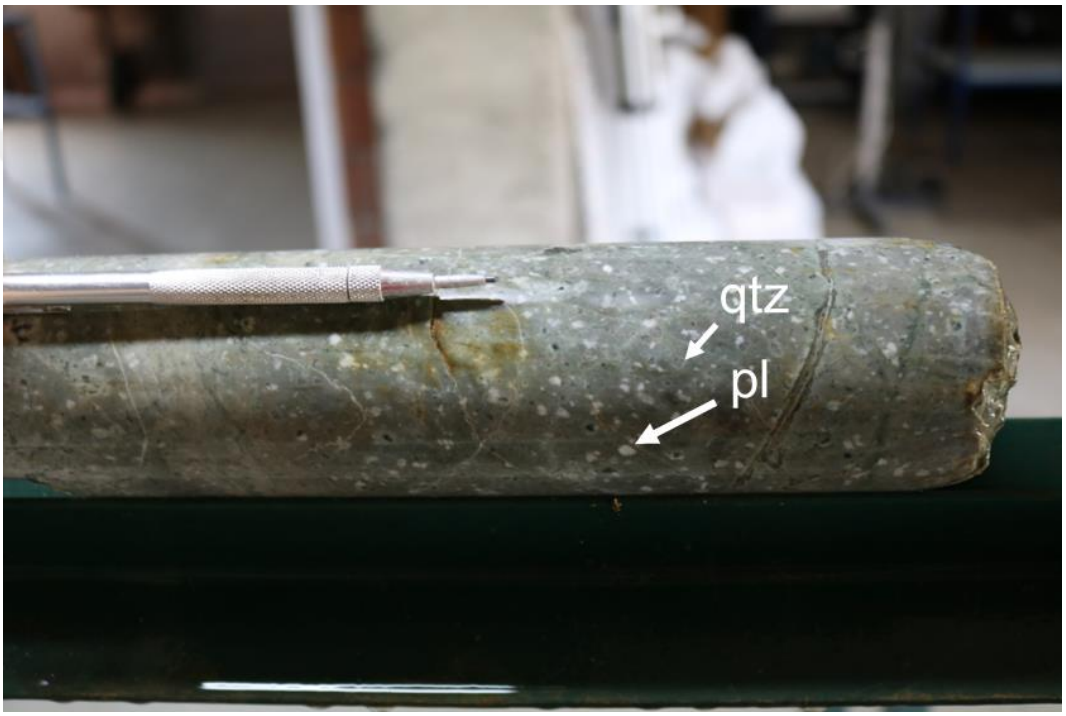


Figure 4-13. Andesite porphyry in the study area (drill hole EU-094, 181.30 m). Abbreviations: qtz = quartz, pl = plagioclase.

Due to extensive hydrothermal alteration, this unit was initially identified as "quartz-feldspar porphyry" by Demir Export geologists. Delibaş et al. (2016) reported an LA-ICP-MS U-Pb zircon age of 131.1 ± 0.9 Ma from this unit.

Petrographic analysis of the quartz-feldspar porphyry shows that it is a groundmass-dominated porphyritic rock, which distinguishes this unit from granodiorite porphyry. Main phenocryst phases are plagioclase and quartz that are generally up to 1.5 mm-long (Figure 4-14). Plagioclase commonly shows polysynthetic twinning,

whereas quartz is generally resorbed as evidenced by its embayed texture (Figure 4-14). Surrounding groundmass is also composed of fine-grained quartz and plagioclase (Figure 4-14). Although ferromagnesian minerals have been completely altered, previous presence of hornblende is suspected as some altered phenocrysts have rhombohedral forms.

The least-altered samples of quartz-feldspar porphyry show weak sericite-chlorite-carbonate alteration (Figure 4-15). This resulted in partial replacement of plagioclase by sericite and late carbonate, whereas mafic phases have been strongly altered into chlorite, sericite, and Fe-Ti oxides. Quartz-feldspar porphyry is also commonly cross-cut by thin carbonate veinlets.

Lithogeochemical data of drill hole intercepts, where this unit is intersected, is used to determine rock compositions. Due to the lack of SiO_2 data within the assays, classification diagram of Pearce (1996) was used. This diagram utilizes immobile elements including Nb, Y, Zr, and Ti (Figure 4-16). Most of the data plotted within the sub-alkaline andesite/basaltic andesite field (Figure 4-16). This, combined with petrographic observations, the quartz-feldspar unit is tentatively identified as andesite porphyry.

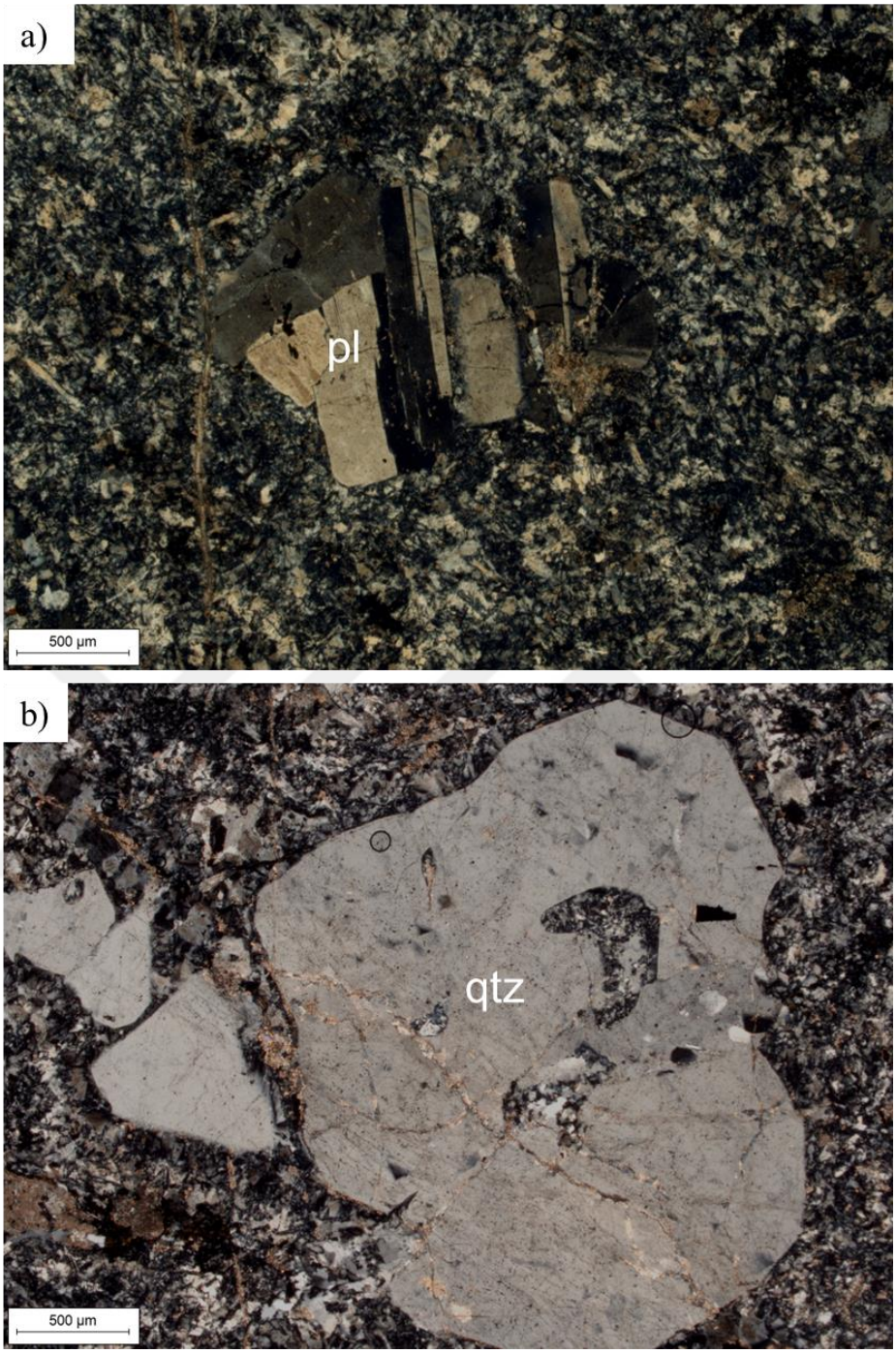


Figure 4-14. a) Microphotograph (XPL, TL image) showing a relatively fresh, twinned plagioclase surrounded by fine-grained groundmass (drill hole EU-094, 181.70 m), b) microphotograph (XPL, TL image) of coarse grained quartz cross cut by carbonate vein (drill hole EU-094, 171.70 m). Abbreviations: pl=plagioclase, qtz=quartz, TL=transmitted light, XPL=cross polarized light, PPL= plane polarized light

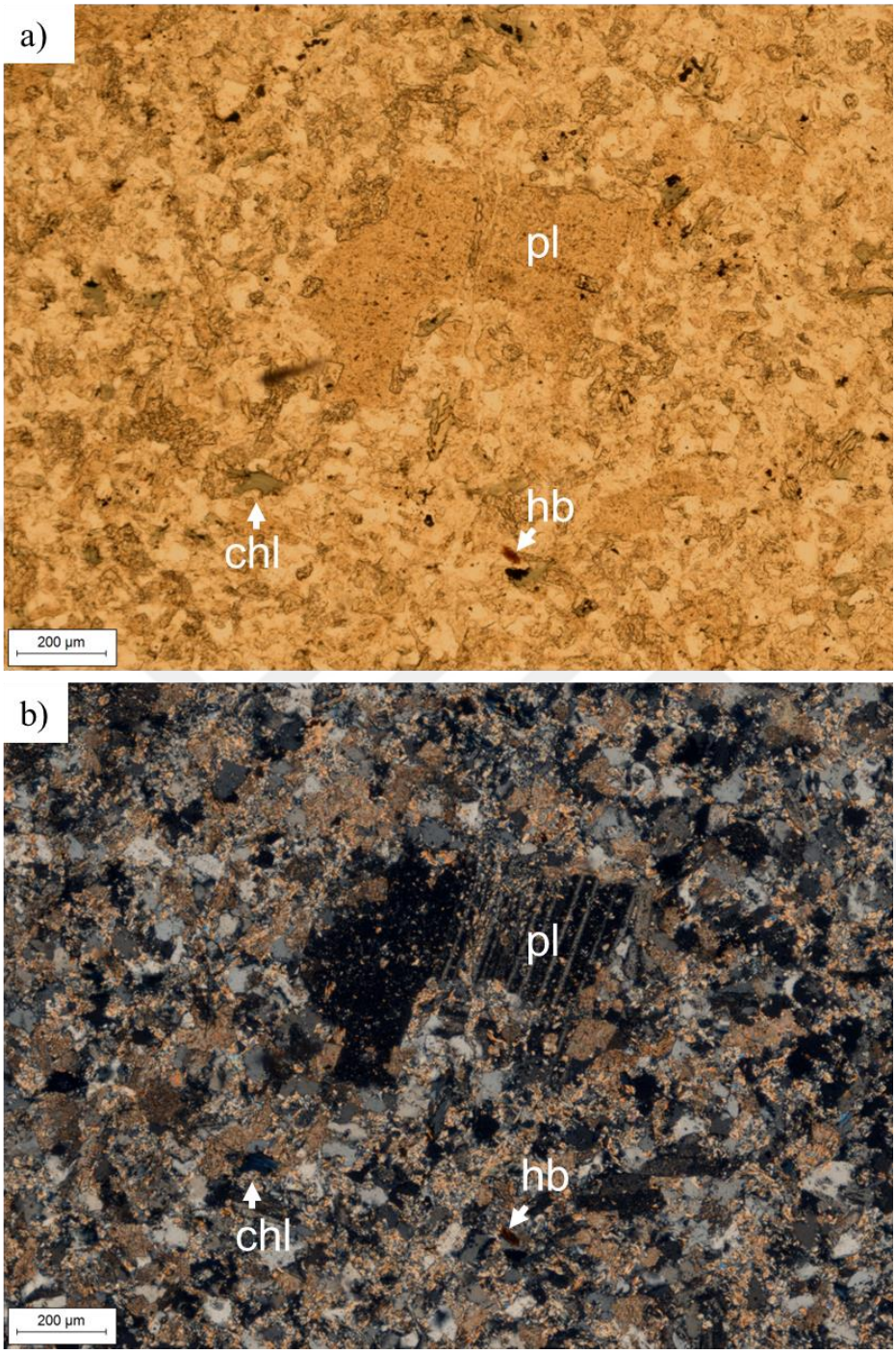


Figure 4-15. a) Microphotograph (PPL, TL image) sericitized and K-feldspar altered plagioclase with chloritized hornblende (drill hole EU-094, 160.70 m), b) Microphotograph (XPL, TL image) sericitized and K-feldspar altered plagioclase with chlorite and hornblende (drill hole EU-094, 160.70 m). Abbreviations: pl=plagioclase, chl=chlorite, hb= hornblende TL=transmitted light, XPL=cross polarized light, PPL= plane polarized light.

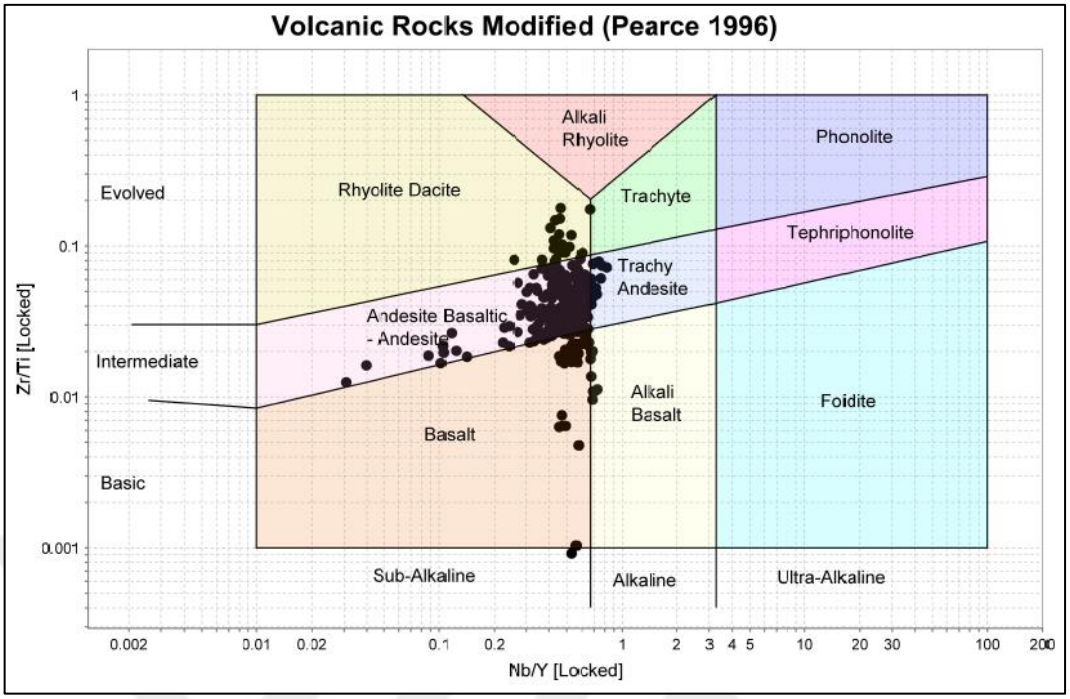


Figure 4-16. Zr/Ti vs. Nb/Y diagram plot (Pearce, 1996) of andesite porphyry unit as based on drill hole assays of the Ulutaş Cu-Zn skarn (lithogeochemical data courtesy of Demir Export).

4.1.2.4 Basaltic Dikes (Cretaceous)

Basement lithologies as well as granodiorite and andesite porphyry intrusions are cross-cut by dikes that are up 3 meters thick. Contacts between these dikes and the units they are quite sharp. Dikes are fine-grained, aphanitic and porphyritic and are greenish in color in hand specimen due to intense chloritic alteration (Figure 4-17).



Figure 4-17. Drill core sample of a basaltic dike from the study area (drill hole EU-094, 179.70 m)

Petrographic analysis of dike samples indicated that the samples are predominantly fine-grained porphyritic in texture. Due to strong alteration, primary mineralogy is largely obscured. Laths of plagioclase are still discernable, although these have been largely replaced by sericite and carbonate (Figure 4-22). Mafic phenocrysts are readily visible in hand specimen (Figure 4-22), but intense chlorite replacement precluded their accurate identification. These were tentatively identified as pyroxene based on their crystal forms. Abundant fine-grained groundmass of dikes are likely rich in plagioclase and particularly in mafic minerals given its dark green color imparted by chloritic alteration.

Pyrite is also a common replacement mineral in basaltic dikes likely formed after Fe-rich mafic minerals such as amphibole or pyroxene. Pyrite occurs as coarse-grained aggregates and displays euhedral cubic crystal forms (Figure 4-22). Late-stage carbonate is present along thin veinlets.

On the Nb/Y vs. Zr/Ti diagram of Pearce (1996) dike samples plot within the sub-alkaline basalt field (Figure 4-18) confirming their mafic (basaltic) composition.

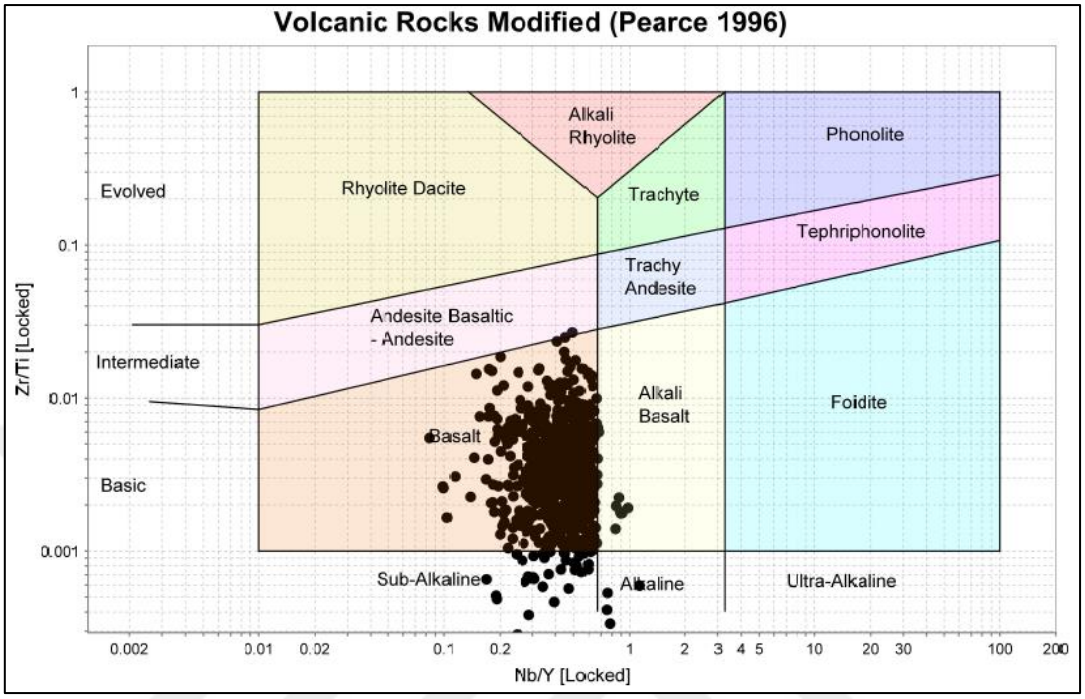


Figure 4-18. Zr/Ti vs. Nb/Y diagram (Pearce, 1996) of basaltic dike intervals from Ulutaş Cu-Zn skarn deposit (lithogeochemical data courtesy of Demir Export).

Some of the observed basaltic dikes are older than the Early Cretaceous granodiorite (Figure 4-21). Some may be present as large rafts (enclaves) of country rock within the granite; it is difficult in drill core to distinguish between these rafts from undisturbed dike.

Other dikes observed in the study area are relatively fresh, and consequently these were interpreted to have a post-mineralization timing. A distinctive feldspar and hornblende porphyritic dacitic andesite was seen both in the outcrop and also in the drill core (Figure 4-19 & Figure 4-20).



Figure 4-19. Drill core interval of andesite porphyry (left) cross-cut by a basaltic dike (drill hole EU-071, 50.70 m). Andesite porphyry shows intense carbonate-chlorite-sericite alteration, whereas the basaltic dike experienced intense chloritization as indicated by its distinct green color.

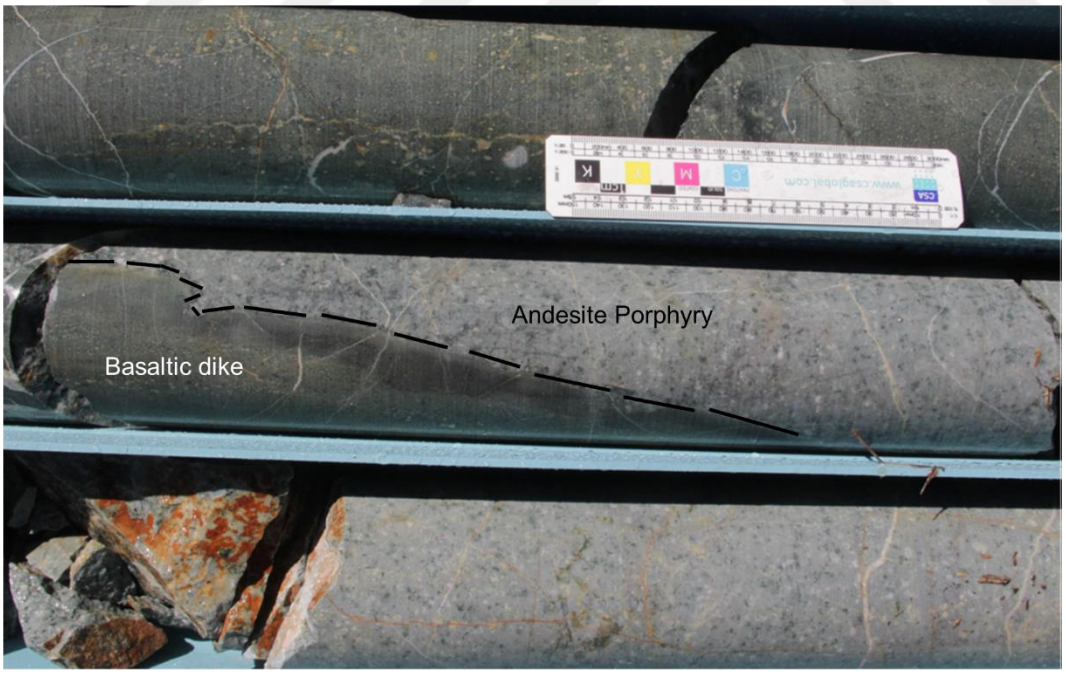


Figure 4-20. Drill core interval with a basaltic dike cross-cutting the andesite porphyry (drill hole EU-102, 159.80 m).



Figure 4-21. Outcrop image showing a basaltic dike cross-cutting the Cretaceous granodiorite (660621 E, 4493406 N, 2.119 m a.s.l., UTM Zone 37).

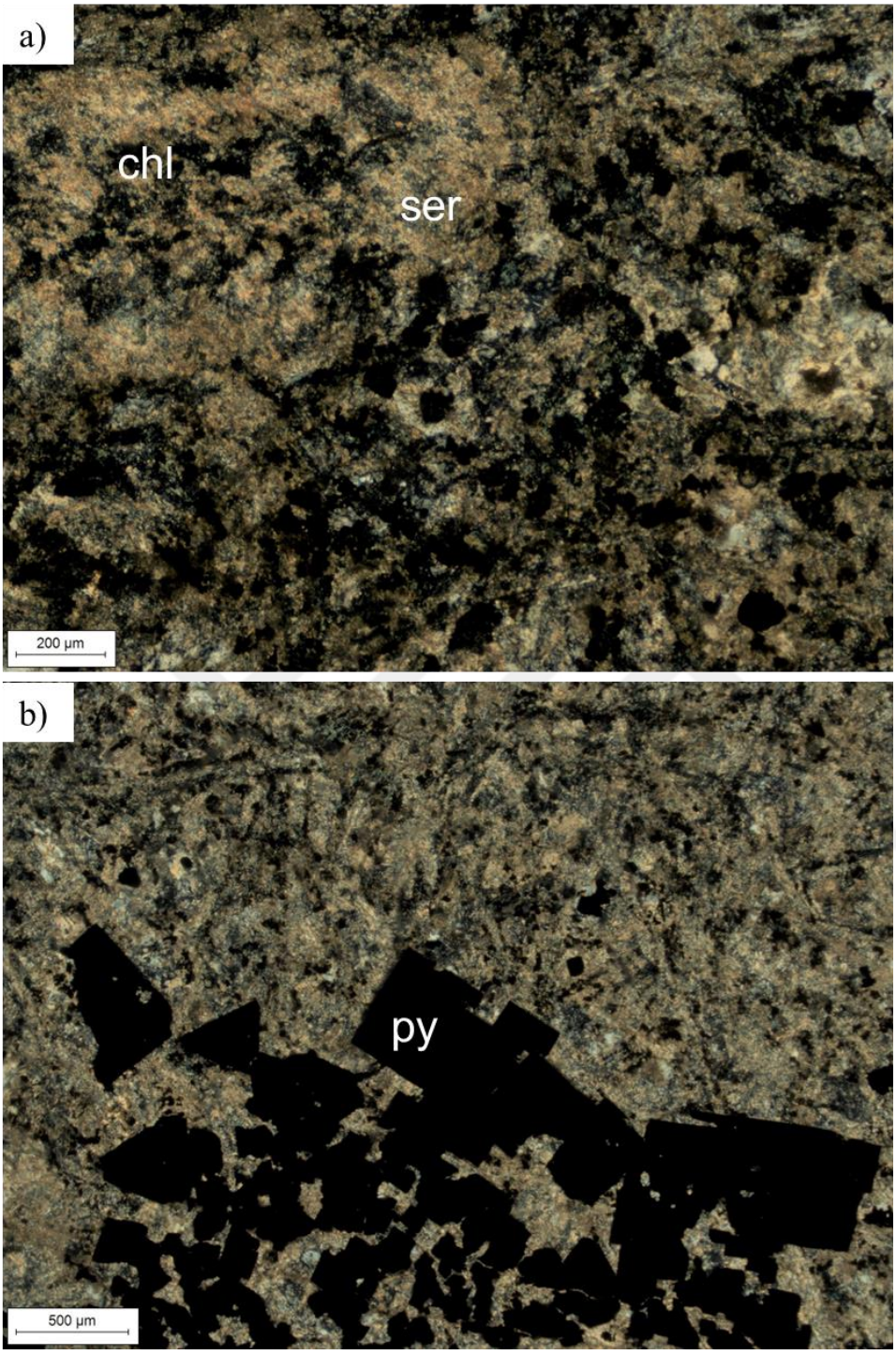


Figure 4-22. a) Microphotograph (XPL, TL image) of chlorite-sericite-altered basaltic dike (drill hole EU-094, 179.70 m), b) microphotograph (XPL, TL image) of euhedral pyrite within basaltic dike (drill hole EU-094, 179.70 m) Abbreviations: chl=chlorite,ser=sericite, py=pyrite, TL=transmitted light, XPL=cross polarized light.

4.1.3 Eocene Volcanic Sequence

The Eocene Volcanic Sequence or the Upper Volcanic Sequence (Giles, 1974) consists of layered andesitic to basaltic flows, tuffs, and agglomerates, which have been deposited particularly on post-mineralization erosional surfaces (Figure 4-23 and Figure 4-24).

This sequence was not sampled during sampling studies but was described in the outcrop. Both the andesites and andesitic breccias are rich in plagioclase phenocrysts alongside hornblende and minor quartz. These have been set in a fine-grained groundmass of quartz and plagioclase. Minor alteration is present in these volcanics in the form of partial chlorite replacement of hornblende and weak sericitization of plagioclase. The base of the sequence consists of pyroclastic rocks with nummulite-bearing marl, conglomerate, and sandstone (Figure 4-25).



Figure 4-23. Polymict andesitic breccia within Eocene Volcanic Sequence



Figure 4-24. Eocene andesite porphyry andesite in the study area (662816 E, 4494629 N, 2538 m a.s.l., UTM Zone 37).



Figure 4-25. Fossiliferous sandstone with abundant bivalves and nummulites within the Eocene Volcanic Sequence (662657 E, 4493415 N, 2328 m a.s.l., UTM Zone 37).

4.1.4 Pleistocene to Quaternary Cover Deposits

Pleistocene glacial till overlies much of the southern sector of the study area, but it has also been occasionally eroded to expose the underlying bedrock (Figure 4-26). It is inferred to represent lateral moraine deposits associated with the glaciation of the main Çayırözü Valley (Giles, 1974). The Ulutaş Zn-Cu skarn deposit is almost entirely covered by these moraine deposits (Figure 4-3). Thicknesses of glacial deposits are generally around 45 meters with a maximum thickness of ~86 meters. Glacial deposits consist of large, rounded to sub-rounded fragments, which range in size from a few centimeters up to about 1.5 m. Fragments of various lithologies were observed, including fresh volcanic and plutonic rock fragments as well as fragments derived from the skarn. These are surrounded by a fine-grained clastic matrix.

A substantial area of landslide cover and scree has been mapped in the southeast of the area, originating in the Eocene volcanic that is relatively susceptible to erosion. Scree exists on some slopes, particularly on the slopes of the Vank Dere valley between the two skarn deposits. Colluvial and alluvial deposits are located in the valley slopes and floors comprising mainly talus, soils, and occasional alluvial terrace gravels.

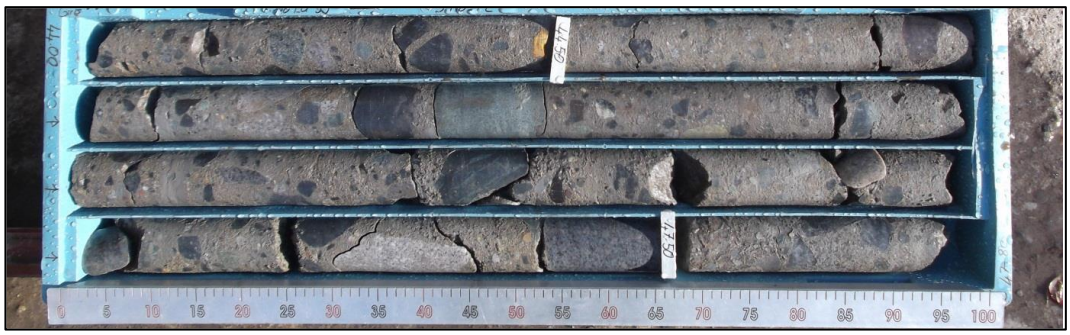


Figure 4-26. Drill core image of Pleistocene glacial till (drill hole EU-55, 44.00-47.80-meter interval).

CHAPTER 5

ALTERATION AND ORE MINERALOGY OF ULUTAŞ SKARN CU-ZN DEPOSIT

5.1 Skarn Alteration

In the Ulutaş area, distinct styles of skarn alteration have affected both the igneous lithologies and their surrounding sedimentary wall-rocks. Porphyry-style alteration is also present in the northeastern sector within the İspir Cu-Mo prospect (Giles, 1974; Soylu, 1999; Oğuz, 2010; Delibaş et al., 2016 and 2019). Porphyry-style alteration has been mapped within the Ulutaş stock, with a core of potassic (secondary K-feldspar and biotite) alteration in outcrops along a creek, below the village. This alteration is accompanied by A- and B-veins and more widespread sericitic alteration (Figure 5-1). Phyllic alteration is far more widespread, and is widely exposed to the west of the İspir porphyry system. This style of alteration is readily identified by bleached outcrops that contain abundant sericite and quartz alongside disseminations of pyrite. Zones of silicification are associated with the late breccias and quartz-porphyry bodies.

To the west of the district, around the Ulutaş Zn-Cu skarn system, surface alteration to skarn minerals is limited. This is due to the presence of glacial deposits covering the skarn domain. Where observed, outcrops commonly contain abundant garnet and minor pyroxene, which have been retrograded into chlorite-epidote-carbonate-tremolite-actinolite assemblages. Hydrothermal alteration due to skarn mineralization at Ulutaş is best developed in the drill core, which enabled identification of various alteration styles. A broad time-relationship has also been established among these alteration types.

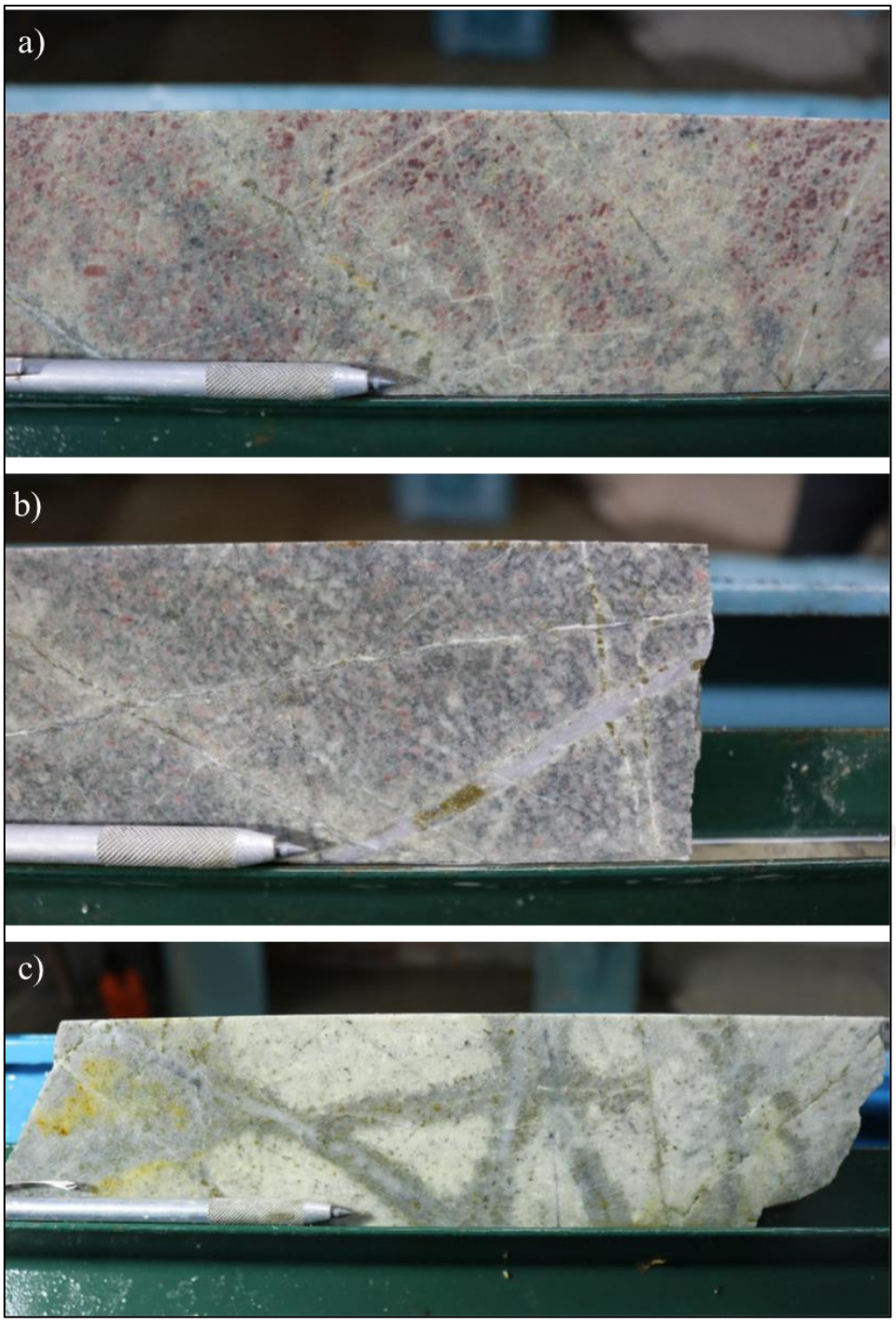


Figure 5-1. Drill core images of porphyry-style alteration in the Ulutaş porphyry area. a) potassic alteration characterized by secondary K-felspar on porphyritic monzonite with minor sericitic overprint along quartz-pyrite veinlets (drill hole EU-040, 312.70 m), b) potassic alteration with secondary K-feldspar on porphyritic diorite with minor sericitic overprint along quartz-pyrite veinlets (drill hole EU040,

294.00 m), c) intensely quartz-sericite-pyrite (phyllic) altered granitoid rock cross-cut by stockworking quartz-pyrite veins (drill hole EU-019, 77.50 m).

Skarn-type alteration (both prograde and retrograde) usually developed around shallowly emplaced andesite porphyry dikes ("quartz-feldspar porphyry) in contrast to being developed around larger intrusive bodies. As such, skarn zones are quite narrow, and these usually run parallel to the main plunge of the dikes.

The dominant alteration associated with the Ulutaş Skarn Cu-Zn deposit is skarn replacement of calcareous rocks with calc-silicate skarn minerals including garnet, pyroxene, and wollastonite (Figure 5-2). The prograde calc-silicate minerals have been extensively replaced by retrograde phases, which were identified as epidote, chlorite, sericite, tremolite-actinolite, carbonate, quartz, and hematite.

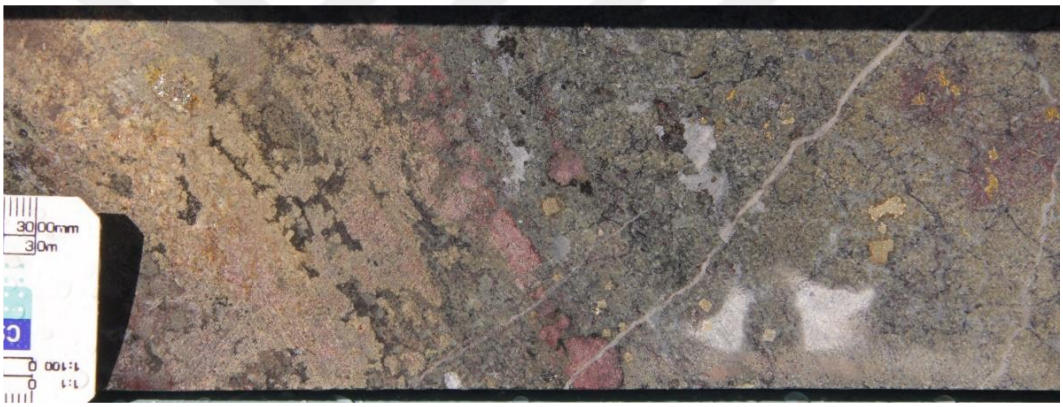


Figure 5-2. Yellowish brown colored garnet with greenish colored pyroxene skarn in the study area (drill hole EU051, 83.00 m)

5.1.1 Stage I - Potassic & Calc-Silicate Alteration (Prograde Stage)

Early-stage alteration at Ulutaş is represented by two distinct alteration styles of potassic and calc-silicate alteration. Potassic alteration is relatively limited and is developed within the intrusive rocks, particularly in the andesite porphyry and less commonly in granodiorite porphyry. Potassic alteration has affected narrow intervals of igneous lithologies and is identified in drill core samples by well-developed pink secondary K-feldspar (Figure 5-3).

In potassically-altered rocks secondary K-feldspar has replaced plagioclase phenocrysts and also the quartzofeldspathic groundmass, leading to K-feldspar flooding of andesite porphyry. Clusters of anhedral fine-grained mica minerals were also observed in the same samples, but their abundance is quite low. These likely represent secondary biotite, but now they have been almost completely chloritized during retrograde overprint (Figure 5-3). This late alteration overprint has also caused sericite and less commonly illite development after K-feldspar, as well as formation of carbonate, pyrite, and rutile. In drill core intercepts of potassically-altered quartz-feldspar porphyry, narrow actinolite or chlorite-epidote veinlets and paragenetically later carbonate veinlets are also present (Figure 5-3a).

The second alteration style associated with the early stages of metasomatic alteration at Ulutaş is calc-silicate alteration. Calc-silicate alteration is far more widespread compared to potassic alteration. The time relationship between these two alteration styles is not clear as these developed in different domains at Ulutaş. As such, their timing should be close to each other, and these even might have developed contemporaneously.

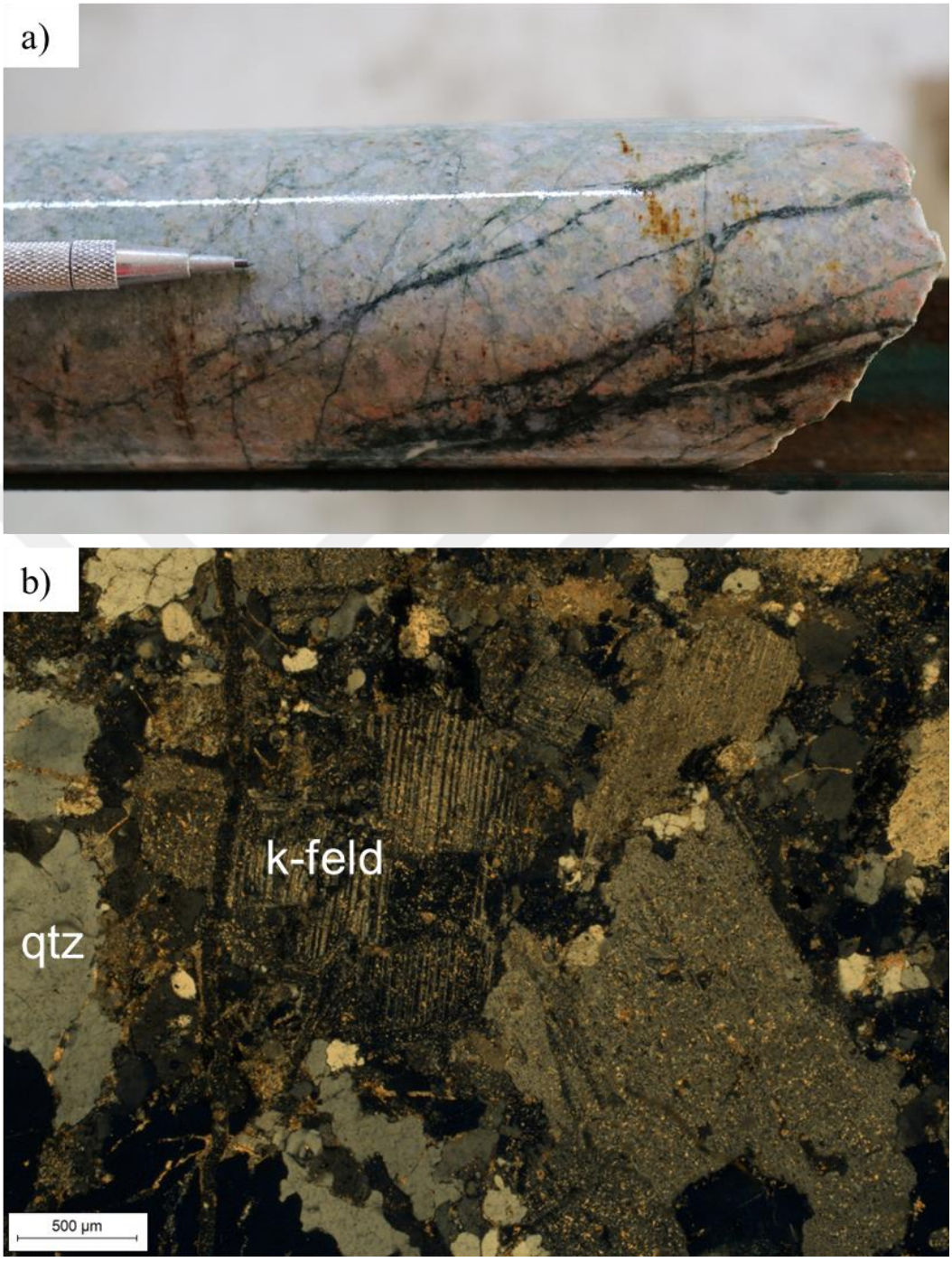


Figure 5-3. a) Drill core image showing early potassic alteration, which is represented by abundant secondary K-feldspar. Altered quartz-feldspar porphyry has been cut by actinolite veins (drill hole EU-051, 111.00 m). b) Microphotograph (XPL, TL image) showing secondary K-feldspar replacing plagioclase in quartz-feldspar porphyry. Fine flakes of sericite have later overgrown K-feldspar (drill hole

EU-051, 111.00 m). Abbreviations: qtz = quartz, K-feld = K-feldspar, XPL= cross-polarized light.

Calc-silicate alteration, represented by early garnet, pyroxene, and occasional wollastonite, developed throughout the entire skarn system at Ulutaş. This alteration type affected both the intrusive phases (endoskarn) and subjacent wall-rocks (exoskarn).

Garnet is the most dominant calc-silicate mineral both in the endoskarn and exoskarn zones. It typically occurs as medium- to coarse-grained, euhedral crystals locally up to a few centimeters in diameter. Massive garnet-pyroxene skarn replaces marble with sharp contacts (Figure 5-4, Figure 5-5, and Figure 5-6).

Impure calcareous clastic lithologies on the other hand have been incompletely replaced by pyroxene skarn and have a banded appearance, reflecting primary bedding and also possible metamorphic foliation. However, a distinct deposit-scale zonation among garnet- and pyroxene-dominant skarn zones is not evident. More commonly, garnet-pyroxene skarn transitions into wollastonite-rich domains at the marble front (Figure 5-5).

Intrusive rocks are also extensively skarn-altered. Endoskarn predominantly contains garnet, pyroxene, and late retrograde epidote. Endoskarn occurs as a replacement within the porphyry dike that cut the mineralized metamorphic basement sequence (Figure 5-7). Thin dikes may be completely replaced by pyroxene skarn or, more commonly, by epidote skarn.

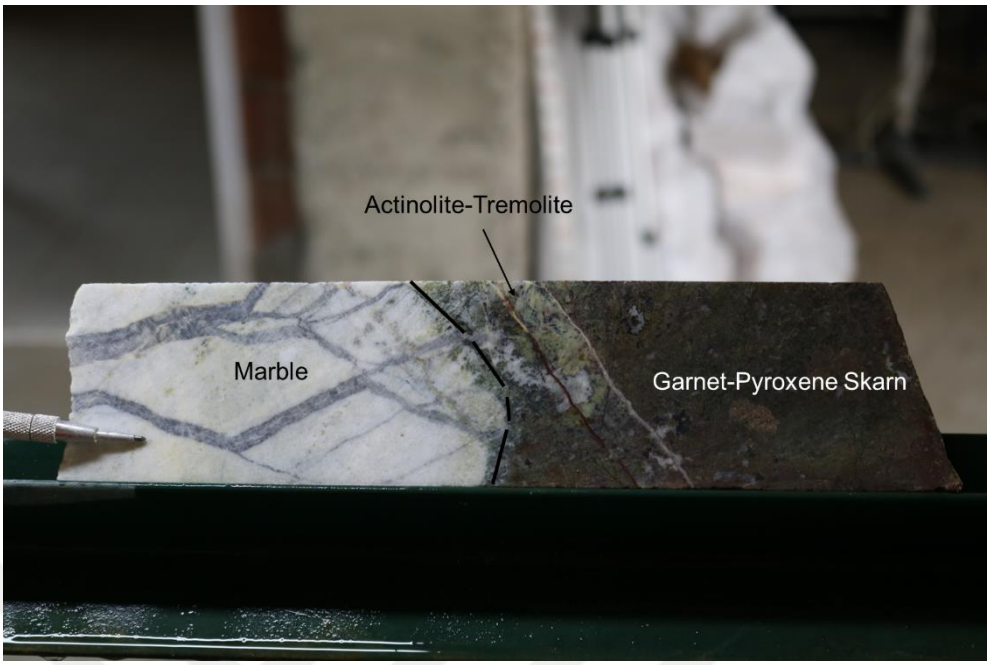


Figure 5-4. Drill core image showing the sharp contact between marble and garnet-dominant garnet-pyroxene skarn. Garnet-pyroxene skarn is replacive towards marble, which has been cut by calcite veins. Late tremolite-actinolite replaces garnet-pyroxene skarn (drill hole EU-094, 108.50 m).

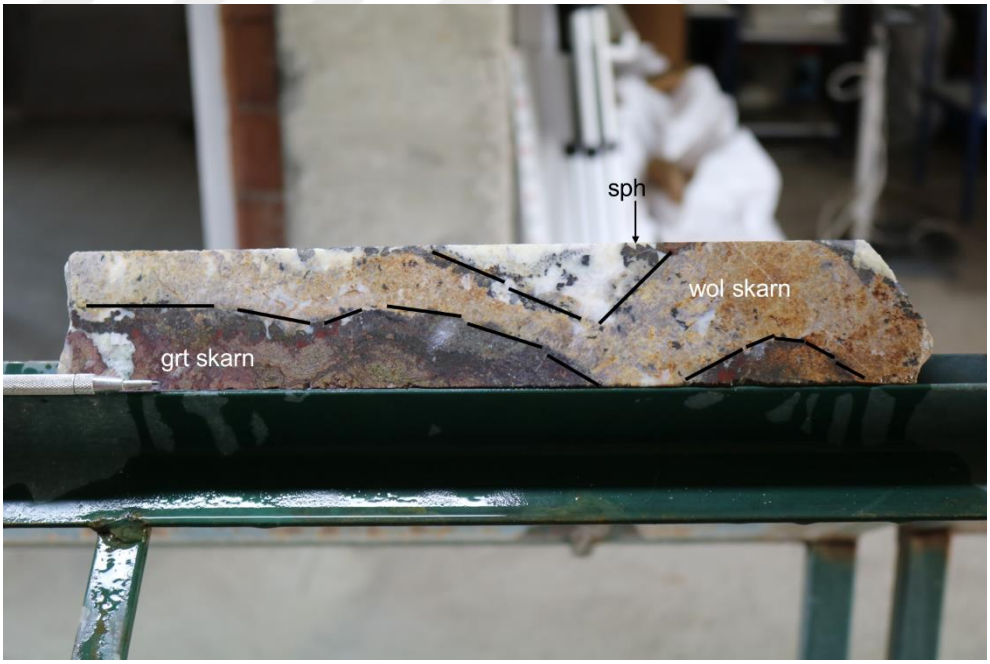


Figure 5-5. Drill core image showing progressive transition from garnet-rich skarn to wollastonite at the marble front. Hematite developed after garnet imparting a reddish color to the sample. Carbonate and sphalerite developed during retrograde

overprint (drill hole EU-094, 88.20 m). Abbreviations: grt = garnet, sph = sphalerite, wol = wollastonite.

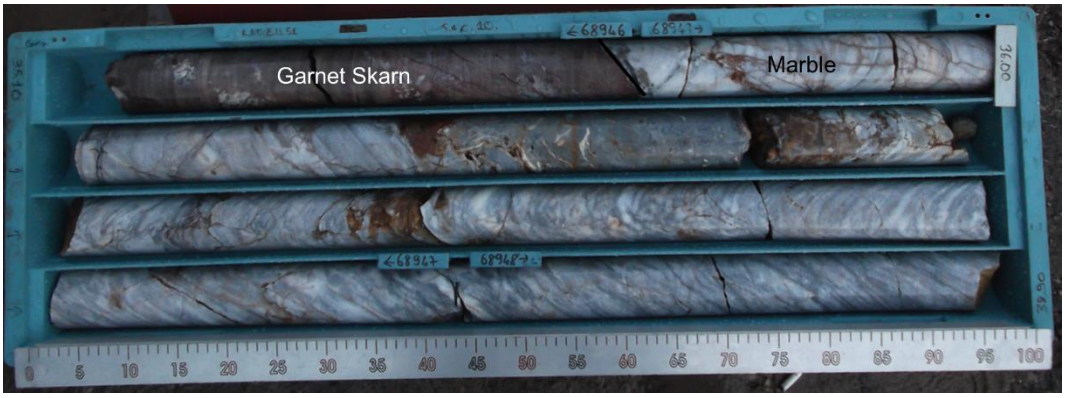


Figure 5-6. Reddish-brown colored garnet skarn in sharp contact with foliated marble (drill hole EU051, 35.40 m).

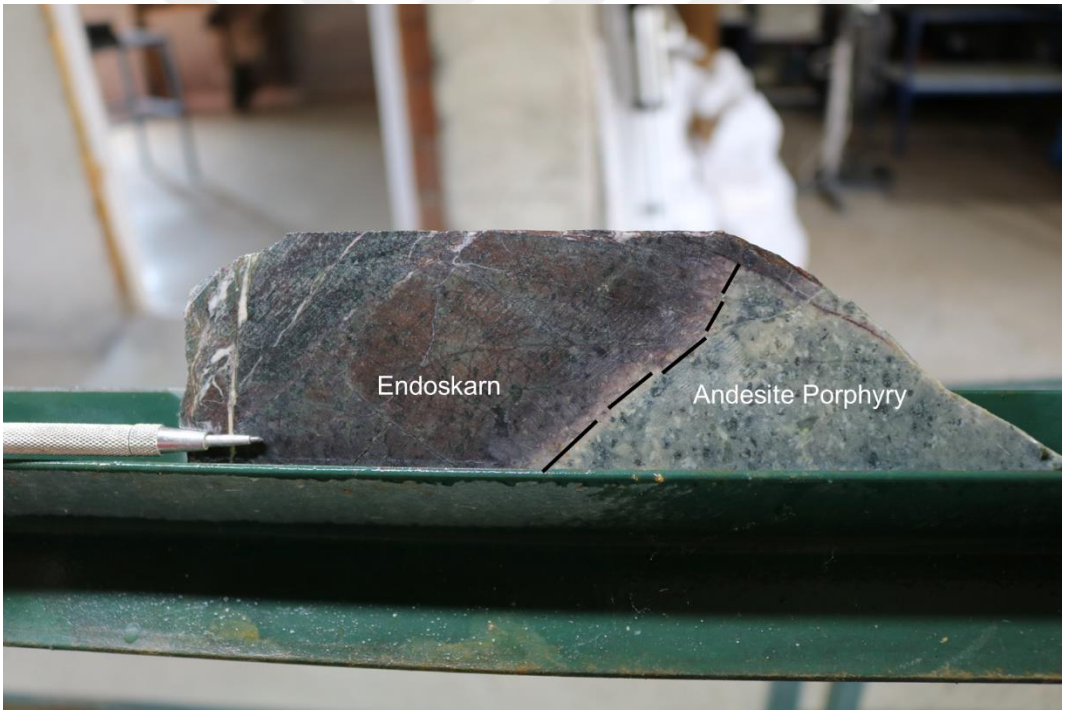


Figure 5-7. Drill core photograph showing the transitional contact between non-skarn andesite porphyry and endoskarn (drill hole EU-094, 160.70 m). Red-green coloring is due to late hematite-chlorite replacement of garnet.

Garnet skarn generally replaces marble and is typically coarse and dominated by dark colored garnet as observed in drill core. Garnets are often dark brown to red,

and less commonly yellowish-brown and pale green in color (Figure 5-9). Garnet in the Ulutaş area occurs as coarse-grained, euhedral crystals.

Garnet skarn has been extensively replaced by retrograde carbonate, quartz, epidote and hematite alteration, with fine-grained hematite resulting in a strongly reddish appearance (Figure 5-10, Figure 5-11). Both under the microscope and in hand specimen, garnet displays well-developed oscillatory zoning (Figure 5-10), where alternating bands of isotropic and anisotropic garnet were observed. Presence of such oscillatory-zoned garnets suggests progressive changes in fluid chemistry (e.g., temperature, fO_2, etc.) during calc-silicate alteration. In addition to oscillatory zoned garnets, sector-zoned garnets are also present at Ulutaş locally. Although most of the skarn in the Ulutaş deposit identified as exoskarn, endoskarn garnet can also occur (Figure 5-7).

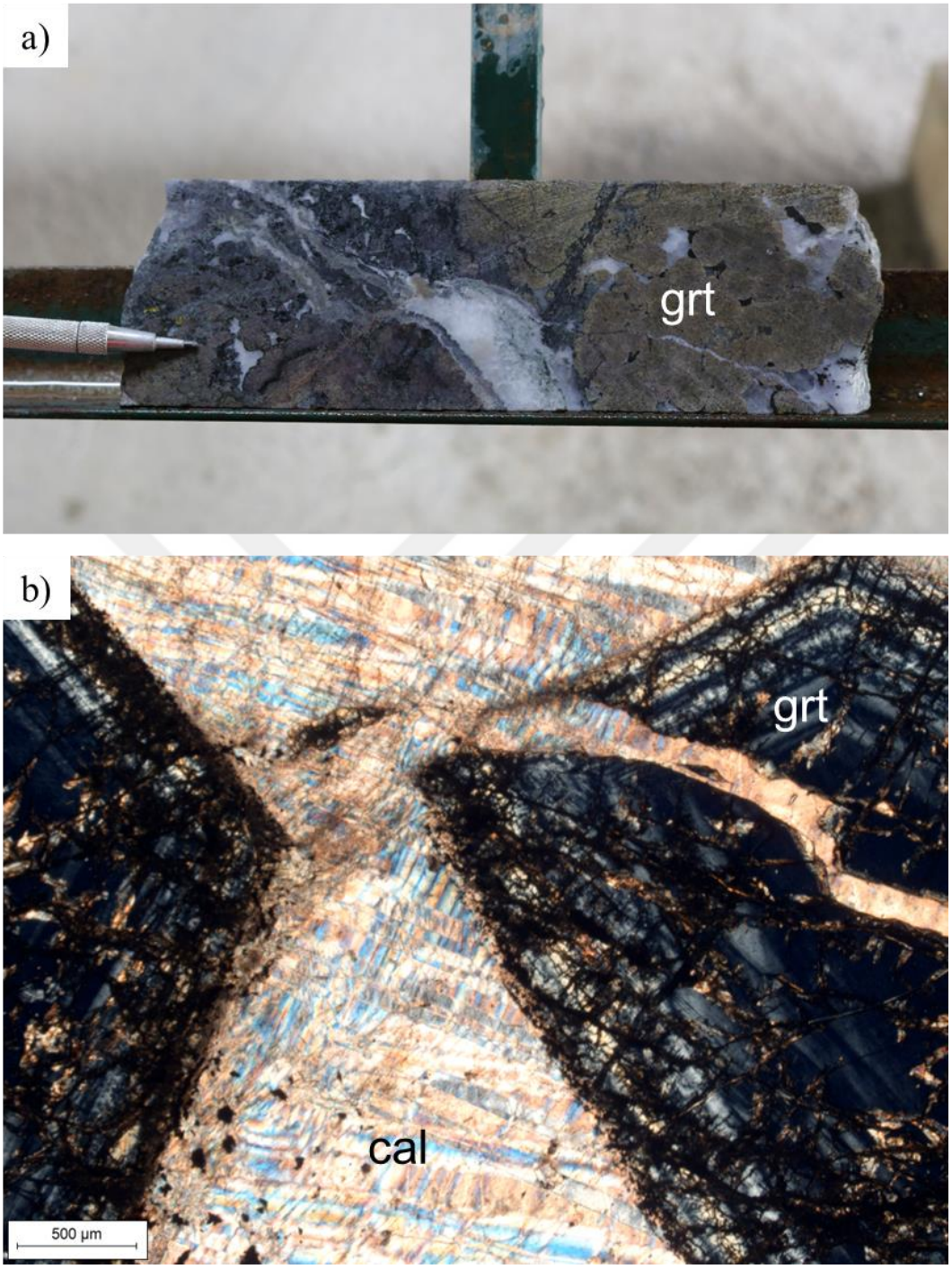


Figure 5-8. a) Drill core image of yellowish brown-colored garnet-rich prograde skarn, intensely overprinted by a late carbonate vein from Ulutaş area (drill hole EU-046, 124.80 m), b) Microphotograph (XPL, TL image) showing compositionally zoned garnets cross-cut and partly replaced by late stage carbonate (drill hole EU-046, 101.30 m). Abbreviations: grt=garnet, cal=calcite TL=transmitted light, XPL=cross polarized light.

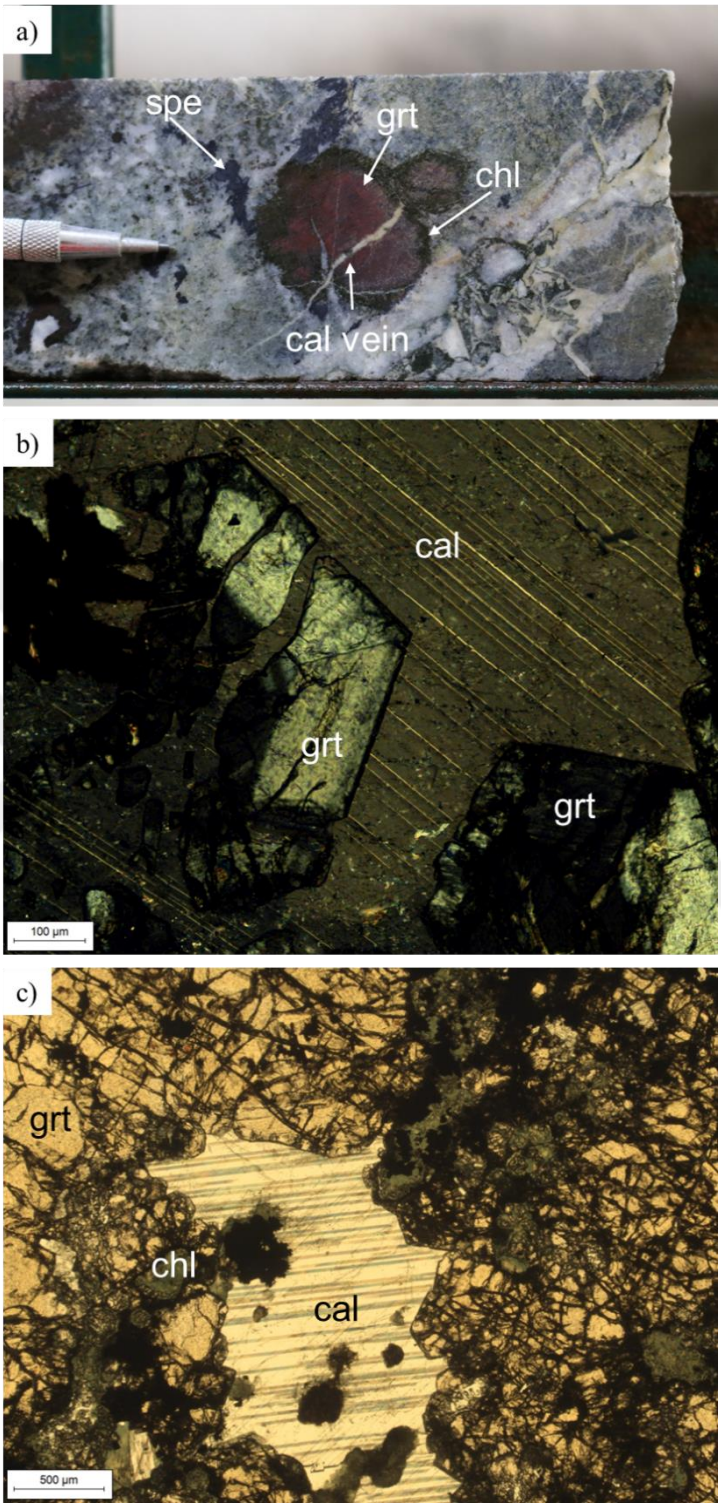


Figure 5-9. Drill core image and microphotographs of retrograde overprinting of garnet-rich calc-silicate alteration. a) Coarse-grained garnet retrograded into hematite (reddish core) and chlorite (green rims). Sample is fractured and brecciated

by fluids that are rich in carbonate. Specularite is also present as a late phase (drill hole EU-046, 101.30 m), b) microphotograph (XPL, TL image) showing sector-zoned garnet crystals fractured and cut by late stage carbonate (drill hole EU-046, 101.30 m), c) microphotograph (PPL, TL image) showing chlorite and carbonate overprinting of garnet (drill hole EU-046, 101.30 m). Abbreviations: grt=garnet, chl=chlorite, spe=specularite, cal=calcite, TL=transmitted light, XPL=cross polarized light, PPL= plane polarized light.

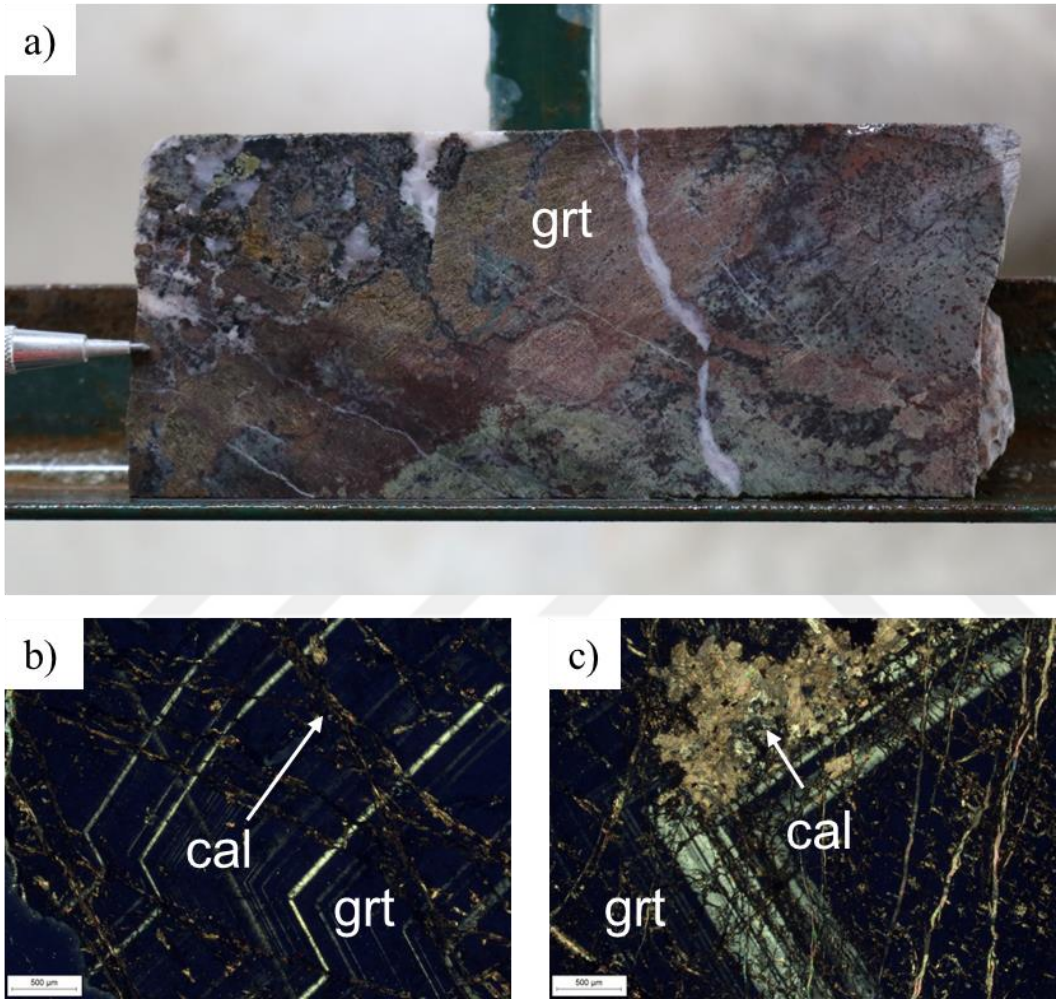


Figure 5-10. Drill core image and microphotographs of early garnet-pyroxene overprinted by late retrograde assemblages. a) drill core image of brown garnet and pale green-beige pyroxene cut and overprinted by carbonate alongside chlorite (drill hole EU-051, 78.90 m), b) microphotograph (XPL, TL image) showing intense carbonate veining after zoned garnet (drill hole EU-051, 78.90 m) c) microphotograph (XPL, TL image) showing partial replacement of garnet by late carbonate (drill hole EU-046, 101.30 m). Abbreviations: grt = garnet, cal = calcite, TL = transmitted light, XPL = cross-polarized light.

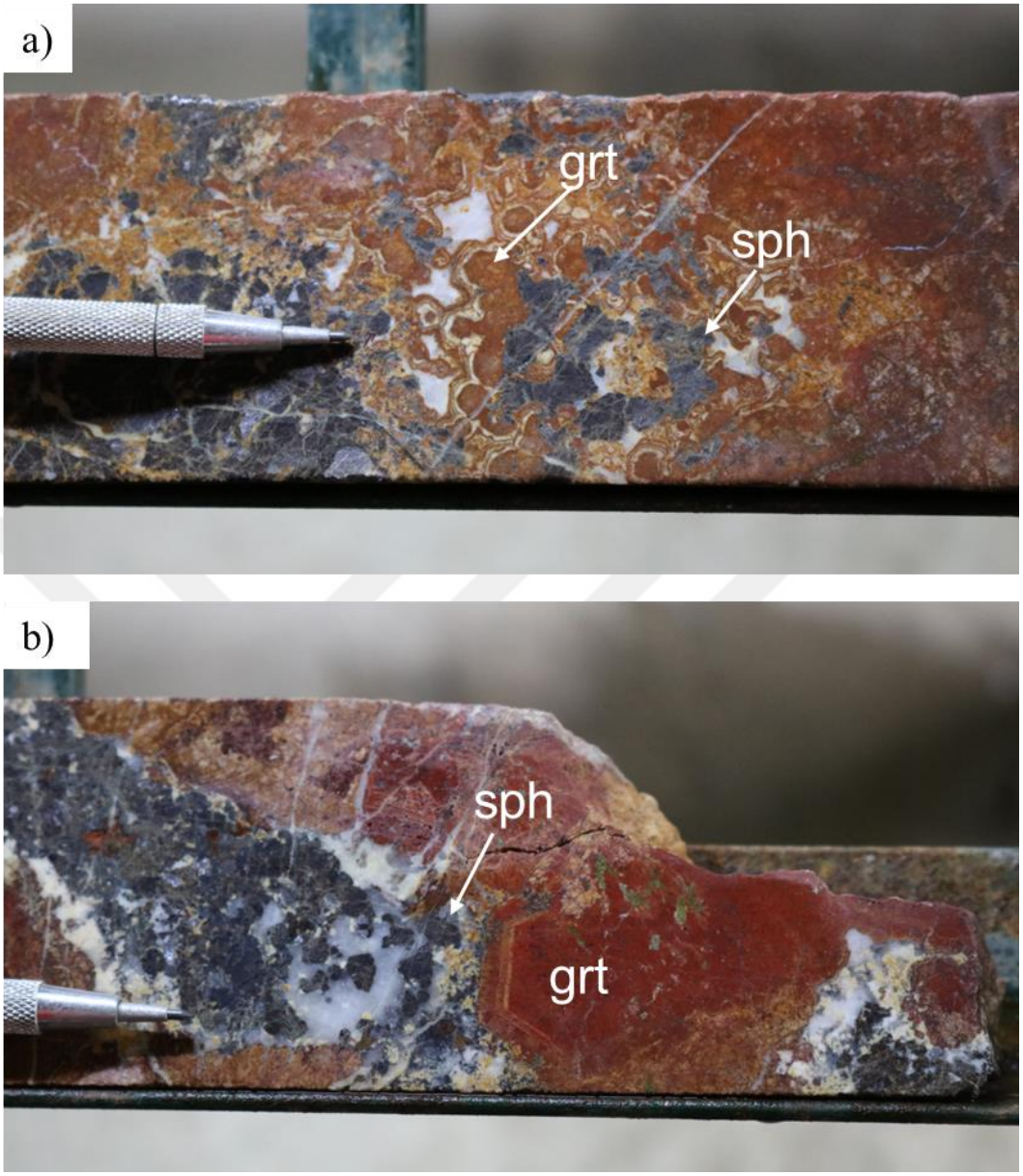


Figure 5-11. a, b) Drill core images showing hematite (red) and carbonate (white) pseudomorphing of early coarse-grained, zoned garnet. Sphalerite (dark gray) is intergrown with carbonate (drill hole EU-038, 86.00 and 85.00 meters, respectively). Abbreviations: grt=garnet, sph=sphalerite.

Pyroxene-rich skarn, characterized by presence of hedenbergite and diopside, also replaces marble as well as impure calcareous clastic metasediments. Pyroxene occurs as medium- to fine-grained, colorless to pale greenish, euhedral to anhedral crystals (Figure 5-12). Pyroxene seems to be more abundant in the exoskarn, particularly

when it developed within bedded and foliated basement metasedimentary lithologies. It can also occur in the endoskarn alongside garnet.

Wollastonite skarn is well-developed particularly along the contact zone with marble (Figure 5-12 and Figure 5-13). As such, carbonate commonly occurs alongside wollastonite. In thin section, wollastonite is readily distinguished by its coarse- to medium-grained, fibrous crystals (Figure 5-12c). In general, wollastonite zones have limited thickness, and these are much less abundant compared to garnet- and pyroxene-rich skarn zones.

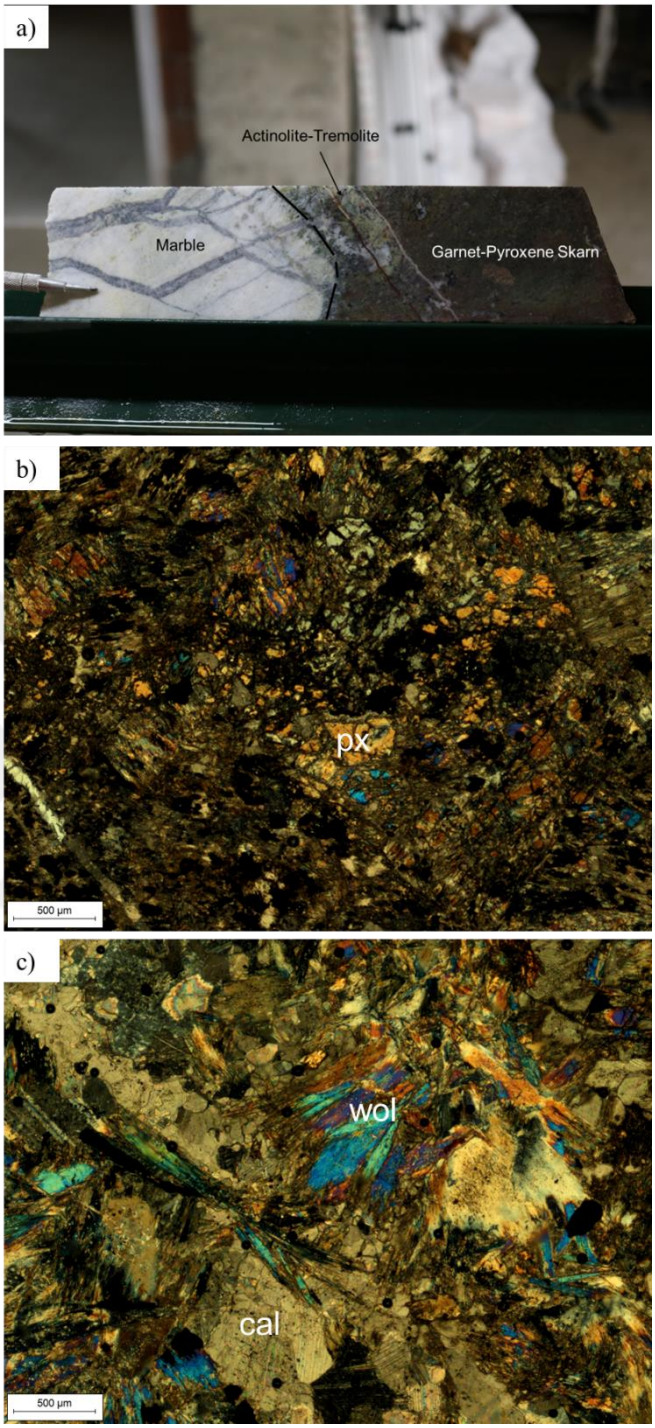


Figure 5-12. a) Marble – garnet-pyroxene skarn contact (drill hole EU-094, 108.50 m). b) microphotograph (XPL, TL image) py which shows high relief and high birefringence color (drill hole EU-094, 108.50 m), c) microphotograph (XPL, TL image) wollastonite show fibrous texture (drill hole EU-094, 108.50 m) Abbreviations: px=pyroxene, wol=wollastonite, carb=carbonate, TL=transmitted light, XPL=cross polarized light.

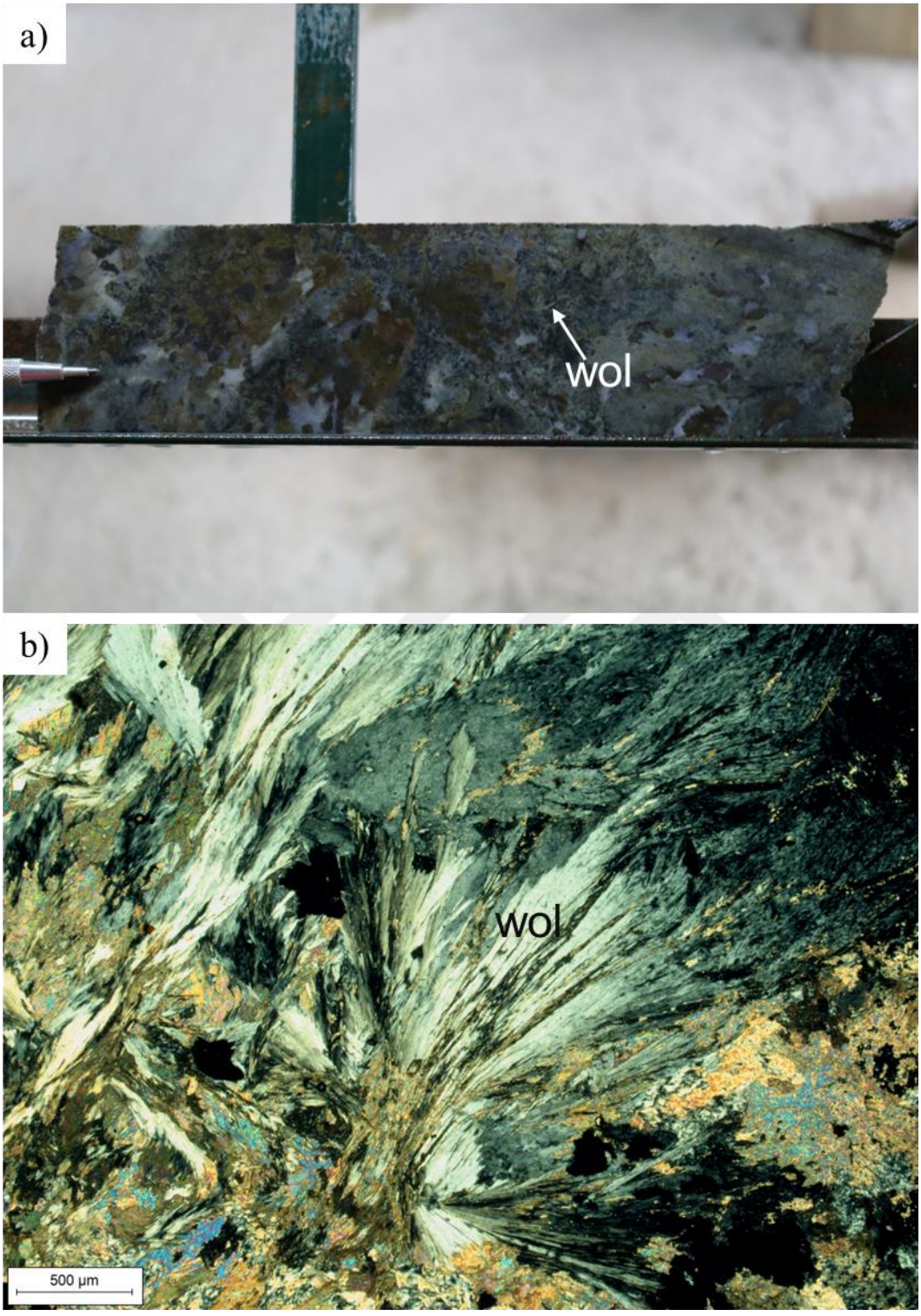


Figure 5-13. Hand specimen and microphotographs of wollastonite-bearing samples. a) drill core photograph of wollastonite showing fibrous texture (drill hole EU-081, 125.00 m), b) microphotograph (XPL, TL image) of wollastonite showing fibrous

texture alongside carbonate (drill hole EU-081, 125.00 m) Abbreviations: wol=wollastonite, TL=transmitted light, XPL=cross polarized light.

5.1.2 Stage II - Retrograde alteration

Retrograde alteration has affected large portions of the Ulutaş skarn system and is also associated with the main Zn-Cu mineralization. This alteration stage is characterized by presence of hydrous mineral phases including epidote, chlorite, sericite, tremolite-actinolite as well as by carbonate, quartz, and hematite. These have intensely overprinted the prograde skarn mineral assemblages (Figure 5-14). The retrograde alteration also affects the host metamorphic rocks and andesite porphyry (Figure 5-15).

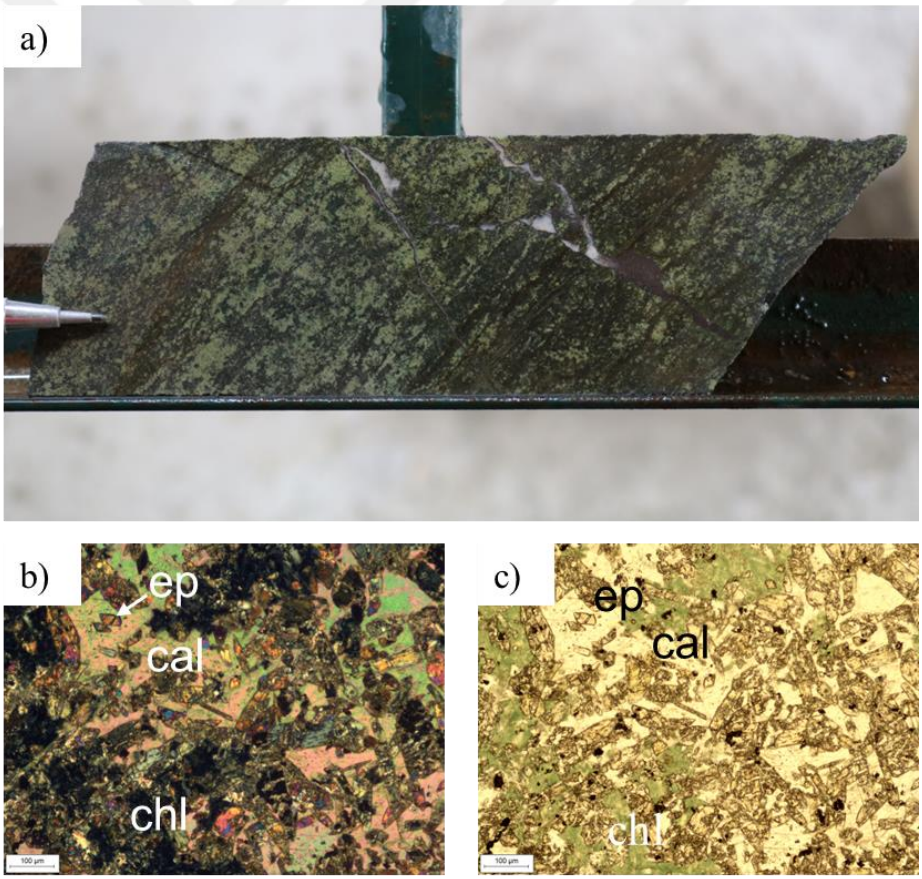


Figure 5-14. Hand specimen and microphotographs of chlorite-epidote skarn sample a) drill core photograph of banded chlorite-epidote skarn (drill hole EU-051, 81.80 m), b) microphotograph (XPL, TL image) of chlorite-epidote skarn (drill hole EU-

051, 81.80 m), c) microphotograph (PPL, TL image) of chlorite-epidote skarn (drill hole EU-051, 81.80 m). Abbreviations: chl = chlorite, cal = calcite, ep = epidote, TL = transmitted light, XPL= cross-polarized light, PPL = plane-polarized light.

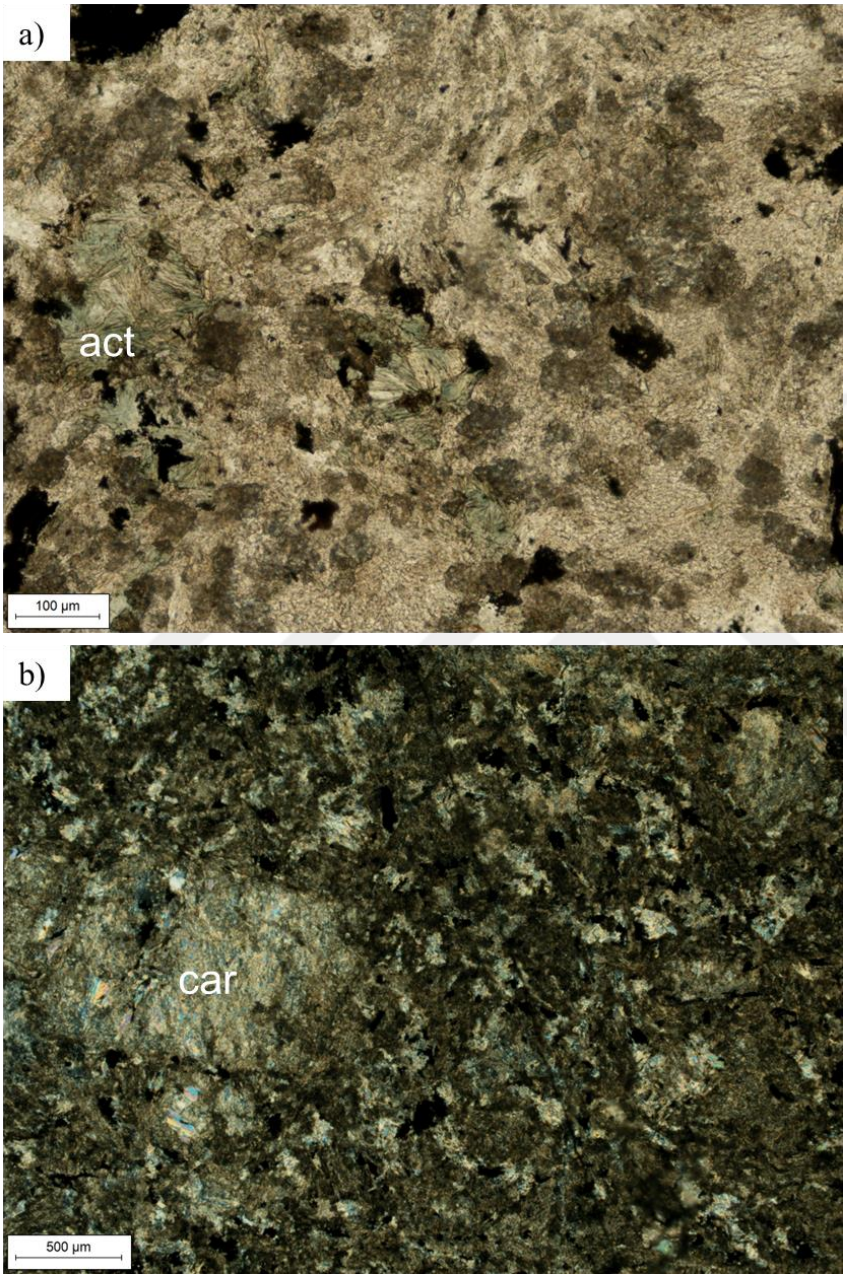


Figure 5-15. a) Microphotograph (PPL, TL image) of actinolite replaces andesite porphyry (drill hole EU-071, 52.70 m), c) microphotograph (XPL, TL image) carbonate altered plagioclase from retrograde altered andesite poprhyry (drill hole EU-071, 52.70 m). Abbreviations: act = actinolite, car = carbonate, TL = transmitted light, XPL= cross-polarized light, PPL = plane-polarized light.

In addition to actinolite-tremolite, chlorite-epidote-carbonate-hematite overprint is also commonly developed after anhydrous calc-silicate minerals. This mineral assemblage is likely formed due to lower fluid temperatures compared to actinolite-tremolite skarn. In such zones, garnet has been variably replaced by carbonate, chlorite, epidote, and hematite. Among these carbonates is the predominant replacement product after garnet, whereas chlorite and epidote are less abundant. Hematite is locally well-developed, and where present it forms alternating bands with carbonate after garnet. Such mineralogical variations are possibly resulted from compositional zonation observed in garnets. Fe-rich domains were selectively replaced by hematite, whereas carbonate is likely developed along layers dominated by Ca-rich garnets.

Various skarn zones at Ulutaş are primarily localized along contacts between intrusive units or dikes and surrounding calcareous sedimentary units. Andesite porphyry in particular seems to be responsible from much of the development of skarn assemblages and it appears to the main heat source for skarn formation. Exoskarn domains in the deposit area developed as a replacement of the upper and lower marble units (Figure 5-16). The interaction of andesite porphyry with upper and lower marble units, and the presence of metamorphic rocks with siliciclastic protoliths between the two units, has resulted in the formation of upper and lower skarn domains at Ulutaş. The obtained zonation of prograde garnet skarn, pyroxene skarn and retrograde skarn with andesite porphyry and mafic dikes is shown in Figure 5-17.

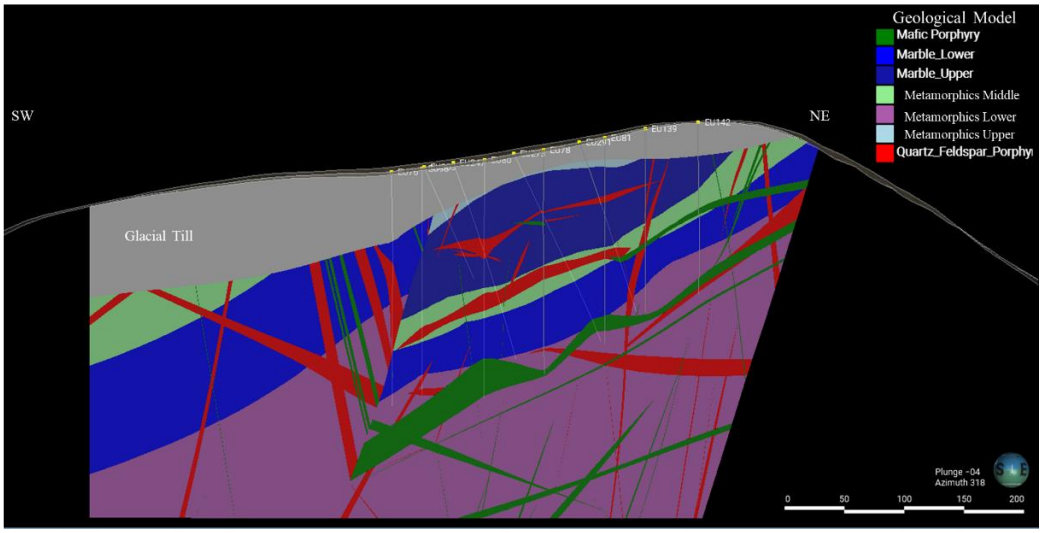


Figure 5-16. Cross-sectional view (looking SE) showing main lithological units and their cross-cutting relationships at the Ulutaş Cu-Zn skarn type deposit. Upper and lower marble units largely localized development of exoskarn. A steeply-dipping fault separates the domains to the northeast and southwest.

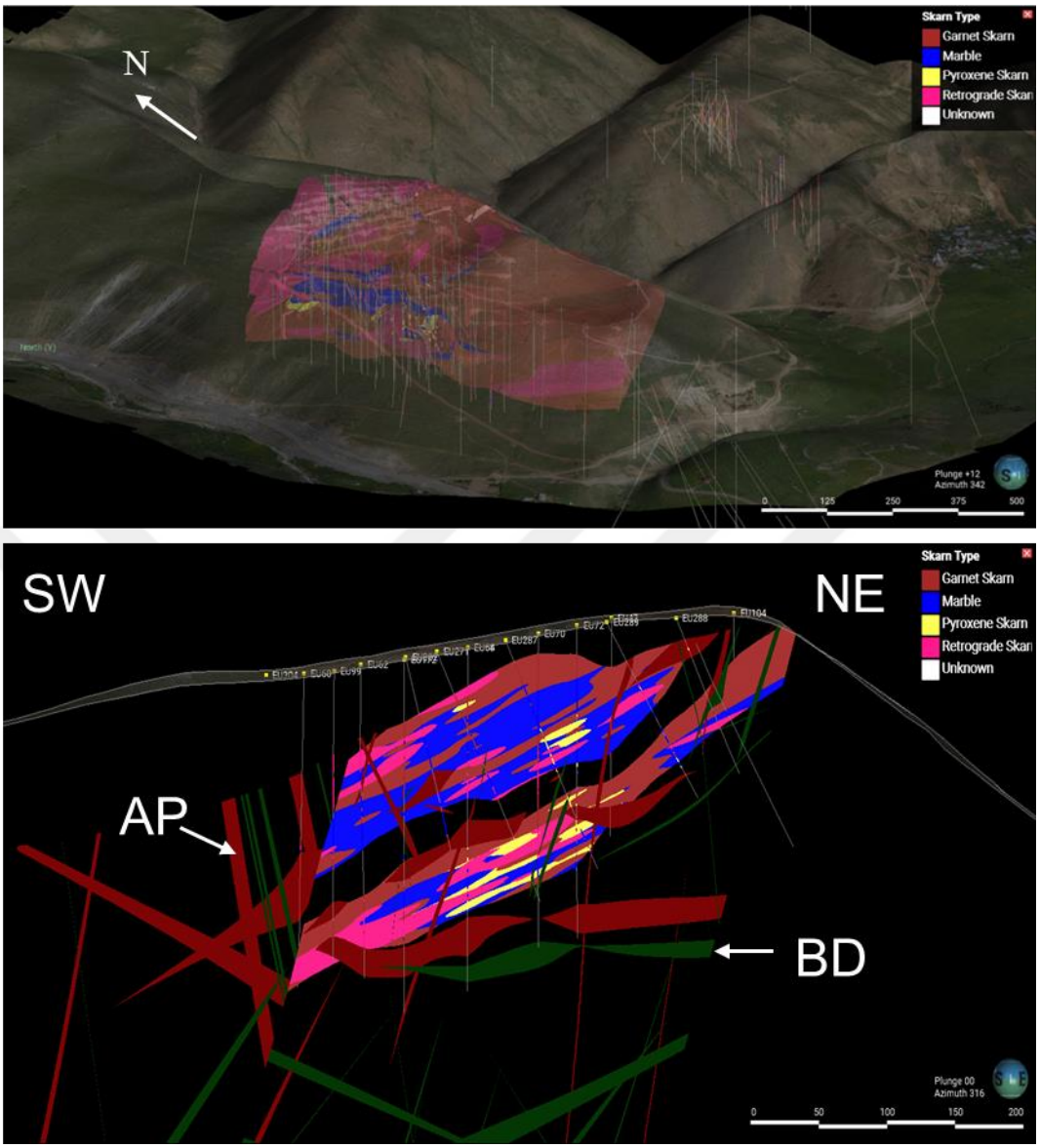


Figure 5-17. Skarn zonation pattern with andesite porphyry (AP) and basaltic dikes (BD) in Ulutaş Cu-Zn skarn type deposit

5.2 Zn-Cu Mineralization

Ulutaş skarn deposit contains economic Zn and Cu mineralization associated with retrograde skarn alteration. Zn and Cu enrichment is almost exclusively related to sphalerite and chalcopyrite, and interestingly the deposit does not contain any galena. This is unusual as most Zn-skarns in the world, including many such examples in Turkey, also have economic zones of Pb mineralization (Meinert et al., 2005). Galena is virtually absent throughout the entire skarn system, which also resulted in absence of Ag mineralization at Ulutaş.

Based on their main ore minerals and the dominant metal contents, the Ulutaş skarn is sub-divided into two mineralized domains: Zn-rich and Cu-rich skarn mineralization. Both of these domains contain abundant sulfide minerals.

The sequence of mineral formations indicating various phases of hydrothermal activity was determined by analyzing the relationship between different mineral assemblages found in both drill core and petrographic studies. The obtained sequence of mineral formations is shown in Figure 5-18.

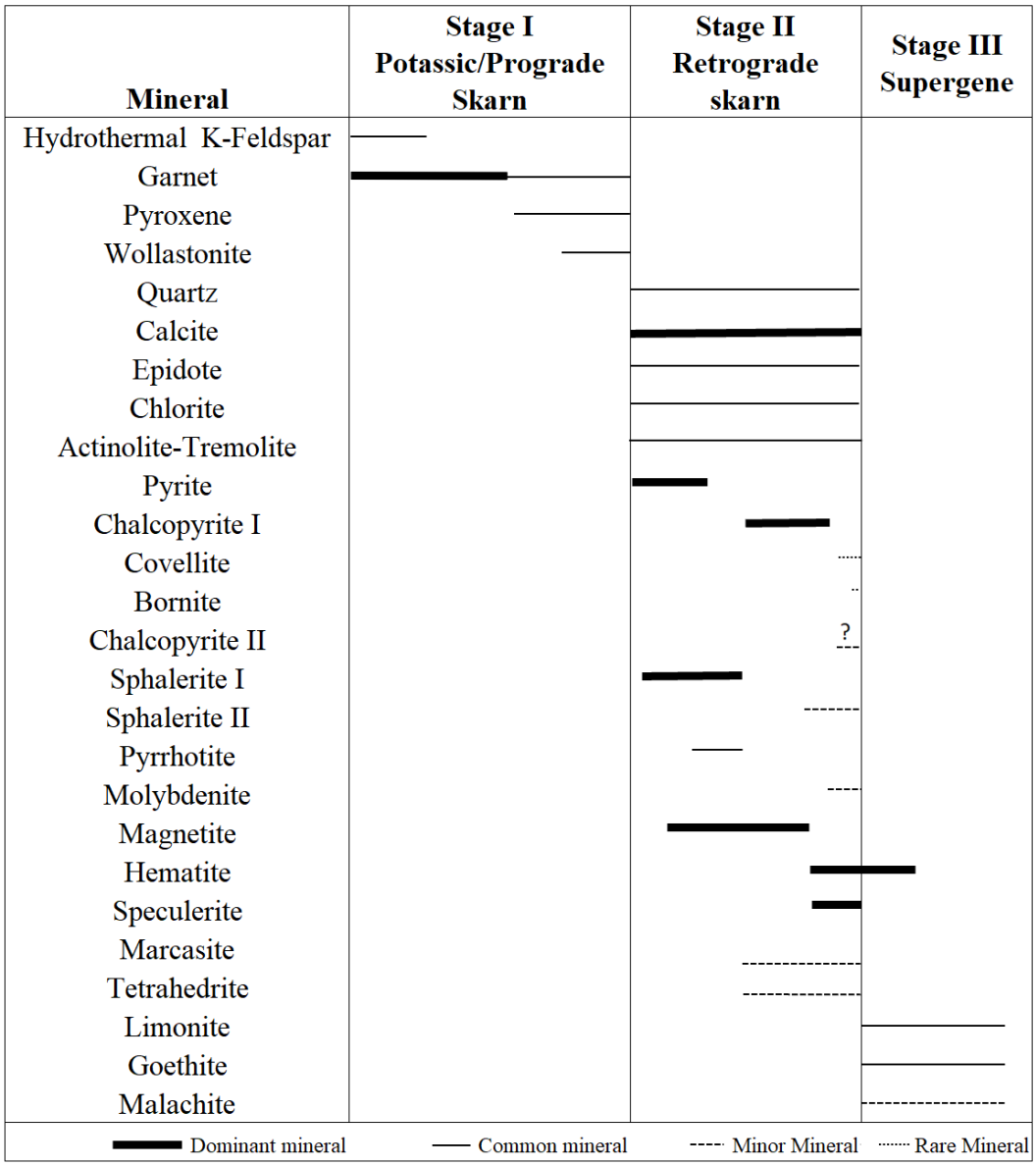


Figure 5-18. Paragenetic sequence of the Ulutaş Cu-Zn skarn type deposit as obtained from petrographic observations of altered and mineralized samples.

The main ore minerals in the Ulutaş Cu-Zn Skarn are pyrite, chalcopyrite, sphalerite, magnetite, hematite and specularite with minor amounts of pyrrhotite, tetrahedrite, marcasite, and rare bornite and covellite (Figure 5-19). Molybdenum contents of drill core samples are quite low (maximum of 122.00 ppm), but significant amounts of disseminated molybdenite was detected in a large number of analyzed samples in this study.

Although most of the sulfide precipitation occurred during the retrograde grade stage, sulfide mineralization also occurs in marble without presence of any skarn minerals. This form of mineralization is commonly represented by an assemblage of with magnetite-specularite-sphalerite (Figure 5-20). The retrogressive stage commences with the sulfide mineralization event and causes prograde skarn calc-silicate minerals to be strongly altered to retrograde stage epidote, chlorite, actinolite/tremolite, and sericite, as well as carbonate and hematite.

Sulfide minerals including pyrite, chalcopyrite and sphalerite occur as massive aggregations, disseminations, or less commonly as vein infill in the Ulutaş deposit (Figure 5-19).

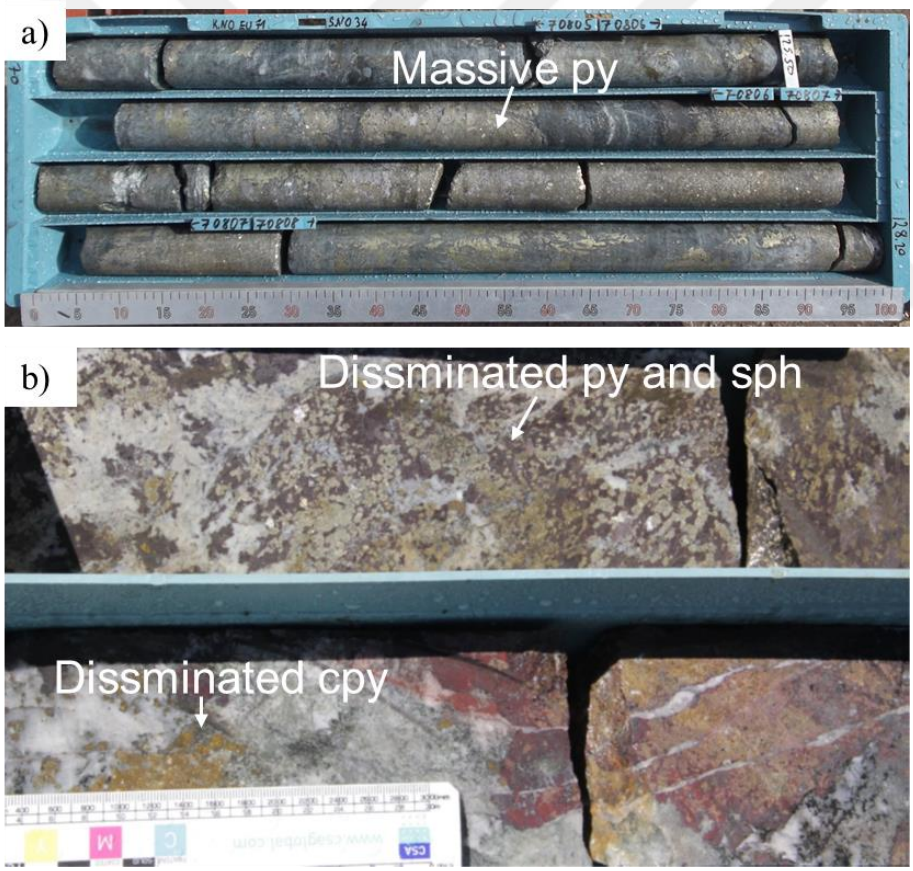


Figure 5-19. a) Drill core sample shows the massive pyrite mineralization in the study area (drill hole EU-071, 126.00 m). b) drill core samples show disseminated sphalerite, pyrite and chalcopyrite mineralization (drill hole EU0102, 111.5-112.00 m). Abbreviations: sph = sphalerite, cpy = chalcopyrite, py = pyrite.

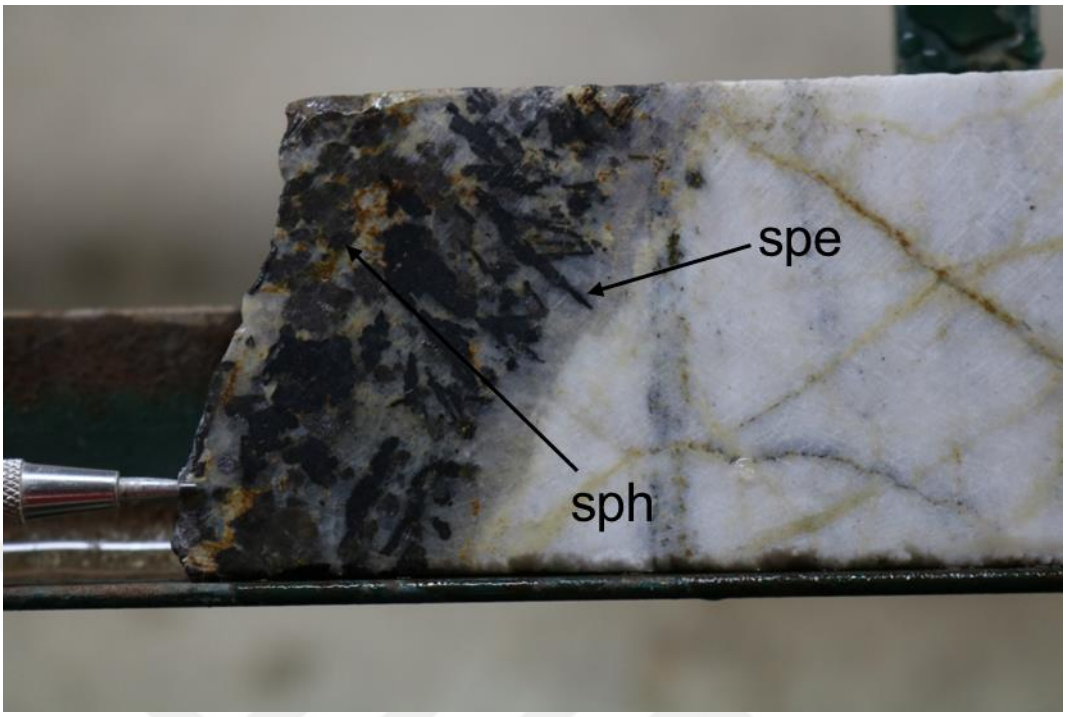


Figure 5-20. Drill core samples shows disseminated sphalerite and specularite mineralization on marble (drill hole EU-081, 83.30 m.) Abbreviations: sph = sphalerite, spe = specularite.

In the study area major ore minerals sphalerite, pyrite, chalcopyrite, magnetite and specularite precipitated across different stages.

Magnetite, which is formed in both prograde and retrograde stages, occurs as disseminations in the Ulutaş skarn deposit. Magnetite forms medium- to coarse-grained discrete crystals. It is commonly accompanied by chalcopyrite, pyrite, and lesser sphalerite. In most of the studied samples, magnetite has been replaced by specularite and hematite associated during the retrograde stage (Figure 5-21). Hematite occurs as a replacement product of magnetite, where it has overgrown magnetite grains along rims and also along micro-fractures (Figure 5-23).

Specularite (or specular hematite) is quite distinct from hematite as it typically occurs as disseminations or aggregates of long, acicular crystals (Figure 5-21). Most specularite is present in shallow depths (<50 m), particularly in drill core intercepts immediately beneath the glacial cover deposits. In addition, specularite commonly

occurs in close association with late stage carbonate and quartz as well as in relation with sphalerite and lesser pyrite and chalcopyrite (Figure 5-20, Figure 5-22, Figure 5-23 and Figure 5-24). The common appearance of hematite and/or specularite after magnetite indicates a progressive change to more oxidizing conditions at Ulutaş.

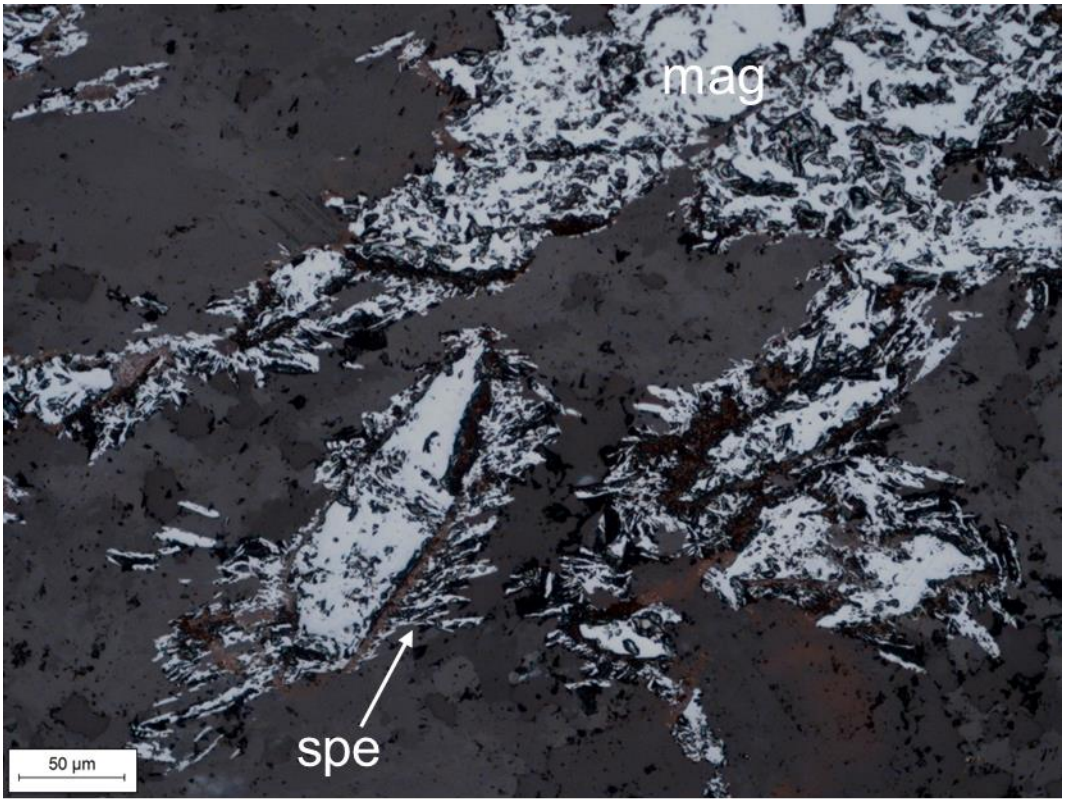


Figure 5-21. Microphotograph (XPL, RL image) of magnetite replaced by acicular specularite (drill hole EU-081, 91.70 m) Abbreviations: mag = magnetite, spe = specularite, hem = hematite RL= reflected light, XPL = cross-polarized light.

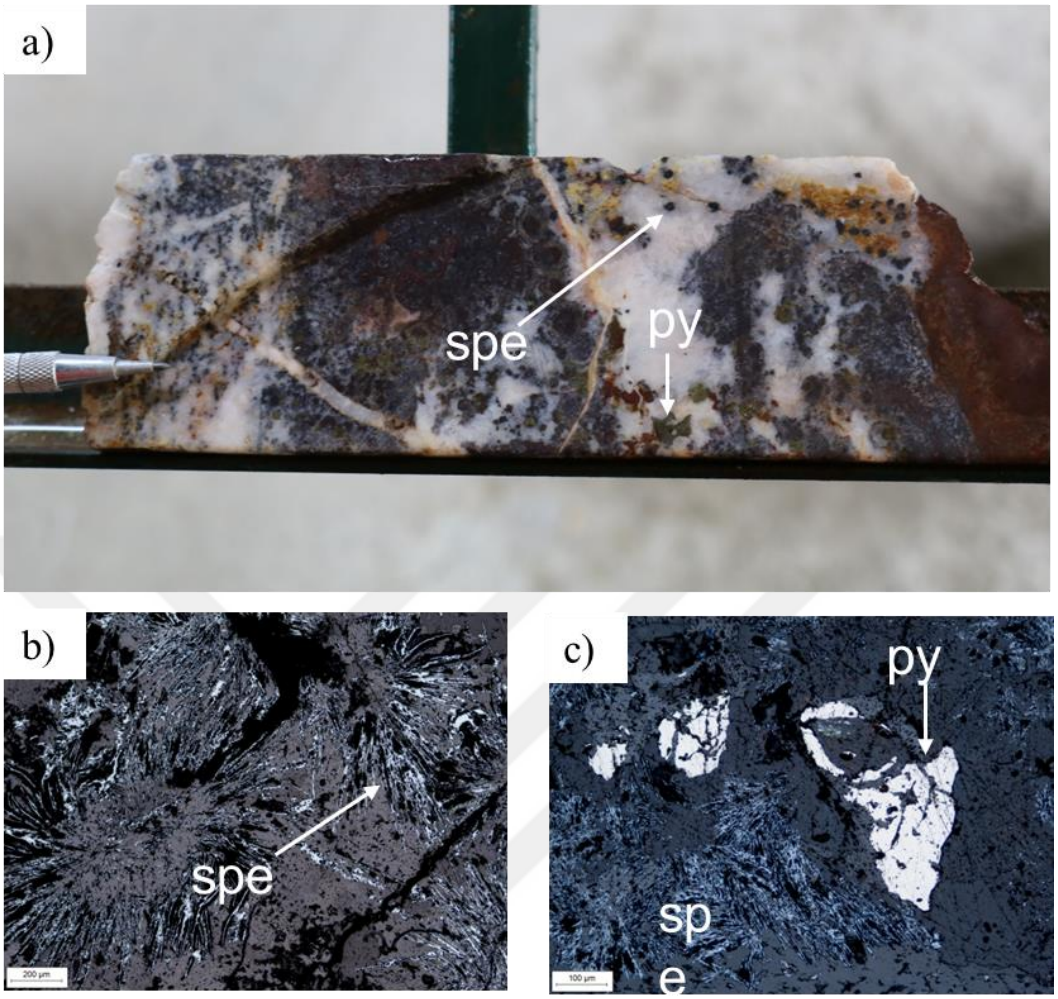


Figure 5-22. Hand specimen and microphotographs showing specularite-pyrite assemblages. a) drill core photograph of retrograde skarn with disseminated acicular specularite and pyrite (drill hole EU-051, 31.10 m), b) microphotograph (XPL, RL image) of fibrous specularite (drill hole EU-051, 31.10 m), c) microphotograph (XPL, RL image) of specularite and pyrite (drill hole EU-051, 31.10 m), Abbreviations: py=pyrite, spe=specularite, RL=reflected light, XPL=cross polarized light.

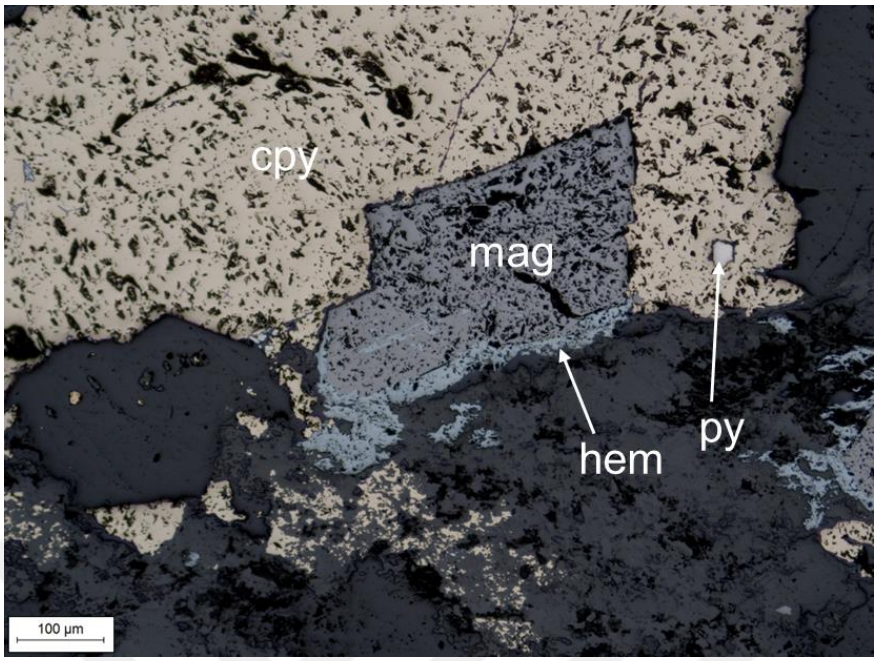


Figure 5-23. Microphotograph (XPL, RL image) of magnetite occurs rims on sphalerite with chalcopyrite and py (drill hole EU-051, 90.00 m), Abbreviations: cpy = chalcopyrite, hem = hematite, py = pyrite, mag = magnetite, RL = reflected light, XPL = cross-polarized light.

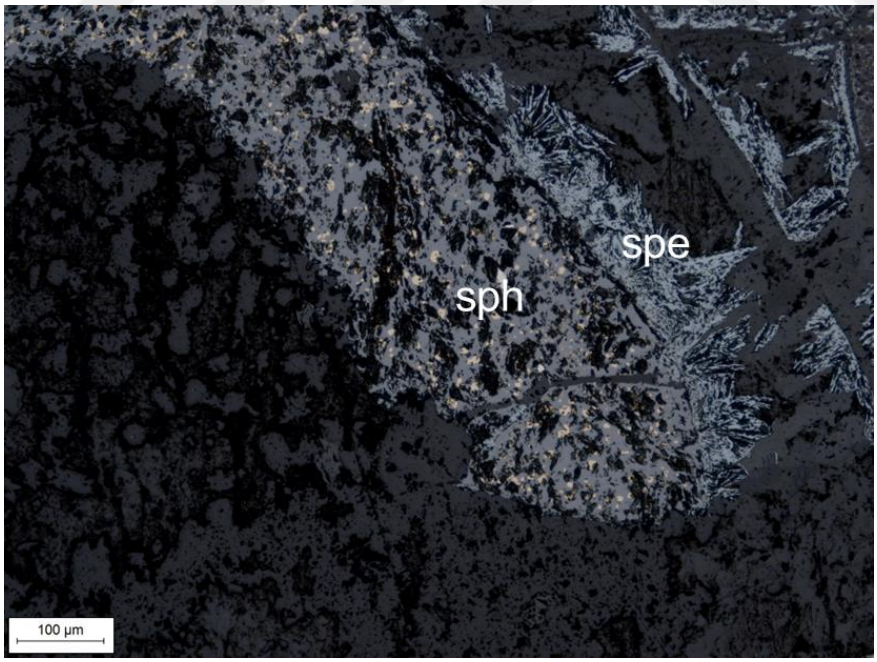


Figure 5-24. Microphotograph (XPL, RL image) showing chalcopyrite (yellow) replacement of sphalerite (gray, center). Sphalerite is rimmed by acicular specularite

(gray, right) (drill hole EU-081, 91.70 m), Abbreviations: spe=specularite, sph=sphalerite, RL=reflected light, XPL=cross polarized light

Sphalerite, the primary Zn ore mineral at Ulutaş skarn system, occurs as medium- to coarse-grained disseminations and massive aggregates. It is generally dark brown in drill core and opaque to reddish brown colored under transmitted light, suggesting an Fe-rich composition. Two distinct sphalerite varieties were identified during petrographic studies. First of these, and also the more common variety, shows typical chalcopyrite disease texture (Figure 5-25, Figure 5-26 and 5-27). In such sphalerites (sphalerite I), tiny blebs of chalcopyrite replace sphalerite abundantly. Chalcopyrite disease in sphalerite is the result of replacement of Fe-bearing sphalerite by chalcopyrite, and that this replacement process is likely related to changes in the chemical environment during or after the deposition of sphalerite (Barton et al., 1987). Replacement process occurs during or after the deposition of sphalerite and is likely related to changes in the chemical environment, such as a incerase in temperature or an increase in sulfur fugacity (Barton et al.1987). Barton et al. (1987) sub-divided "chalcopyrite disease" textures as watermelon (fine-grained, disseminated chalcopyrite), dusting (veinlets of chalcopyrite) and biomodal (massive aggregates of chalcopyrite) textures. Sphalerite in Ulutaş area commonly shows watermelon texture. According to Barton et al. (1987), these textures are clearly the result of replacement, rather than exsolution or other processes, because they involve a complete or partial replacement of original Fe-bearing sphalerite by an aggregate of chalcopyrite and low-Fe sphalerite as an integral part of the mineralization process.

Although most sphalerite at Ulutas is dark brown to dark red in color, single crystals locally color variations (Figure 5-26), where darker colored sphalerite cores are surrounded by progressively lighter brown to orange colored sphalerite at the rims. The brownish grey colored sphalerites under cross-polarized light has relatively poorly-developed chalcopyrite disease texture, whereas bluish grey sphalerite generally displays much significant development of chalcopyrite replacement. This

likely indicates that Fe contents of sphalerite varies across different generations of this mineral.

The second sphalerite variety (sphalerite II) on the other hand does not display chalcopyrite replacement, and in fact it overprints chalcopyrite (Figure 5-28). In some samples, sphalerite II was further replaced by a later stage of chalcopyrite (chalcopyrite II). Sphalerite II replaces chalcopyrite I, however sphalerite II also shows chalcopyrite disease texture in some samples and this chalcopyrite is indicated as chalcopyrite II.

Apart from chalcopyrite, pyrrhotite was also observed locally to have replaced sphalerite as tiny blebs together with some chalcopyrite (Figure 5-27).

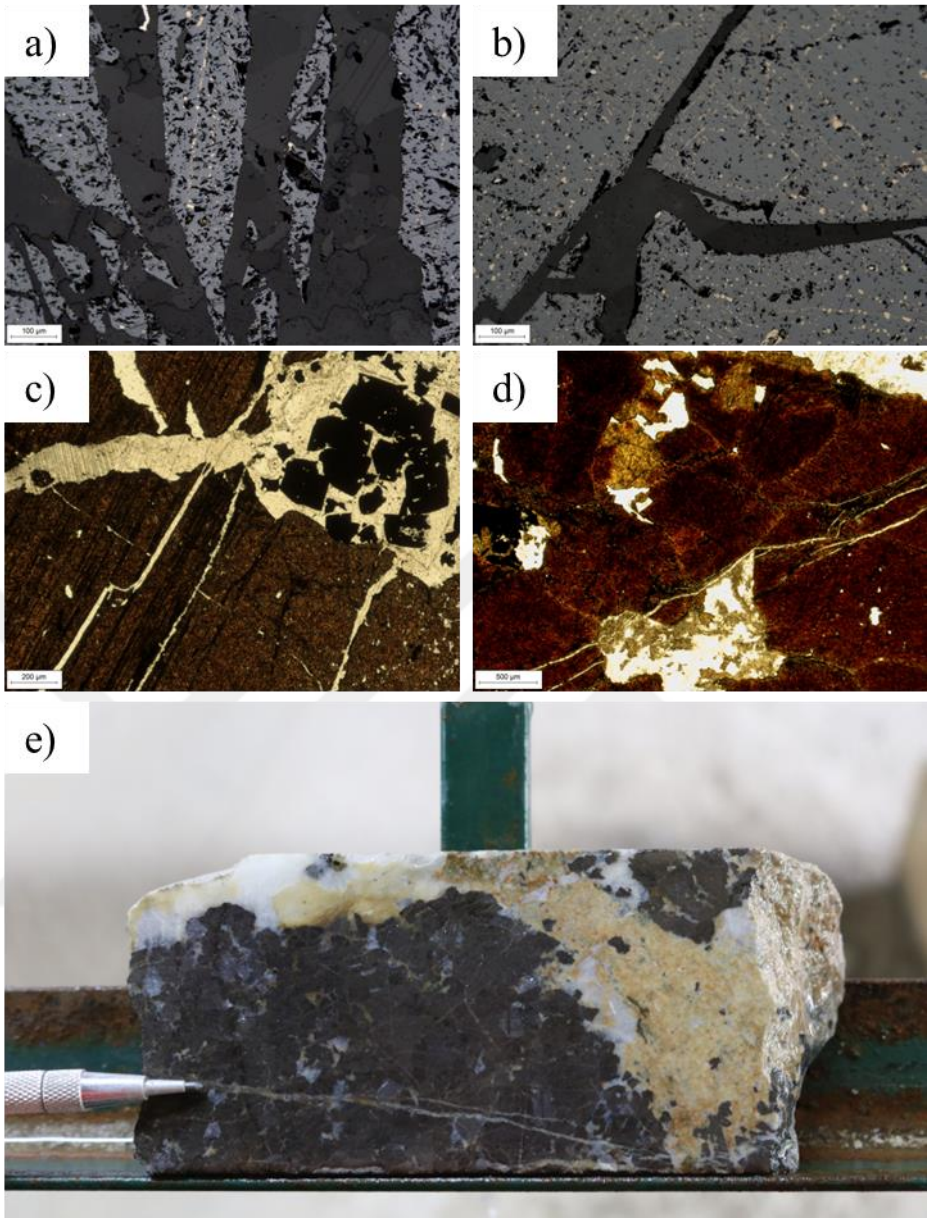


Figure 5-25. Hand specimen and microphotographs of sphalerite mineralized samples a) microphotograph (XPL, RL image) of sphalerite with chalcopyrite disease texture cross-cut by calcite (drill hole EU-046, 102.00 m), b) microphotograph (XPL, RL image) of sphalerite with chalcopyrite disease texture cross-cut by calcite (drill hole EU-046, 102.40 m), c) microphotograph (PL, TL image) of brownish colored sphalerite cross-cut by calcite with opaque minerals (possible pyrite) (drill hole EU-046, 102.40 m), d) microphotograph (PL, TL image) of reddish brown colored sphalerite cross-cut by calcite (drill hole EU-081, 82.80 m), e) drill core photograph of massive and disseminated sphalerite (drill hole EU-046, 102.40 m) Abbreviations: cpy = chalcopyrite, sph = sphalerite, RL = reflected

light, TL = transmitted light, PPL = plane-polarized light, XPL= cross-polarized light.

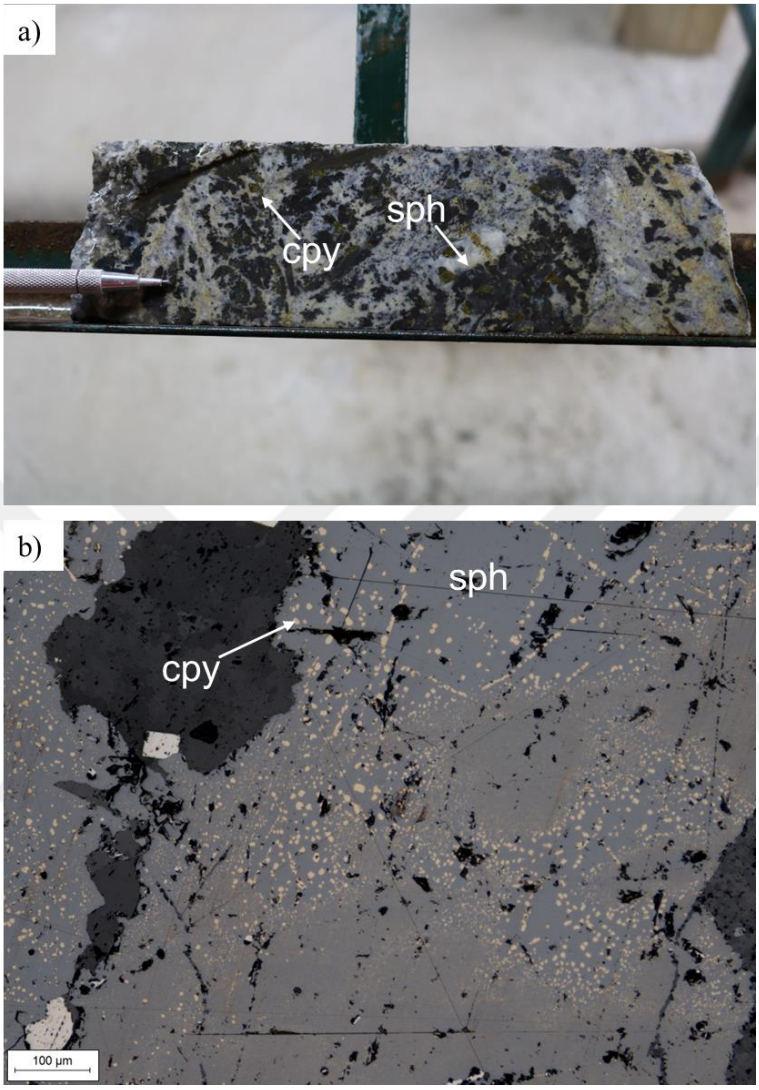


Figure 5-26. Hand specimen and microphotographs of sphalerite and chalcopyrite mineralized samples. a) drill core photograph of retrograde skarn with disseminated sphalerite and chalcopyrite (drill hole EU-081, 85.00 m), b) microphotograph (XPL, RL image) of sphalerite showing chalcopyrite disease texture (sample EU81-8150, drill hole EU-081, 81.50 m), Abbreviations: cpy = chalcopyrite, sph = sphalerite, RL = reflected light, XPL = cross-polarized light.

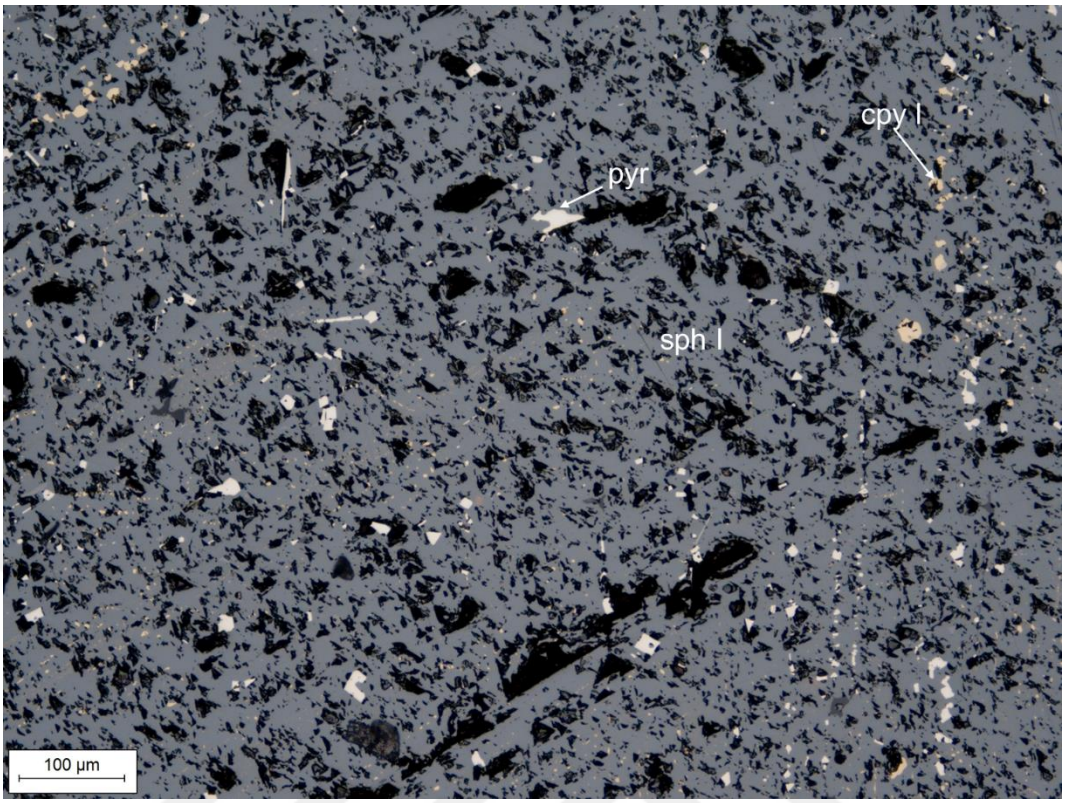


Figure 5-27. Microphotograph (XPL, RL image) microphotograph (XPL, RL image) of pyrrhotite replacement of sphalerite showing chalcopyrite disease texture (drill hole EU-094, 86.60 m), Abbreviations: pyr = pyrrhotite, sph = sphalerite, cpy = chalcopyrite, RL=reflected light, XPL = cross-polarized light.

Chalcopyrite occurs as medium- to coarse-grained crystals forming massive aggregations or disseminations. Chalcopyrite is generally accompanied by pyrite and magnetite in the studied samples. Pyrite occurs as euhedral, medium- to coarse-grained crystals. In most studied samples, pyrite has an early timing from the magnetite. Disseminated crystals of pyrite have been subsequently surrounded by sphalerite, chalcopyrite, magnetite, and specularite, or fractures within pyrite were filled by these minerals.

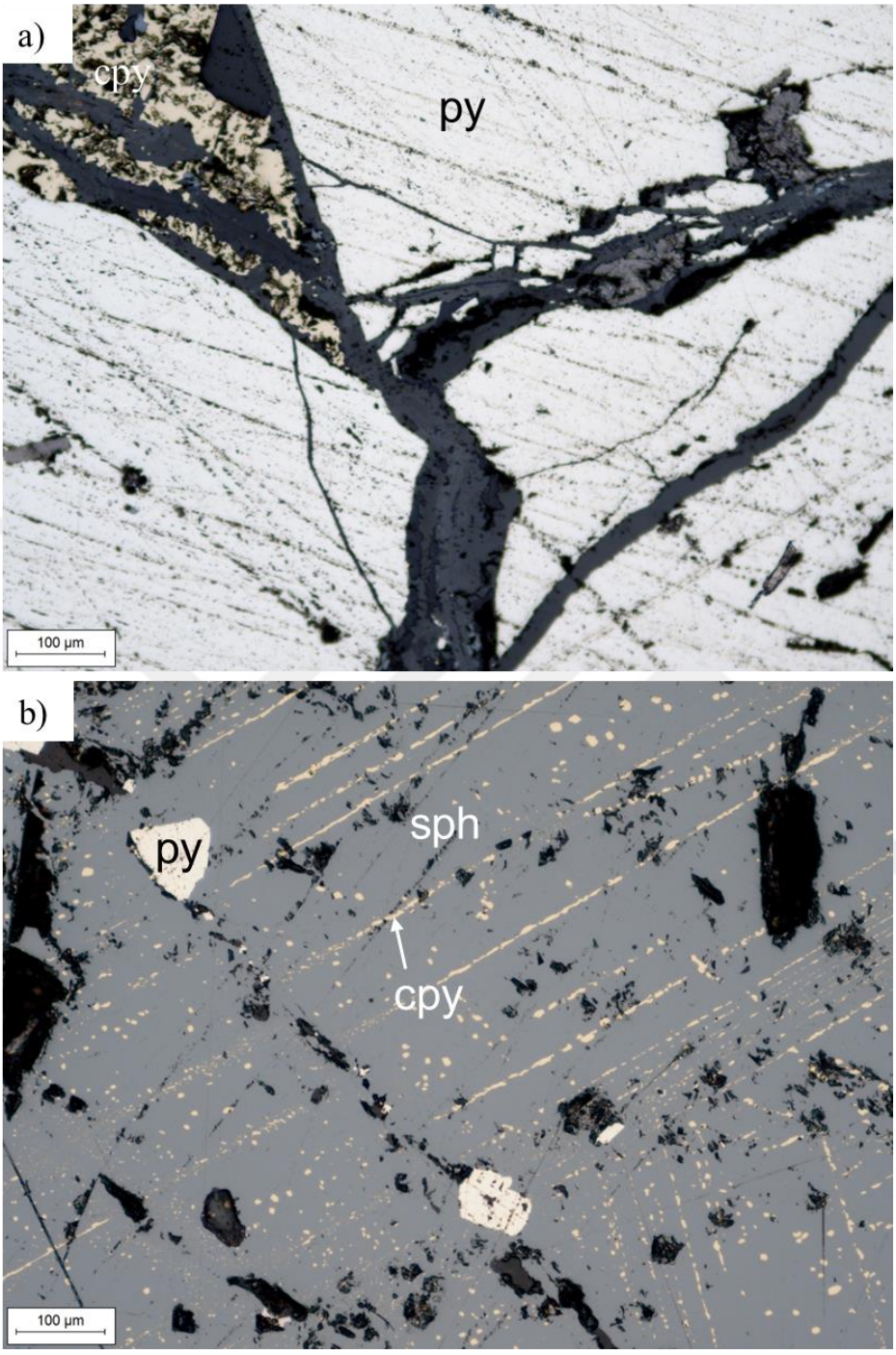


Figure 5-28. a) Microphotograph (XPL, RL image) of euhedral pyrite with chalcopyrite (drill hole EU-046, 115.00 m), b) microphotograph (XPL, RL image) of sphalerite I (chalcopyrite disease) which is intersected by pyrite (drill hole EU-046, 112.00 m), Abbreviations: py = pyrite, sph = sphalerite, cpy = chalcopyrite, RL = reflected light, XPL = cross-polarized light.

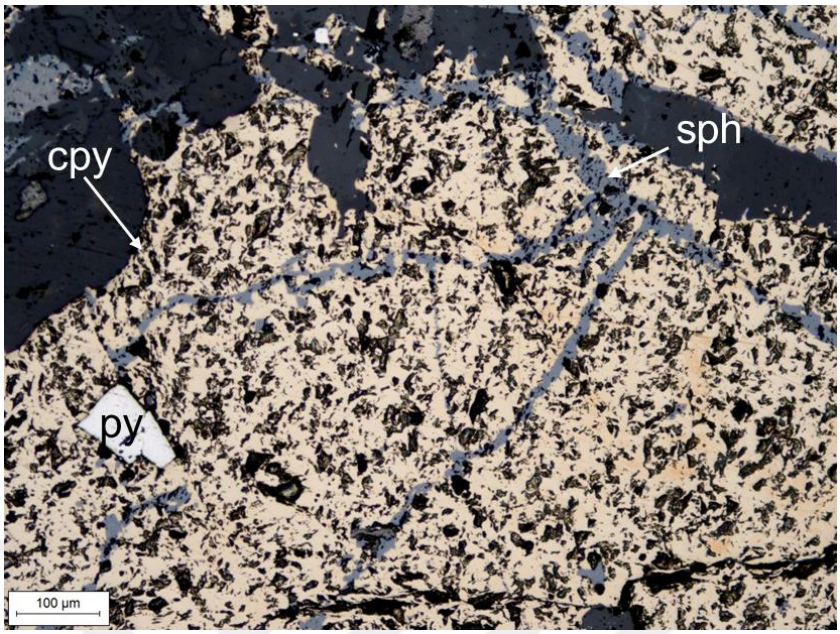


Figure 5-29. Microphotograph (XPL, RL image) showing early euhedral pyrite surrounded by coarse-grained chalcopyrite, which in turn is cross-cut by sphalerite II (drill hole EU-038, 90.40 m). Abbreviations: py = pyrite, sph = sphalerite, cpy=chalcopyrite, RL = reflected light, XPL = cross-polarized light.

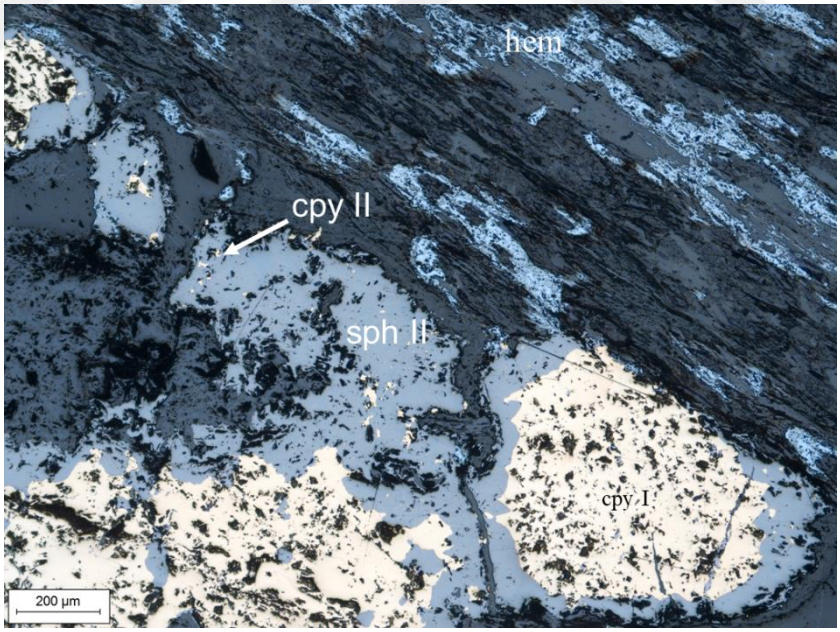


Figure 5-30. Microphotograph (XPL, RL image) showing early coarse-grained chalcopyrite surrounded and partly replaced by sphalerite II, which was later replaced by fine-grained chalcopyrite (chalcopyrite II; drill hole EU-046, 116.10 m).

Abbreviations: py = pyrite, sph = sphalerite, cpy = chalcopyrite, hem = hematite, RL = reflected light, XPL = cross-polarized light.

Molybdenite was not reported in any of the previous studies on the Ulutaş skarn system. In addition, drill hole assays do not show significant molybdenum values. However, petrographic investigations indicated presence of molybdenite within the Ulutaş skarn samples, particularly in Cu-rich skarn mineralization associated with chalcopyrite-magnetite assemblages. Molybdenite almost never displays cross-cutting or intergrowth textures with other sulfide and oxide minerals. It rather occurs as fine- to medium-grained disseminations of tabular crystals within the exoskarn and rarely in endoskarn rocks in close association with sphalerite I, chalcopyrite, magnetite, and hematite (Figure 5-31).

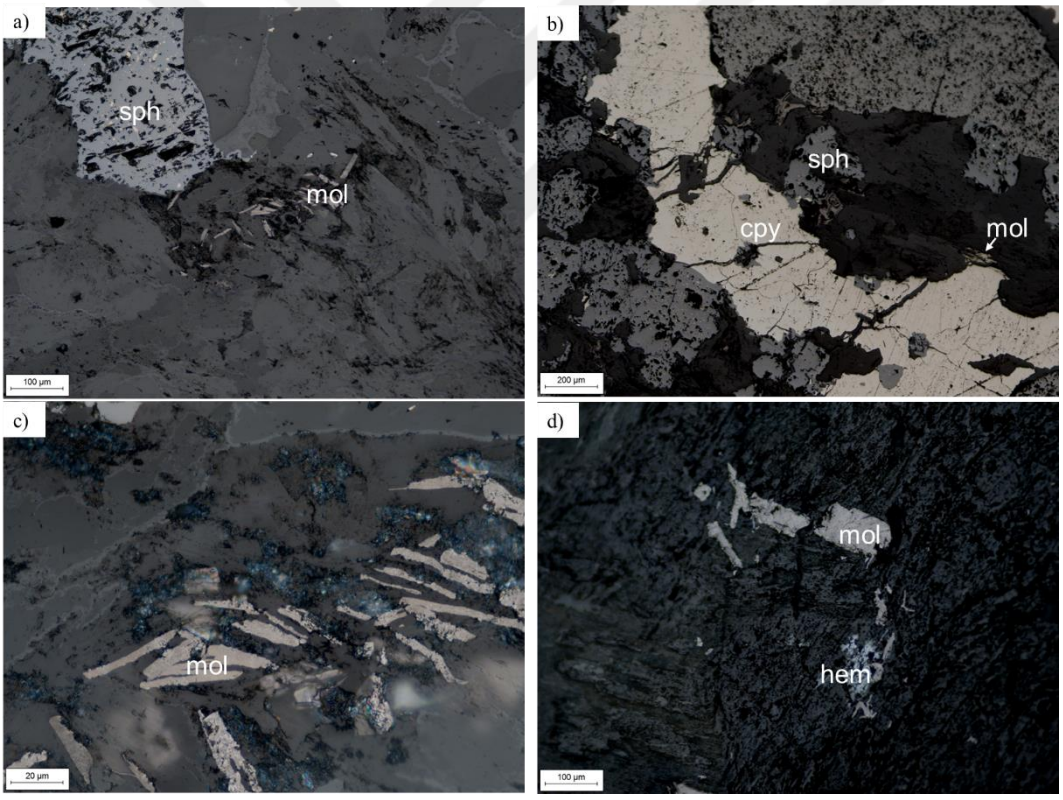


Figure 5-31. a) Microphotograph (XPL, RL image) showing coarse-grained sphalerite I with chalcopyrite disease and disseminations of tabular molybdenite crystals (drill hole EU-081, 125.00 m). b) Microphotograph (XPL, RL image) showing coarse-grained sphalerite, which is cross-cut and replaced by chalcopyrite, alongside tabular molybdenite crystals (drill hole EU-081, 125.00 m). c) Microphotograph (XPL, RL image) showing a cluster of medium-grained, tabular

molybdenite (drill hole EU-081, 125.00 m). d) Microphotograph (XPL, RL image) showing medium-grained, tabular molybdenite with hematite (drill hole EU-046, 116.10 m). Abbreviations: mol = molybdenite, sph = sphalerite, cpy = chalcopyrite, hem = hematite, RL = reflected light, XPL = cross-polarized light.

Marcasite is observed as disseminations of fine- to medium-grained diffuse crystals in close spatial association with pyrite, where it commonly replaces the latter (Figure 5-32). Marcasite is accompanied by pyrite, chalcopyrite, magnetite and hematite in the Ulutaş deposit.

Tetrahedrite is a rare ore mineral at the Ulutaş deposit. It was detected as fine- to medium-grained, subhedral crystals (Figure 5-32). It is accompanied by pyrite, chalcopyrite, and sphalerite. Weak Ag enrichment as indicated by drill core assays is likely associated with tetrahedrite in the Ulutaş Cu-Zn skarn deposit.

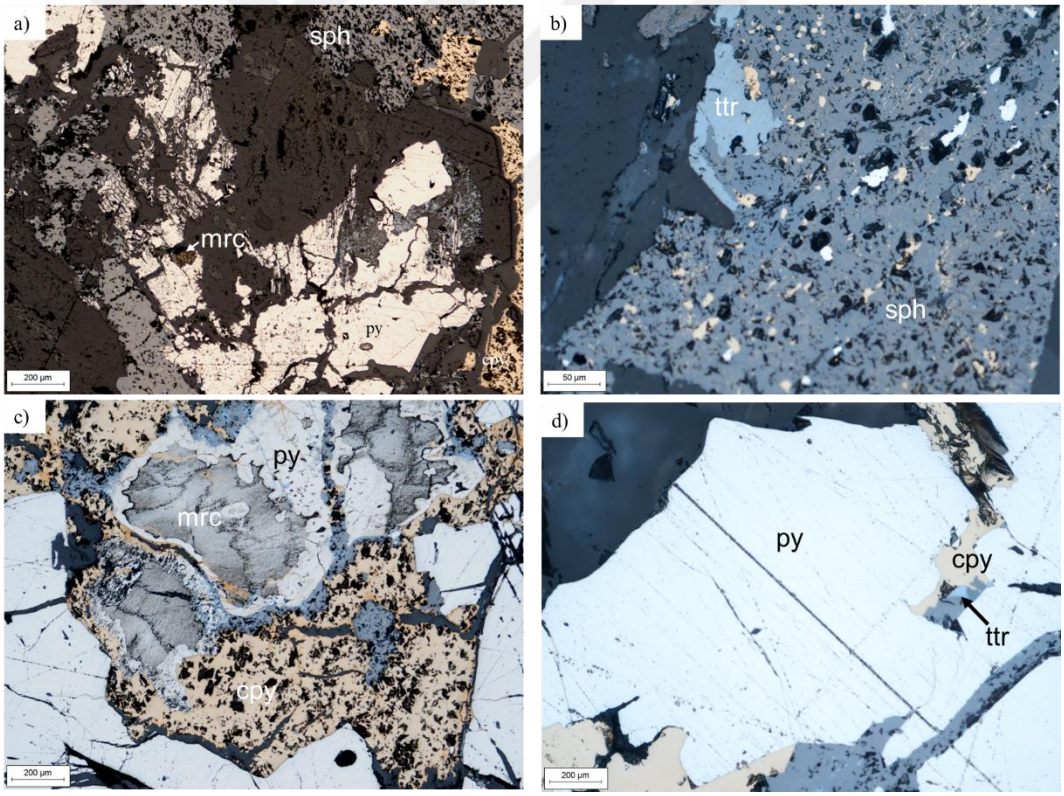


Figure 5-32. a) Microphotograph (XPL, RL image) of anhedral marcasite replaces the euhedral, cataclastic pyrite with chalcopyrite and sphalerite I (drill hole EU-046, 112.00 m), b) microphotograph (XPL, RL image) of tetrahedrite marcasite replaces sphalerite (drill hole EU-038, 90.40 m), c) microphotograph (XPL, RL image) of marcasite replaces py with cpy (drill hole EU-046, 116.10 m), b) microphotograph

(XPL, RL image) of tetrahedrite marcasite accompanied with pyrite and chalcopyrite replaces sphalerite I (drill hole EU-046, 116.10 m). Abbreviations: mrc = marcasite, py = pyrite, sph = sphalerite, cpy = chalcopyrite, ttr = tetrahedrite, RL = reflected light, XPL = cross-polarized light.

Covellite and bornite were also observed locally to have replaced chalcopyrite (Figure 5-33). They are accompanied by pyrite at Ulutaş deposit.

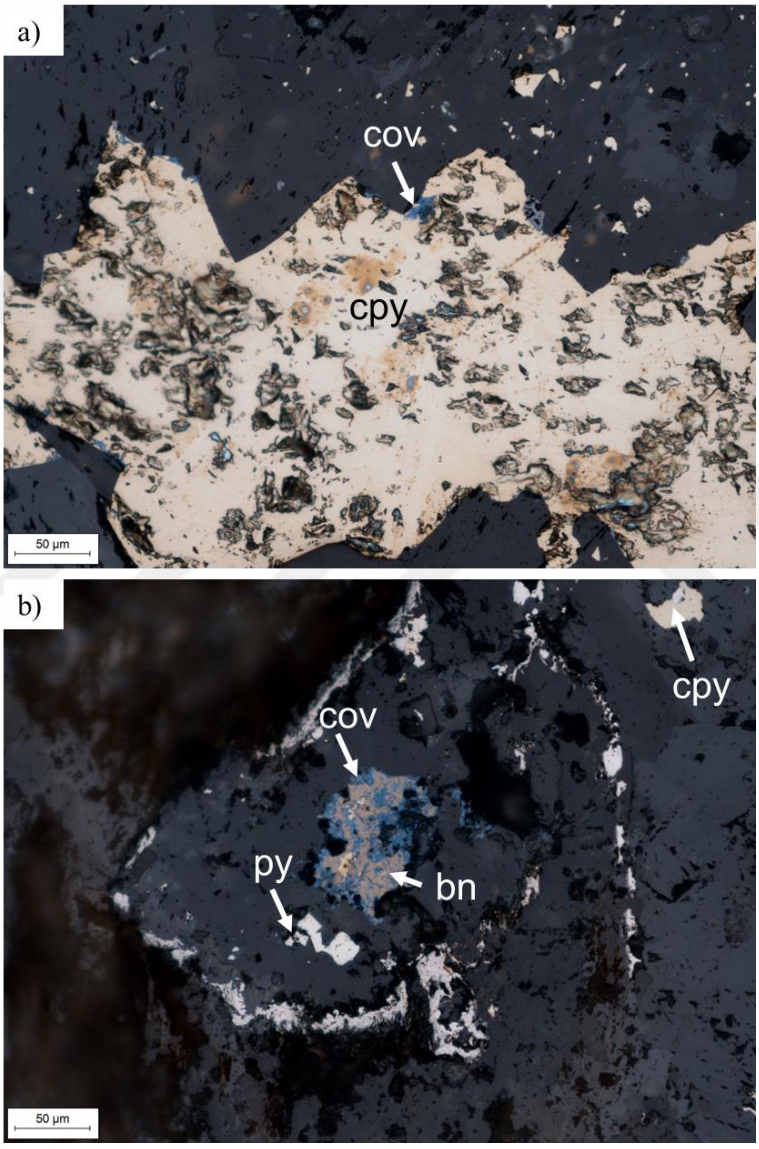


Figure 5-33. a) Microphotograph (XPL, RL image) of covellite replaces the chalcopyrite (drill hole EU-046, 73.00 m), b) microphotograph (XPL, RL image) of bornite replaces covellite with pyrite and chalcopyrite (drill hole EU-046, 73.00 m). Abbreviations: cov = covellite, py = pyrite, bn = bornite, cpy = chalcopyrite, RL = reflected light, XPL = cross-polarized light.

5.3 Supergene Oxidation and Weathering

At Ulutaş, supergene oxidation does not have significant effect on skarn mineralization. However, some near surface oxidation occurs particularly beneath the moraine cover. Strong oxidation usually reaches down to 5–10 m depth with partial oxidation traced to depths of up to 40 meters (Figure 5-34 & Figure 5-35). Deeper partial oxidation is restricted to fault zones. The extent of partial oxidation plays an important role in flotation performance and metallurgical recovery. Due to strong weathering, secondary ore minerals like limonite, goethite, hematite and malachite formed in Ulutaş Cu-Zn skarn type deposit.

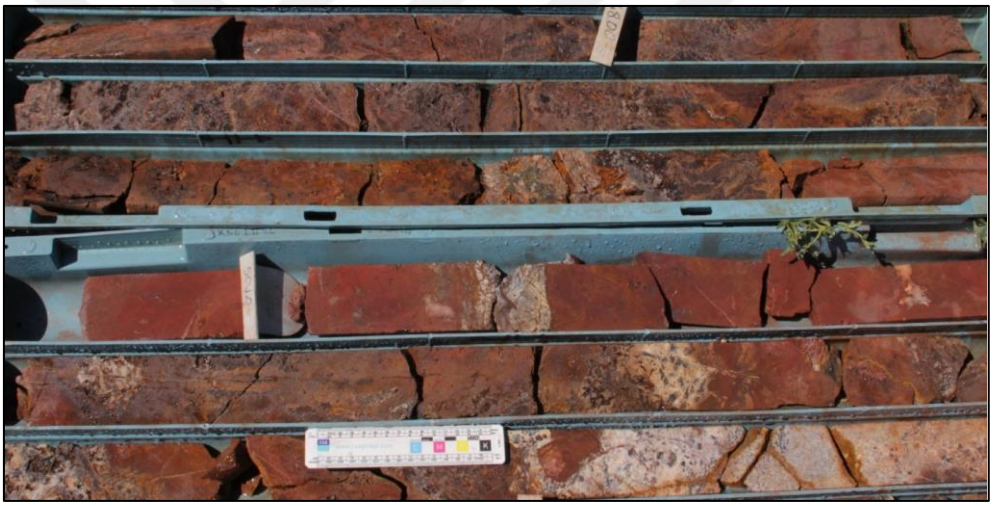


Figure 5-34. Strongly-weathered mineralized skarn (drill hole EU-051, 47-53 meters).



Figure 5-35. Moderately-weathered garnet skarn (drill hole EU-051, 26- 30 meters).

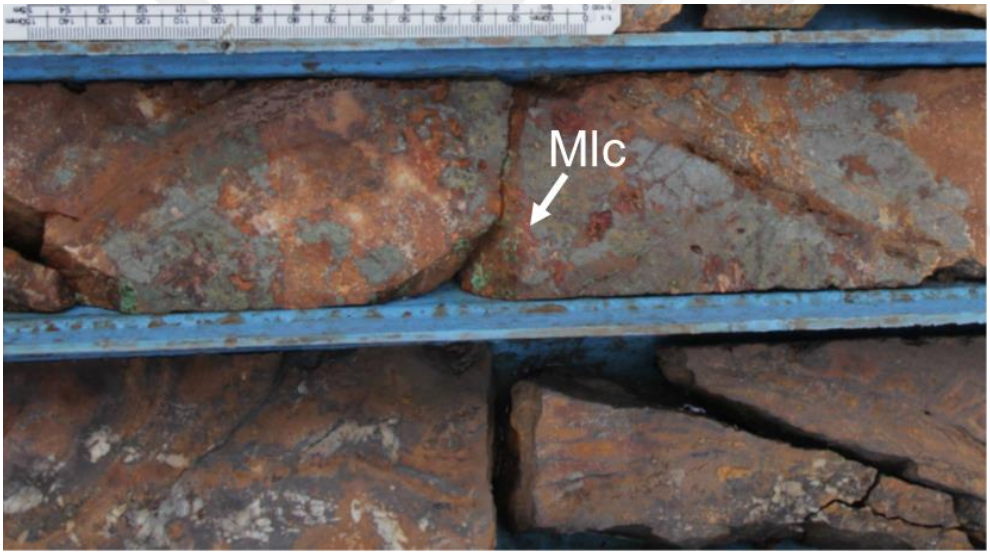


Figure 5-36. Drill core image showing weathered skarn samples represented by limonite and malachite (drill hole EU-038, 50.00 m).

5.4 Metal Associations/Correlations

The interaction of andesite porphyry with the upper and lower marble units, and the presence of clastic type metamorphic rocks between the two units, has resulted in the formation of upper and lower skarn domains at the Ulutaş deposit.

Descriptive statistical studies were conducted to understand the variations of metals in the upper and lower skarns (Table 5-1and Table 5-2). For this study, unpublished dril core data from 244 drill holes from Demir Export's drilling campaign were used. This consisted of 1497 samples from the upper skarn and another 2297 samples from the lower skarn.

Table 5-1. Descriptive statistical parameters for the upper skarn domain as calculated from assay data (lithogeochemical data courtesy of Demir Export)

UPPER SKARN						
	Cu_ppm	**Zn_ppm**	**Ag_ppm**	**Au_ppm**	**Mo_ppm**	**Pb_ppm**
Sample Number	1497	1497	1497	1497	1497	1497
Minimum	0.5	9.0	0.0	0.0	0.3	1.0
Maximum	85,700.00	216,000.00	190.00	0.71	80.00	579.00
Mean	3,984.78	10,393.81	9.90	0.03	5.88	20.41
Median	149.50	384.00	0.80	0.01	3.00	10.00
Range	85,699.50	215,991.00	189.96	0.71	79.70	578.00
Interquartile Range	1,878.50	1,360.00	7.10	0.02	5.12	13.00
Standard Deviation	10,706.11	31,787.92	23.88	0.06	9.12	44.86
1 percentile	1.00	26.00	0.10	0.00	0.50	1.00
5 percentile	3.38	54.90	0.10	0.00	0.50	1.00
10 percentile	7.00	84.80	0.10	0.00	0.50	2.00
25 percentile	24.00	155.00	0.25	0.00	1.00	5.00
75 percentile	1,902.50	1,515.00	7.35	0.02	6.12	18.00
90 percentile	11,810.00	21,940.00	29.24	0.08	13.15	37.00
95 percentile	22,684.00	85,910.00	52.23	0.12	21.00	69.10
99 percentile	61,923.60	168,130.00	138.00	0.30	52.06	251.10

Table 5-2. Descriptive statistical parameters for the lower skarn domain as calculated from assay data (lithogeochemical data courtesy of Demir Export)

LOWER SKARN						
	Cu_ppm	**Zn_ppm**	**Ag_ppm**	**Au_ppm**	**Mo_ppm**	**Pb_ppm**
Sample Number	2267	2267	2267	2267	2267	2267
Minimum	0.50	1.00	0.02	0.00	0.26	1.00
Maximum	97,550.00	347,000.00	238.00	0.49	122.00	470.00
Mean	6,477.99	30,248.05	17.32	0.04	6.51	19.25
Median	637.00	1,080.00	2.50	0.01	3.00	9.00
Range	97,549.50	346,999.00	237.98	0.48	121.74	469.00
Interquartile Range	5,542.00	16,595.00	17.45	0.04	5.00	13.00
Standard Deviation	13,661.08	64,995.97	33.26	0.06	12.47	37.78
1 percentile	1.00	40.00	0.10	0.00	0.50	1.00
5 percentile	4.00	74.40	0.10	0.00	0.50	1.00
10 percentile	9.00	114.00	0.10	0.00	0.50	2.00
25 percentile	38.00	255.00	0.25	0.00	1.00	5.00
75 percentile	5,580.00	16,850.00	17.70	0.04	6.00	18.00
90 percentile	20,252.00	117,000.00	56.54	0.10	15.00	40.00
95 percentile	35,566.00	183,700.00	91.08	0.17	25.12	69.00
99 percentile	70,213.20	301,320.00	161.32	0.31	73.00	183.56

Based on the statistical analysis for the upper skarn and lower skarn domain samples, Ulutaş skarn deposit seems to be enriched in Zn and Cu, but it is poor in terms of Mo, Pb and Au. The maximum Pb value obtained in drill core is 470 ppm over a meter length, and no galena was observed in the studied samples from the Ulutaş deposit. Galena was also not reported during drill core logging. Sphalerite is the main source of Zn, whereas chalcopyrite is the main source of Cu. Bornite and covellite are the other copper ore minerals, but these are rarely observed in the entre skarn system. Minor tetrahedrite detected petrographically is the possible source of Ag and some Cu in Ulutaş.

An elemental correlation analysis was conducted using drill hole assay data in order to understand metal associations of the lower and upper skarn domains in the Ulutaş Zn-Cu skarn deposits (Figure 5-37 & Figure 5-38). Bivariate correlation charts are used to show the relationships between any two metals such as Cu vs. Zn, Cu vs. Ag, etc. The variables are plotted on a scatterplot, with one variable on the x-axis and the other variable on the y-axis. The data points are then plotted on the graph, and a line of best fit is drawn through the data points.

The bivariate scatter plots of Cu, Zn, Pb, Ag, Au, and Mo from the upper skarn domain revealed positive correlations between Cu and Ag, Cu and Au, and Ag and Au, but no correlation is evident between Cu and Zn, Cu and Pb, Cu and Mo, Zn and Pb, Zn and Ag, Zn and Mo, Mo and Pb, Mo and Ag, and Ag Pb and Ag (Figure 5-37).

The bivariate scatter plots of Cu, Zn, Pb, Ag, Au, and Mo from the lower skarn domain indicated similar positive correlations between Cu and Ag, Cu and Au, and Ag and Au. Again, in close similarity to the upper skarn domain, there are no significant correlations between Cu and Zn, Cu and Pb, Cu and Mo, Zn and Pb, Zn and Ag, Zn and Mo, Mo and Pb, Mo and Ag, and Pb and Ag in the lower skarn domain (Figure 5-38).

Table 5-3 shows the correlation coefficients between Cu, Zn, Ag, Au, Pb, and Mo. At both lower and upper skarn, there is a strong correlation between the Cu - Ag, Cu - Au and Ag - Au but not between those variables and Zn.

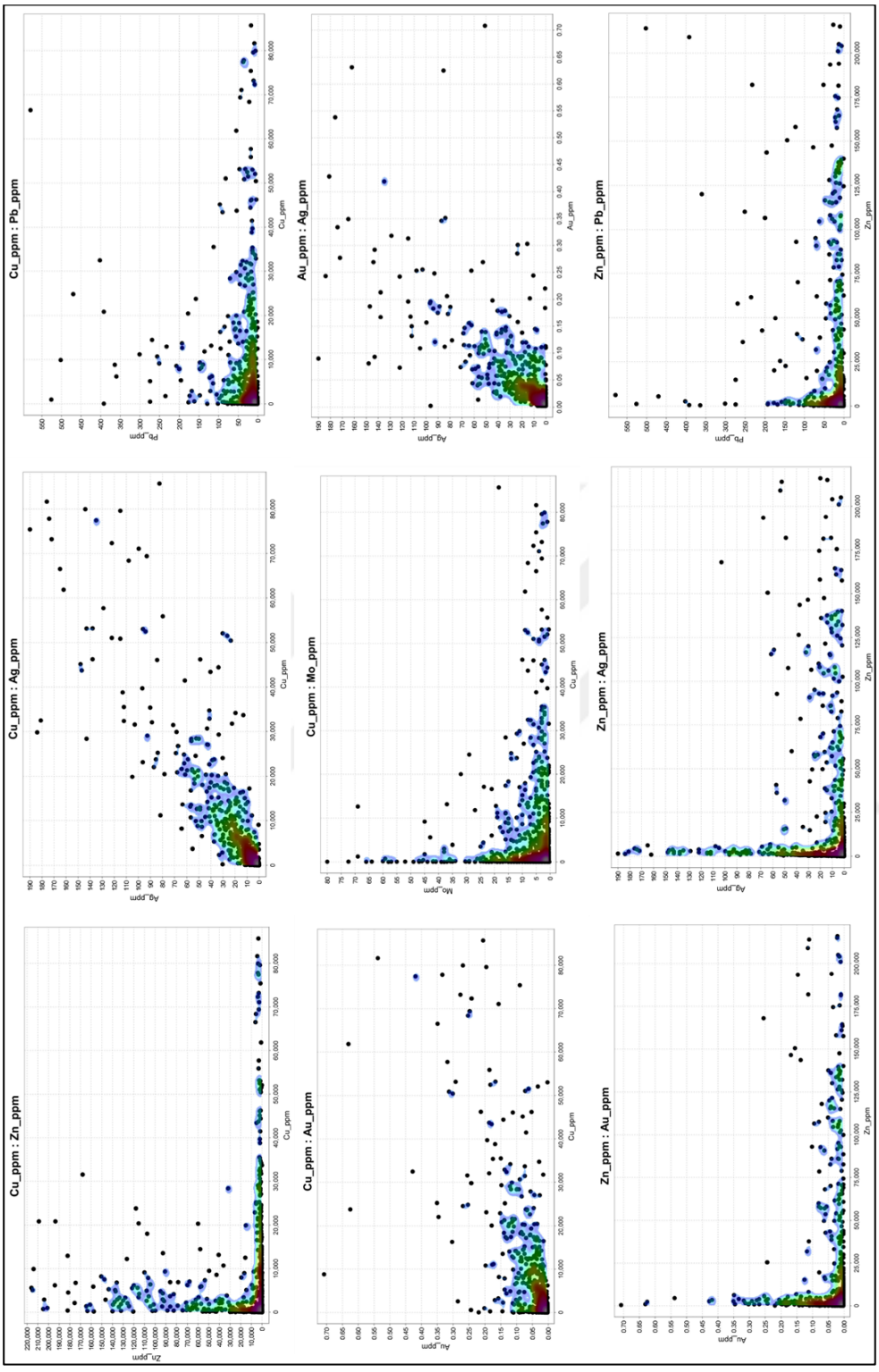


Figure 5-37. Bivariate correlation diagrams for selected metals of Cu, Zn, Ag, Au, Mo, and Pb for the upper skarn domain at Ulutaş (assay data courtesy of Demir Export).

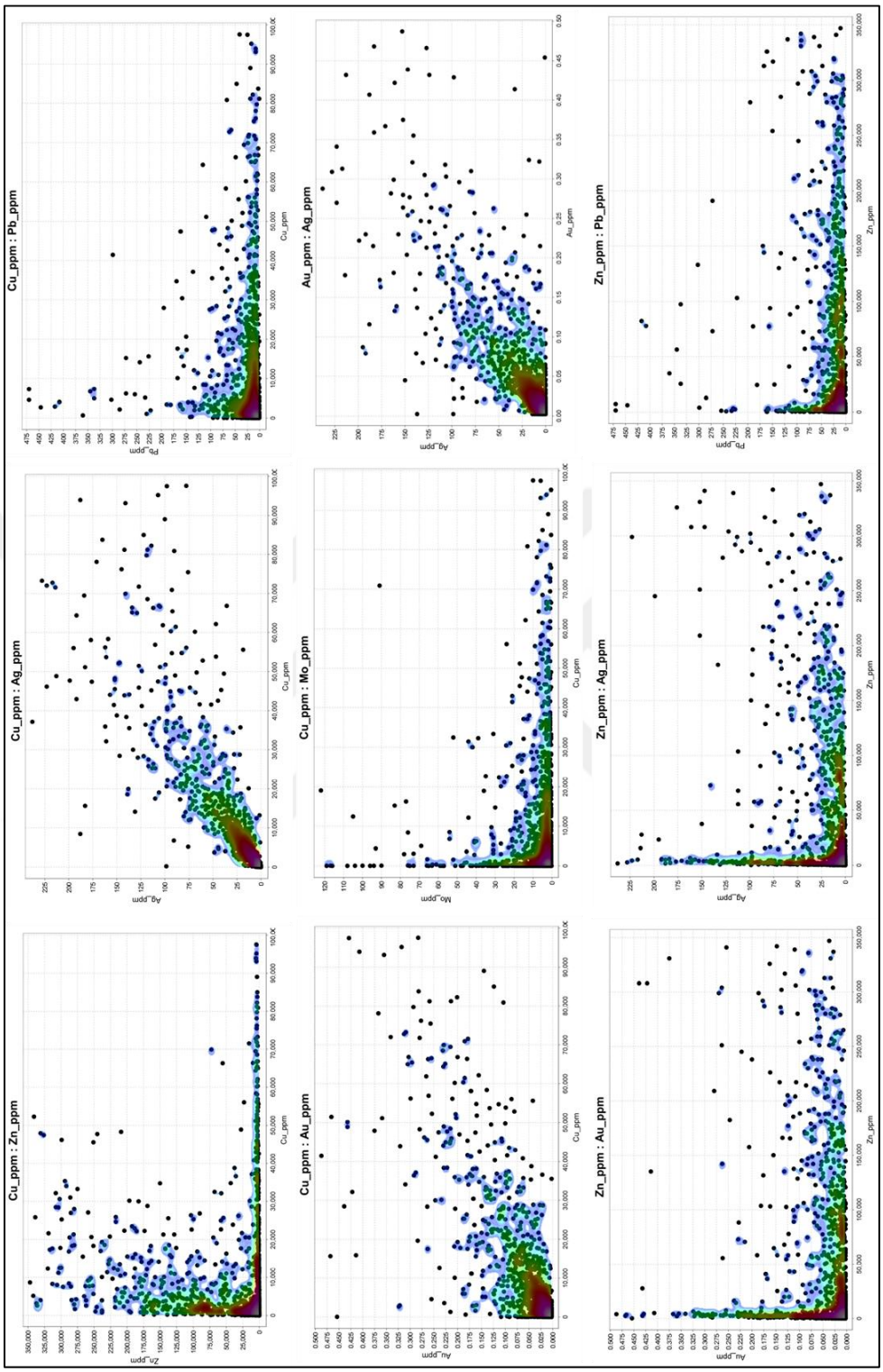


Figure 5-38. Bivariate correlation diagrams for selected metals of Cu, Zn, Ag, Au, Mo, and Pb for the lower skarn domain at Ulutaş (assay data courtesy of Demir Export).

Table 5-3. Correlation coefficients for Cu, Zn, Ag, Au, Mo, and Pb for both Upper and Lower Skarn domains at Ulutaş (assay data courtesy of Demir Export)

UPPER SKARN						
Correlation	**Cu_ppm**	**Zn_ppm**	**Ag_ppm**	**Au_ppm**	**Mo_ppm**	**Pb_ppm**
Cu_ppm	1.00	0.04	0.89	0.72	-0.02	0.21
Zn_ppm	0.04	1.00	0.11	0.06	-0.11	0.22
Ag_ppm	0.89	0.11	1.00	0.78	-0.01	0.34
Au_ppm	0.72	0.06	0.78	1.00	0.01	0.40
Mo_ppm	-0.02	-0.11	-0.01	0.01	1.00	0.05
Pb_ppm	0.21	0.22	0.34	0.40	0.05	1.00

LOWER SKARN						
Correlation	**Cu_ppm**	**Zn_ppm**	**Ag_ppm**	**Au_ppm**	**Mo_ppm**	**Pb_ppm**
Cu_ppm	1.00	0.14	0.87	0.79	0.00	0.13
Zn_ppm	0.14	1.00	0.28	0.21	-0.09	0.22
Ag_ppm	0.87	0.28	1.00	0.80	0.00	0.26
Au_ppm	0.79	0.21	0.80	1.00	0.01	0.26
Mo_ppm	0.00	-0.09	0.00	0.01	1.00	0.06
Pb_ppm	0.13	0.22	0.26	0.26	0.06	1.00

As the correlation coefficients shown in Table 5-3 indicate, Cu is strongly correlated with both Ag and Au. This is likely due to deportment of at least some of the Au and Ag in chalcopyrite and possibly the contribution of tetrahedrite group minerals in Cu and Ag enrichments.

In order to understand the metal distribution and economic resource potential at Ulutaş, a domaining study was carried out for Cu and Zn. The information for this study is obtained from Demir Export with data in Excel format, which contains collar, lithology, assay, and survey files. The data also includes a digital map of the geological surface, specific gravity measurements, digital topographic contours with one-meter intervals. These data are gathered to enhance the comprehension of mineralization characteristics. The drillhole database comprised 244 holes (32.077 samples) with depths ranging between 50 and 290.70 m (average: 166.6 m). Preliminary statistical review of assays was completed. Histograms for Zn and Cu are presented in Figure 5-39 and Figure 5-40 respectively. The histogram for Zn was characterized by several populations – below 1% Zn (non-mineralized), between 1%

and approximately 5% Zn and greater than 5% Zn, both representing the mineralized populations. For Cu, 0.3% represents a break in the histogram, indicating a reasonable natural boundary between ore and waste. After considering the mineralization cut-off (0.3 % grade for Cu and 1% grade for Zn) by using histogram trends, ore domaining study was conducted (Figure 5-41).

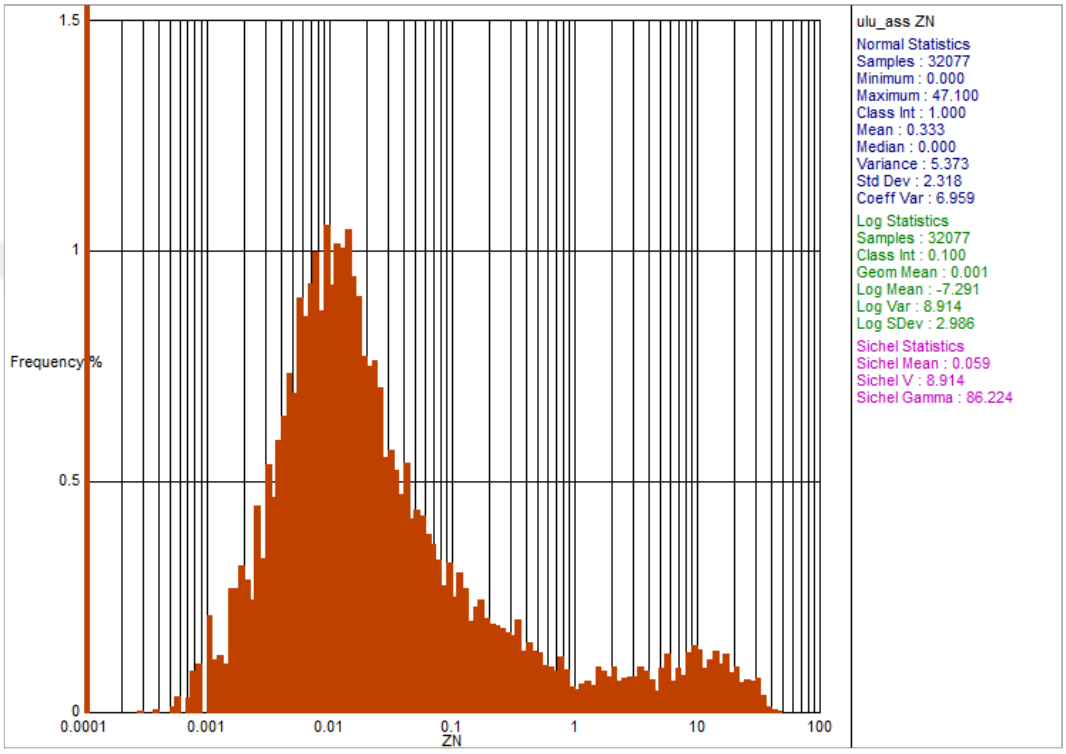


Figure 5-39. Log histogram of Zn assays of the Ulutaş skarn deposit.

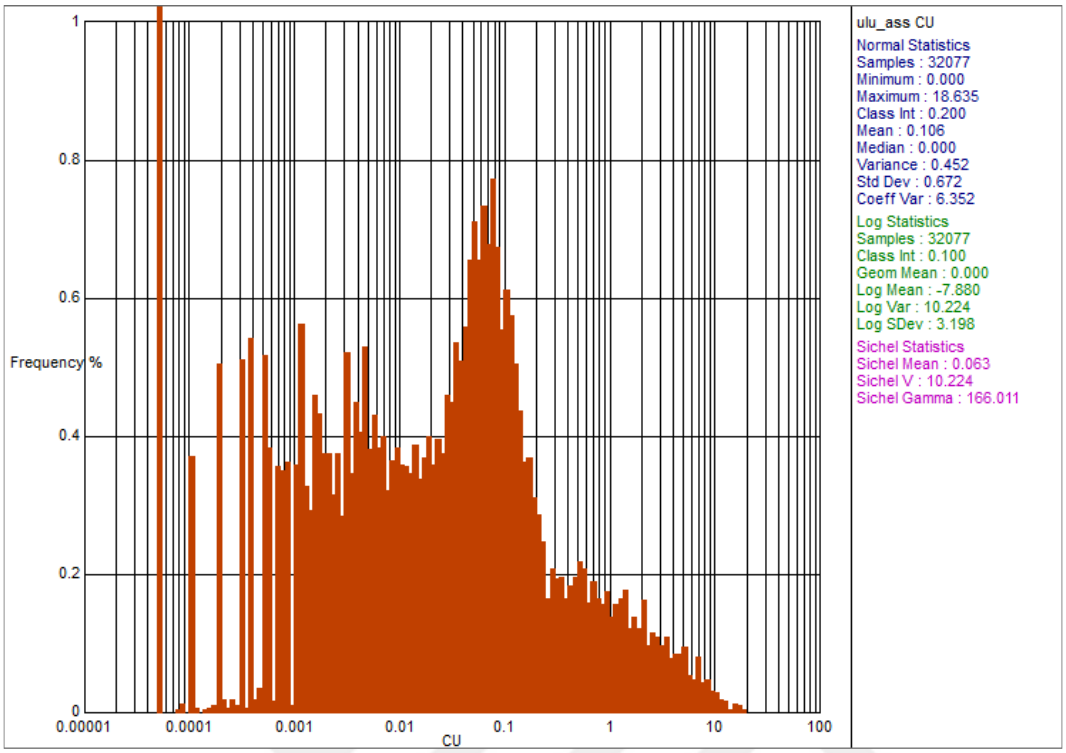


Figure 5-40. Log histogram of Cu assays of the Ulutaş skarn deposit.

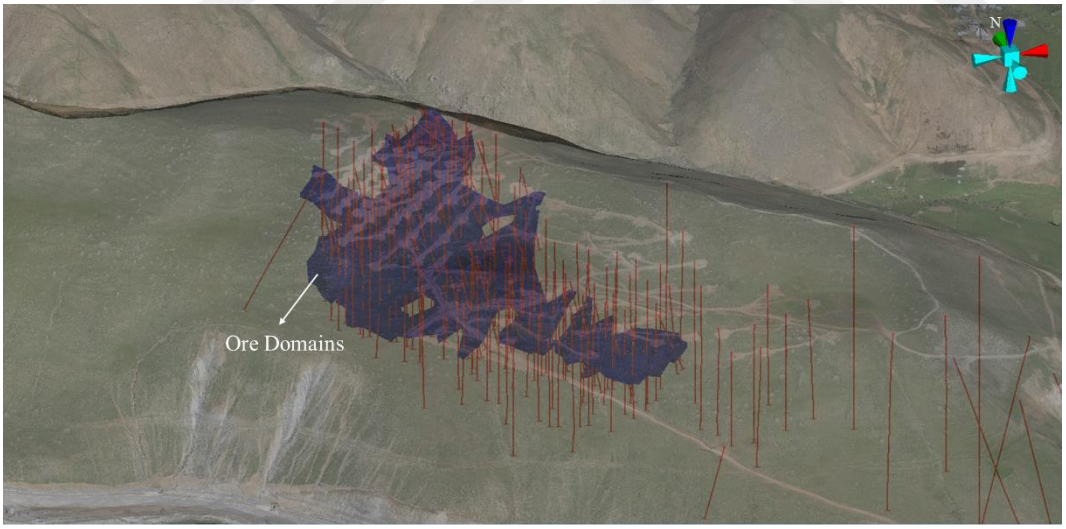


Figure 5-41. General view of ore domains in the Ulutaş skarn deposit (red traces represent the drill holes).

Samples that show Cu and Zn mineralization were used to conduct a sample length analysis. The majority of raw sample intervals are approximately 1 m in length (Figure 5-42)

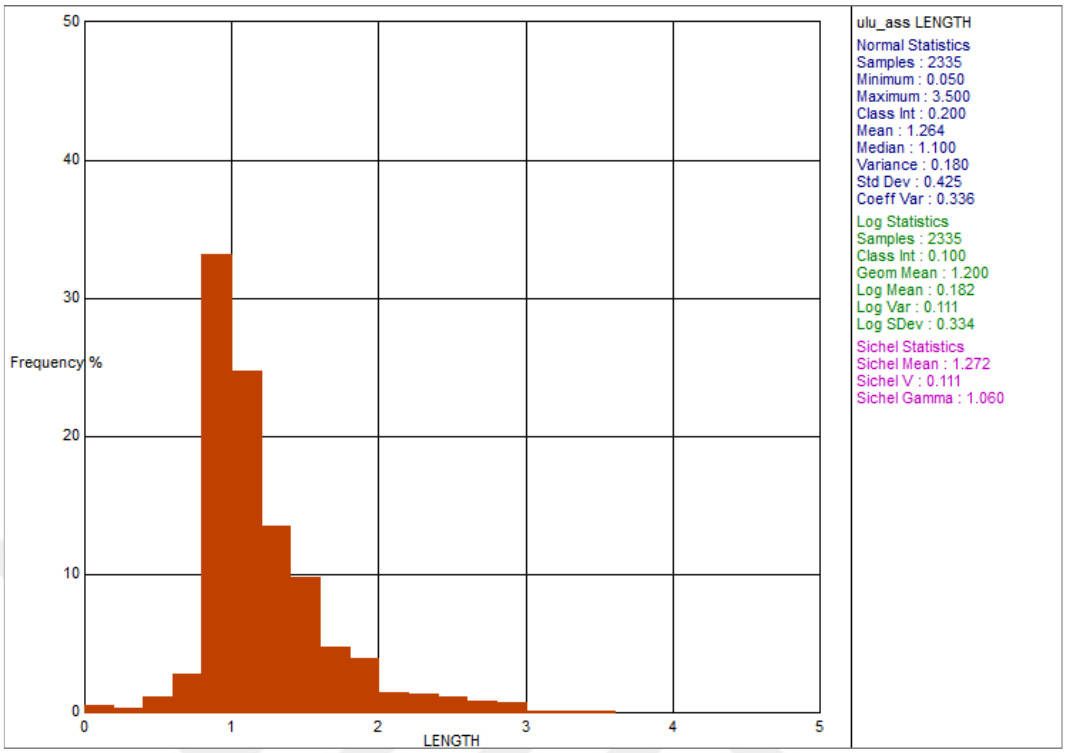


Figure 5-42. Histogram of sample lengths.

Metal zonation is developed at deposit scale in the Ulutaş Cu-Zn skarn system (Figure 5-43). Mineralization is classified as Cu-rich with 0.5% wt. Cu cut-off grade and 1.0 wt.% Zn cut-off grade. The definitions of copper-rich and zinc-rich zones were determined based on the 75 percentile values in descriptive statistics (Table 5-1 and Table 5-2). In general, the Lower Skarn domain is more Zn-rich compared to the Upper Skarn domain, while the Upper Skarn is more enriched in terms of Cu (Figure 5-44 & Figure 5-45). Using drillhole data, a total resource of 3.35 million tons of Cu at an average grade of 1.22 wt.% and an average Zn grade of 3.02 wt.% have been estimated from the numerical modeling study of the Ulutaş Zn-Cu skarn deposit. Ore tonnage of the Lower and Upper Skarn domains with different skarn types are listed in Table 5-4. The obtained result for the Ulutaş Zn-Cu deposit is consistent with the findings of Cihan (2018) and Delibaş et al. (2019), in which a total resource of 3 Mt ore at 1.3 wt.% Cu, 4.77 wt.% Zn were indicated.

To validate the numerical model, various checks are conducted to confirm that the output is both internally and globally consistent. In this study, the validation process includes comparing the model against input data and alternative methods (Table 5-5). This is done to ensure the accuracy and reliability of the resource model. Swath plots were created to compare the model grades and sample grades in a certain direction. As seen in Figure 5-46 and Figure 5-47 the model grades and the sample grades shows the sample trend, and this indicates that numerical model represents the drill hole assay data from Ulutaş Cu-Zn skarn type deposit.

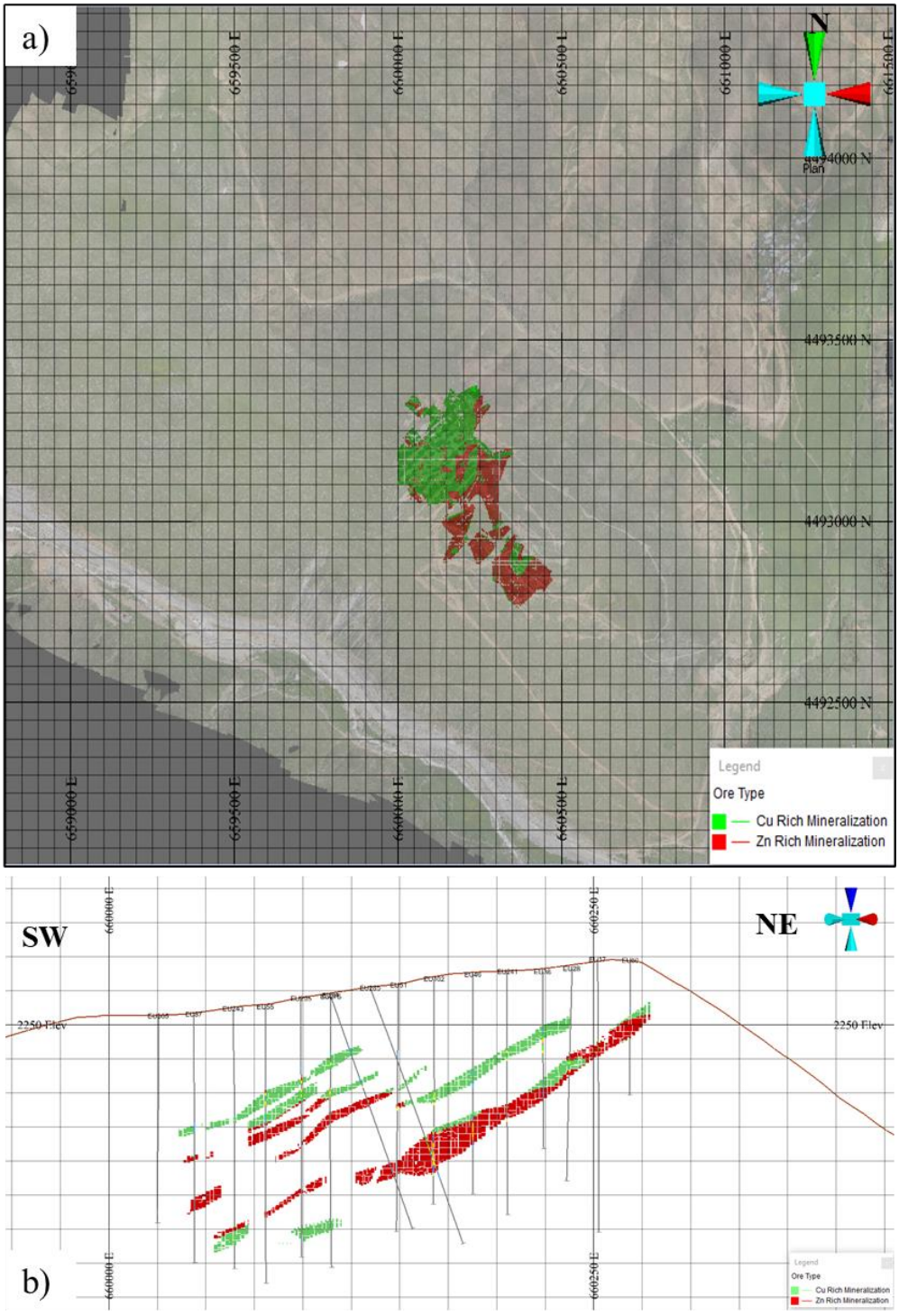


Figure 5-43. a) Plan view, and b) Cross-sectional view showing spatial distribution of Cu- and Zn-rich domains at the Ulutaş Zn-Cu skarn deposit as based on drill hole data of Demir Exports.

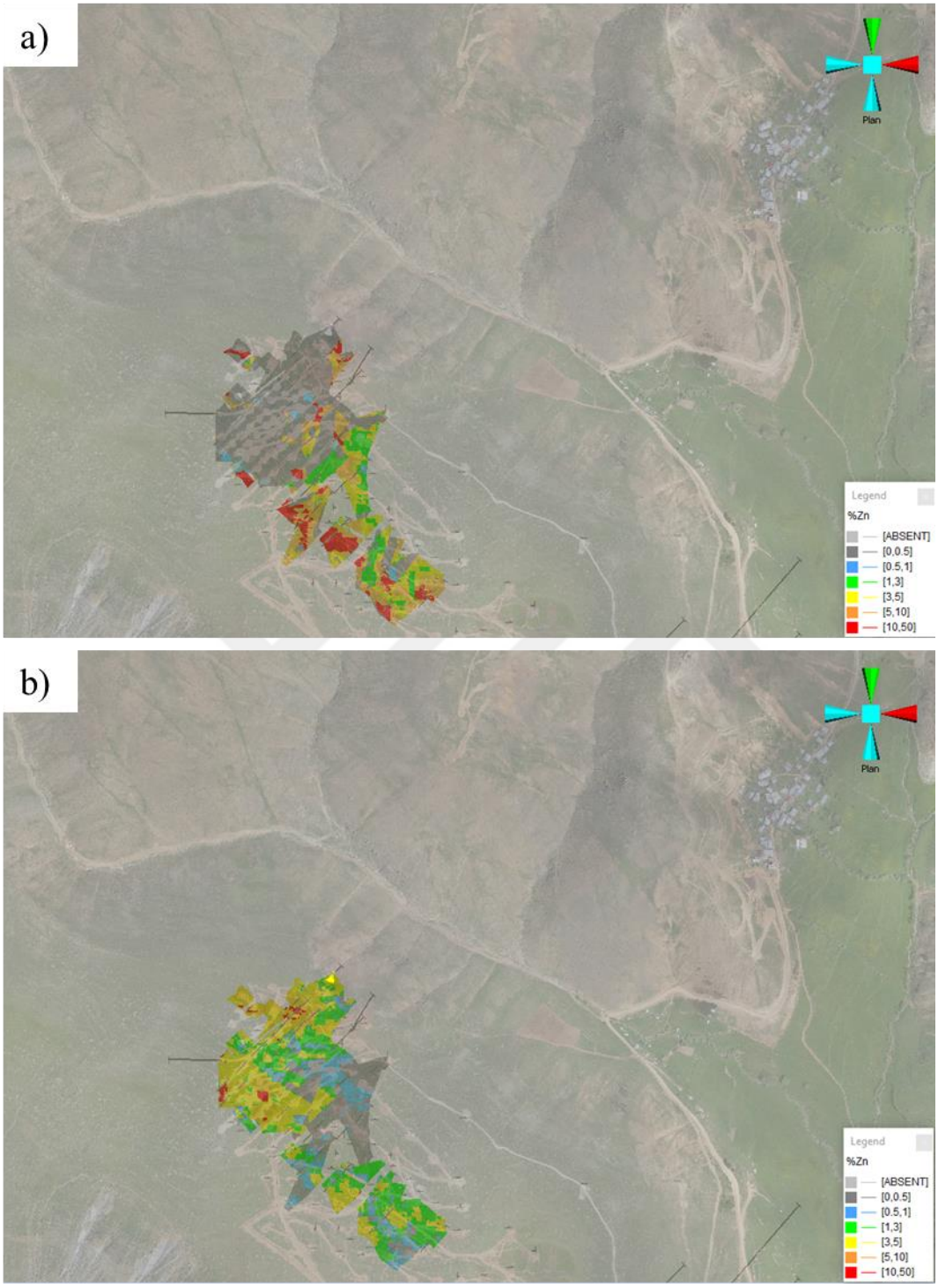


Figure 5-44. Spatial distribution of a) Cu and b) Zn grade shells at Ulutaş as projected on to surface (assay data courtesy of Demir Export).

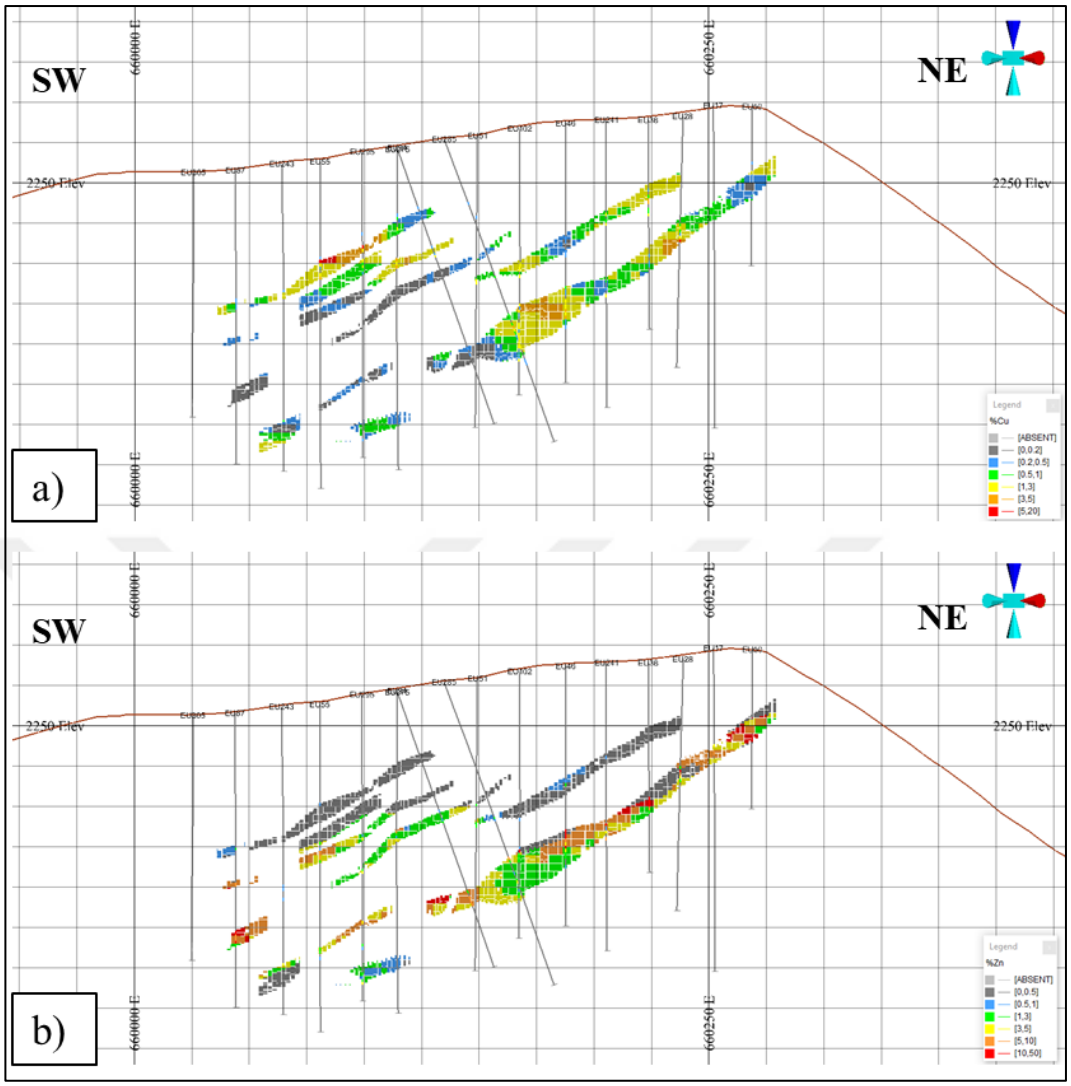


Figure 5-45. Cross-sectional views of a) Cu and b) Zn grade shells at the Ulutaş Cu-Zn skarn deposit (assay data courtesy of Demir Export).

Table 5-4. Total tonnage and metal grade values estimated for various skarn domains at the Ulutaş deposit as calculated from assay data of Demir Export

Ulutaş Cu-Zn Skarn Type Deposits				
Skarn Locality	**Skarn type**	**Tonnes**	**Cu %**	**Zn %**
Upper Skarn	Garnet	342,190.68	1.26	0.71
	Pyroxene	42,603.69	0.39	4.03
	Retrograde	1,149,281.58	1.06	2.58
Lower Skarn	Garnet	437,855.09	0.92	3.85
	Pyroxene	172,484.81	0.94	4.41
	Retrograde	1,207,647.21	1.53	3.57
Total		**3,352,063.05**	**1.22**	**3.02**

Table 5-5. Raw samples grade vs. numerical model grade comparison

Variable	Samples	Numeric Model	% difference
Cu	1.14	1.05	-7%
Zn	3.85	3.69	-4%

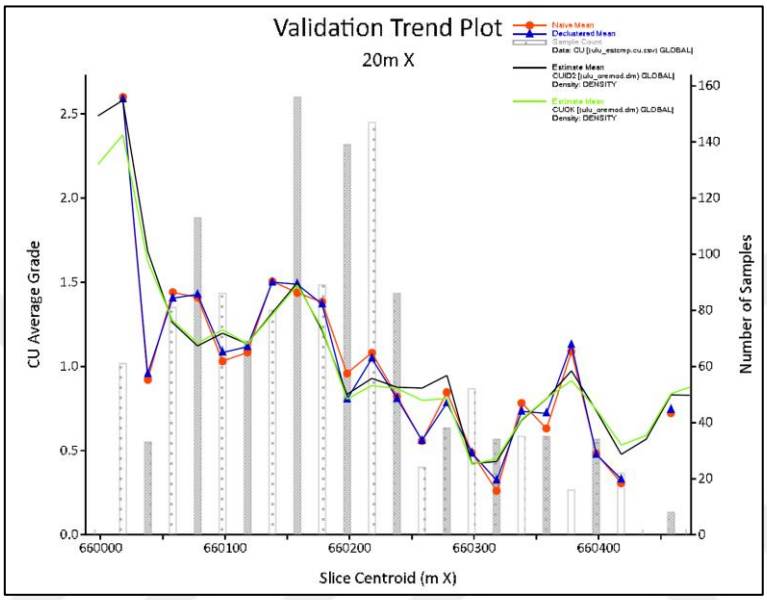


Figure 5-46. Swath plot of Cu grades for raw data vs. numerical model.

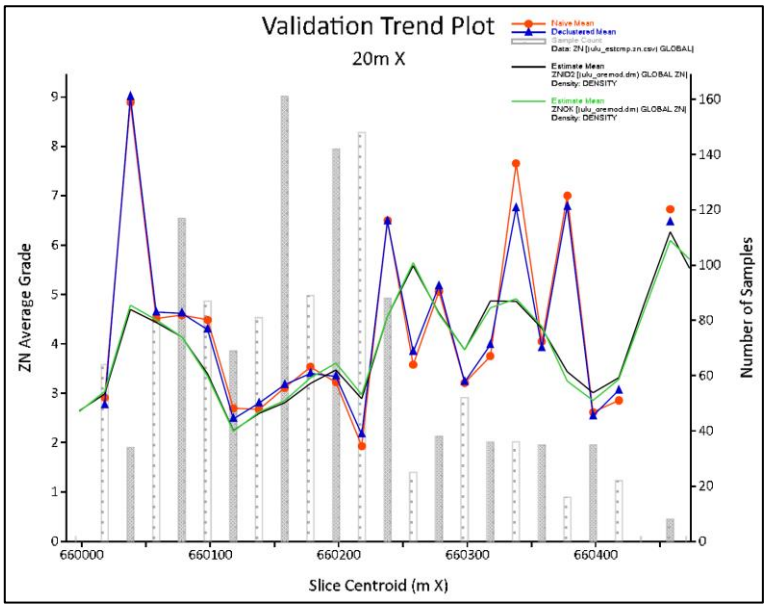


Figure 5-47. Swath plot of Zn grades for raw data vs. numerical model.

CHAPTER 6

DISCUSSIONS AND CONCLUSIONS

6.1 Discussions

6.1.1 Geodynamic Evolution of Ulutaş Cu–Zn Skarn Type Deposit

The Ulutaş Cu-Zn skarn type deposit, which is located in the İspir district in Erzurum (NE Turkey), is currently the most significant base metal skarn system in the entire Eastern Pontide magmatic belt. Copper and zinc mineralization developed within calcareous sedimentary and metamorphic rocks of the pre-Jurassic metamorphic basement, and also partly within the Cretaceous andesite porphyry, granodiorite porphyry, and basaltic dike units.

Due to lack of geochronological data from the skarn and the magmatic host rocks, the timing of the mineralization at Ulutaş is currently unclear. However, by considering the relationship between endoskarn formation within the andesite porphyry and the reported LA-ICP-MS U-Pb zircon age of 131.1 ± 0.9 Ma from the same unit (Delibaş et al., 2016), it is likely that the Ulutaş Zn-Cu skarn system formed during Early Cretaceous. Delibaş et al. (2016) also dated the porphyritic granodiorite, which is the main host lithologies for adjacent İspir Cu-Mo porphyry prospect through LA-ICP-MS U-Pb zircon geochronology and obtained an age of 132.9 ± 0.9 Ma. Delibaş et al. (2019) further dated a molybdenite sample from the İspir Cu-Mo porphyry prospect through Re-Os dating and obtained an age of 131.0 ± 0.7 Ma.

If zircon and molybdenite ages reported by Delibaş et al. (2016 and 2019) from the Ispir-Ulutaş district are accepted to reflect the broad age of formation of the Ulutaş Zn-Cu skarn deposit, then this indicates that Ulutaş (similar to Ispir) has a much

earlier timing compared to the main metallogenic periods of Late Cretaceous and Eocene in the Eastern Pontides. In addition, this timing possibly corresponds to the early initiation stage of magmatism in the Eastern Pontide magmatic arc (REFS).

Early Cretaceous period is not known for widespread alteration and mineralization throughout the Eastern Pontides and most of the economic metallic ore deposits in the region are restricted to two distinct time periods: Late Cretaceous (92–78 Ma) and middle Eocene (51–40 Ma; Kuşcu et al., 2019; Rabayrol et al., 2022). Late Cretaceous deposits are mainly represented by VHMS, porphyry Mo-Cu or VHMS-epithermal hybrid deposits, whereas middle Eocene deposits tend to be of porphyry-epithermal Au-Ag-Cu-Mo style mineralizations (REFS: Revan, Delibas, Kuscu, Rabayrol). The Cu-Zn±Mo association at Ulutaş significantly differs from the younger Cu-Zn-Pb-Au-Ag systems of the belt. The unusual lacking of Pb mineralization at Ulutaş may be related to this early timing of mineralization, in an incipient continental arc setting. In such a tectonic environment, the interaction between ascending arc-related magmas and the overriding continental plate would be limited, which might explain the absence of Pb, a lithophile element, in the Ulutaş skarn system.

Most of the known skarn systems in the Eastern Pontides are also of Late Cretaceous or middle Eocene age (Kuşcu et al., 2019). Although the economic potential and metal contents of these systems differ from that of Ulutaş, there are some common features of Ulutaş and these other regional skarn deposits. The Ulutaş skarn system can be classified as a calcic skarn based on the main marble host rock for Cu and Zn mineralization similar to the majority of the skarn system in the Eastern Pontide belt. Moreover, prograde garnet, pyroxene, and wollastonite with retrograde alteration assemblages mainly including chlorite, epidote, quartz, and calcite is present in Ulutaş skarn system. Cretaceous-aged, sub-alkaline, andesitic/andesitic basalt composition porphyries seem to be the main source of metals and heat in the Ulutaş Cu-Zn skarn type deposit.

Lithogeochemical plots of the precursor quartz-feldspar porphyry and mafic dikes at Ulutaş as based on immobile element concentration such as Nb/Y and Zr/Ti indicated that quartz-feldspar porphyry is mainly of andesitic composition with sub-alkaline character and mafic dikes are mainly of basaltic composition, again with sub-alkaline character. These geochemical features correlate well with other Late Cretaceous igneous systems of the magmatic belt (Giles, 1974; Delibaş et al., 2016 and 2019; Kuşcu, 2019).

6.1.2 Nature of Alteration and Mineralization at Ulutaş Cu–Zn Skarn Type Deposit

Ulutaş can be classified as an exoskarn-dominated, calcic, Cu- and Zn-rich skarn deposit. Although endoskarn within the andesite porphyry, which is probably the main metal and heat source of the skarn system, Ulutaş Cu-Zn deposit is dominated by the presence of exoskarn-hosted mineralization. Main calc-silicate alteration minerals are garnet, pyroxene, and wollastonite. Retrograde alteration, which mainly includes calcite, quartz, chlorite, epidote and hematite overprints these prograde assemblages.

Due to development of multiphase porphyry intrusions, a well-developed skarn zonation cannot be traced at Ulutaş. Skarn zones formed near horizontally horizontal due to the structural orientation of marble units and the sill-like development of the igneous units. Common skarn zonation at skarn deposits can be identified as distal garnet, proximal pyroxene and wollastonite at marble front (Meinert et al., 2005). However, at Ulutaş, garnet-rich calc-silicate alteration extends towards the marble front, where it often terminates into marble (Figure 5-6). Also, garnet is the most dominant calc-silicate mineral within the Ulutaş deposit. Moreover, garnet skarn is replaced by retrograde carbonate, quartz, epidote and hematite alteration, with fine-grained hematite resulting in a strongly reddish appearance.

Mineralization at the Ulutaş Cu-Zn skarn deposit is mainly associated with the retrograde stage alteration. Pyrite, chalcopyrite, sphalerite, magnetite, and hematite/ specularite are the main ore minerals with minor marcasite, tetrhedrite, and molybdenite. Although most Zn-skarns also contain appreciable amounts of Pb (Meinert, 1987; Meinert et al., 2005), there is only anomalous level of Pb and galena was not observed in any of the studied samples. Cu and Zn does not correlate, although these two metals are often observed together where sphalerite has been replaced partially by chalcopyrite. Cu-Ag, Cu-Au, and Au-Ag, on the other hand, show positive correlation, which suggests that Au and part of Ag is associated with chalcopyrite, whereas some Ag is also potentially related to tetrahedrite precipitation.

The siliciclastic metamorphic sequence restricted skarn formation and ore mineralization to between upper and lower marble levels, which resulted in formation of the Upper and Lower Skarn domains. Although there is some economic Cu mineralization within the Lower Skarn, the Upper Skarn zone is more Cu enriched, whereas the Lower Skarn zone is more enriched in terms of Zn.

Most of the skarn deposits in the Eastern Pontides are Fe, Fe-Cu and Cu rich skarns. Ulutaş skarn is Cu and Zn rich which makes that Ulutaş deposit is unique and economically important skarn type in the Eastern Pontide.

6.1.3 Regional Significance of the Ulutaş Cu-Zn Skarn Deposit

Most of the skarn deposits in the Eastern Pontides are related to Late Cretaceous or Middle Eocene intrusions (Yiğit, 2009, Kuşcu, 2019). These intrusions cross-cut older clastic-carbonate rocks from the Jurassic-Cretaceous periods or Late Cretaceous volcanic-volcanoclastic rocks (Kuşcu, 2019). The main skarn types in respect to their metal contents are Fe, Fe-Cu or Cu skarns with no or very limited Zn-Pb skarns (Yiğit, 2009). The majority of skarn deposits in Eastern Pontides are calcic skarns and main calc-silicate minerals are garnet, pyroxene, wollastonite with

retrograde alteration minerals like actinolite, tremolite, epidote, chlorite, calcite and quartz (Kuşcu, 2019).

The Sivrikaya Fe skarn deposit which is located in Rize formed during the Late Cretaceous period along the carbonate layer of a volcanic and sedimentary formation, as well as the İkizdere granitoid which intruded during the Late Cretaceous to Eocene era (Demir et al., 2017). The minerals found in the deposit are andradite-rich garnet, diopside-rich pyroxene, magnetite, hematite, and epidotes (Demir et al., 2017. The main ore minerals of Sivrikaya are hematite and magnetite with lesser amount of pyrite and chalcopyrite (Demir et al., 2017.

Eğrikar Fe-Cu skarn deposit which is located Gümüşhane is classified as calcic exoskarn (Yılmaz, 2016). The main prograde minerals in Eğrikar are garnet, pyroxene and retrograde minerals are epidote, calcite, quartz, actinolite and tremolite (Yılmaz, 2016). Ore minerals of Eğrikar Fe-Cu skarn deposit are hematite, magnetite, pyrite and chalcopyrite. The main intrusion which is related to the formation of Eğrikar Fe-Cu skarn deposit is Late Cretaceous aged monzogranite (Yılmaz, 2016). There is no indication about the deposit economic or not.

Kotana Fe skarn deposit which is located 30 km south of Giresun is also classified as calcic exoskarn which is hosted by pre-Lower Jurassic Pınarlar metamorphics which cross-cut by Late Cretaceous-Eocene aged Aksu biotite monzogranite (Çiftçi, 2010). The principal ore minerals of Kotana Fe skarn pyrrhotite and magnetite with minor pyrite and chalcopyrite which is replaced by trace sphalerite (Çifçi, 2010). There is no indication about the deposit economic or not.

The Ulutaş skarn system differs from the Fe, Cu and Fe-Cu skarn deposits in the Eastern Pontides in that it contains both copper and zinc and has economic potential (Table 6-1). There is no documented economic Cu-Zn skarn system in the Eastern Pontide rather than Ulutaş Cu-Zn skarn type deposit.

Table 6-1. Summary characteristics of Cretaceous skarn deposits in the Eastern Pontides Abbreviations: grt=garnet, px= pyroxene, wol=wollastonite, ep=epidote, chl=chlorite, cal=calcite, qtz=quartz, tr=tremolite, act=actinolite, mag=magnetite,

hem=hematite, cpy=chalcopyrite, py=pyrite, sph=sphalerite, mo=molybdenite, po=pyrrhotite

	Ulutaş	Sivrikaya	Eğrikar	Kotana
Basement	pre-Jurassic metamorphics	Liassic volcano-sedimentary rocks	Late Cretecceous dacite and	pre-Jurassic Pınarlar
Intrusion type	Quartz feldspar porphyry	Granitoid	Monzogranite	Monzogranite
Host Lithology	Marble	Dolomitic Limestone	Limestone	Marble
Skarn Type	Calcic exoskarn	Calcic exoskarn	Calcic exoskarn	Calcic exoskarn
Mineralization	Zn, Cu	Fe	Fe-Cu	Fe
Alteration Minerals	grt, px, wol, ep, chl, cal, qtz	grt, px, ep, tr, act, mag, hem, qtz, cal	grt, px, ep, tr, act, qtz, cal	grt, px, ep, tr, act, qtz, cal
Ore Minerals	cpy, py, sph, mag,hem, mo	mag, hem, py, cpy	mag, hem, py, cpy	mag, hem, py, po, sph
Ore Texture	Massive, disseminated	Nodular, massive, disseminated	Massive, disseminated	Massive, disseminated
Intrusion age	Early Cretaceous (1,2)	Late Cretecceous	Late Cretecceous	Late Cretecceous
Data Source	1, in this study	3	4	5

Data Sources: 1= Giles (1974), 2=Delibaş et al. (2016) 3= Demir et al. (2017), 4= Yılmaz (2016)

6.1.4 Global Significance of Ulutaş Cu-Zn Skarn Type Deposit

Cu-Zn skarns are uncommon because Zn sulfides dissolve more easily than Cu sulfides, resulting in a zonation pattern where Cu mineralization is found close to the source and Zn mineralization is found farther away due to fluids moving away from the source and depositing sphalerite (Chang & Meinert, 2008). However, in Cu-Zn skarns, this zonation pattern is condensed, and Zn mineralization occurs in close proximity to Cu mineralization (Chang & Meinert, 2008). One of the most well known Cu-Zn skarn deposits are Empire Cu-Zn, Antamina Cu-Zn and Velerdeña Zn-(Pb-Cu) skarn deposits.

Empire Cu-Zn Skarn which is located Idaho is economically important Cu-Zn skarn type deposit which has resources of 18 Mt grading 0.49 % Cu and 0.19 % Zn, 13.5 g/t Ag and 0.48 g/t Au (Chang & Meinert, 2008). Generally, endoskarn occurs in granite porphyry and Empire Cu-Zn skarn is endoskarn dominated system. Prograde alteration characterized by garnet, pyroxene and wollastonite in Empire Cu-Zn skarn and retrograde alteration consists of quartz, calcite and chlorite. Primary Cu mineralization consists of chalcopyrite, and it occurs as dissemination or veinlets. Sphalerite which is the primary source of Zn mineralization occurs both endoskarn and exoskarn. Cu and Zn mineralization is accompanied by magnetite and minor molybdenite in the Empire Cu-Zn Skarn (Chang & Meinert, 2008).

Antamina Cu-Zn skarn deposit in Peru has resources of 2,968 Mt grading 0.89 % Cu and 0.77 % Zn, 11 g/t Ag and 0.002 % Mo (Mrozek, 2018). Antamina Cu-Zn skarn shows skarn alteration and mineralization around multi-phase porphyry intrusion. The alteration pattern consists of potassic alteration to transition into endoskarn then exoskarn. Distinct zonation pattern which is identified by garnet color change, garnet:clinopyroxene ratio and garnet and clinopyroxene composition. Skarn mineralogy is dominated by garnet with lesser clinopyroxene. Retrograde alteration in Antamina Cu-Zn skarn is characterized by quartz, calcite, calcite, chlorite, epidote and vesuvianite. The main ore minerals of Antamina Cu-Zn are chalcopyrite, pyrite, sphalerite, magnetite with molybdenite, galena bornite, pyrrhotite (Mrozek, 2018).

The nature of the precursor magmatism for the Velardeña skarns is dikes and stocks of porphyritic texture with granitic to granodioritic composition (Jiménez-Franco et al., 2020). The type of intrusion related to skarn formation is dike-related and has a granitic to granodioritic composition. The main calc-silicates minerals in the Velardeña are calcic clinopyroxene and garnet in the exoskarn and wollastonite in the endoskarn (Jiménez-Franco et al., 2020). Calcite, quartz, actionolite, epidote and chlorite are the main retrograde minerals with sulfides (Jiménez-Franco et al., 2020). Main ore minerals in the Velardeña are sphalerite, galena, chalcopyrite, pyrite and pyrrhotite (Jiménez-Franco et al., 2020).

Ulutaş Cu-Zn deposit have similarities and differences between Empire Cu-Zn, Antamina Cu-Zn and Velerdeña Zn-(Pb-Cu) skarn deposits. Ulutaş Cu-Zn skarn deposit is more exoskarn dominated rather than endoskarn unlike with Empire Cu-Zn skarn deposit. Prograde and retrograde alteration minerals are similar in Ulutaş skarn with Empire, Antamina and Velardeña. Moreover, potassic alteration can observed in Ulutaş Cu-Zn skarn system like Antamina. Formation of Ulutaş Cu-Zn skarn deposit also related with the multi-phase porphyry system like Antamina and Velardeña. Galena is observed in Empire, Antamina and Velardeña skarn deposits however, Ulutaş skarn deposit does not contain any galena. Although it is low in tonnage, Ulutaş skarn is an economic skarn mineralization like Antamina, Empire Velardeña skarn deposits.

6.2 Conclusions

Ulutaş Cu-Zn skarn type deposit in Eastern Pontides, northeastern Turkey, was analyzed through a combination of techniques including geological mapping, core sample collection, petrography, identification of ore and gangue minerals, determination of alteration assemblages through drill hole data, correlation of metal contents and numerical modelling of Cu and Zn mineralization. The study's results can be summarized as follows:

- The main host lithology for Cu-Zn mineralization is pre-Jurassic aged metamorphic unit which contains marble lenses. The metamorphic unit cross-cut by Early Cretaceous aged quartz feldspar porphyry. The main heat source of formation of skarn system is related with the quartz feldspar porphyry intrusions.
- According to Nb, Ti, Y and Zr concentration results of 306 samples from 23 drillhole of Ulutaş Cu-Zn skarn deposit, quartz feldspar porphyry can be classified as andesitic rock with sub-alkaline characteristics.
- According to Nb, Ti, Y and Zr concentration results of 648 samples from 31 drillhole of Ulutaş Cu-Zn skarn deposit, mafic dike can be classified as basaltic rock with sub-alkaline characteristics.
- Both endoskarn and exoskarn were observed in Ulutaş Cu-Zn skarn deposit. Also, early potassic alteration was also observed within quartz feldspar porphyry. Exoskarn is classified as calcic exoskarn which replaces marble unit. Prograde alteration consists of garnet, pyroxene and wollastonite. Prograde alteration is also replaced by retrograde alteration which is characterized by chlorite, epidote, carbonate and quartz. Below glacial till, skarn also observed as weathering. Due to weathering, limonite, goethite and secondary Cu minerals like malachite observed.
- The main ore minerals in Ulutaş Cu-Zn skarn deposits are pyrite, chalcopyrite and sphalerite with magnetite and hematite with minor molybdenite, tetrahedrite and marcasite and rare covellite and bornite.
- By considering the metal correlation, Cu and Ag shows good correlation and Cu and Zn shows no correlation although sphalerite is replaced by chalcopyrite.
- Metal zonation also occurs in Ulutaş Cu-Zn skarn. Lower skarn is Zn rich whereas upper skarn is Cu rich.
- As a result of numerical modelling for Cu and Zn, a resource of 3.35 million tons of Cu with a grade of 1.22 % wt and Zn with a grade of 3.02 wt % has been estimated.

REFERENCES

Atkinson, W.W., Jr., and Einaudi, M.T., 1978, Skarn formation and mineralization in the contact aureole at Carr Fork, Bingham, Utah: Economic Geology, v. 73, p. 1326–1365.

Bektaş O, Şen C, Atıcı Y, Köprübaşı N (1999). Migration of the upper Cretaceous subduction related volcanism towards the back arc basin of the eastern Pontide magmatic arc (NE Turkey) Geological Journal 34: 95-106.

Bilir, M.E., 2015. Geochemical And Geochronological Characterization of The Early-Middle Eocene Magmatism And Related Epithermal Systems Of The Eastern Pontides, Turkey, MSc. Thesis, Muğla Sıtkı Koçman University (117 pp.).

Bozkurt, E., & Mittwede, S. K. (2001). Introduction to the geology of Turkey—a synthesis. International Geology Review, 43(7), 578–594. https://doi.org/10.1080/00206810109465034

Boztuğ, D., Harlavan, Y., 2008. K–Ar ages of granitoids unravel the stages of Neo-Tethyan convergence in the eastern Pontides and central Anatolia, Turkey. Int. J. Earth Sci. 97, 585–599. http://dx.doi.org/10.1007/s00531-007-0176-0.

Burt, D.M., 1977, Mineralogy and petrology of skarn deposit: Soc. Italiana Mineralogia Petrologia Rend., v. 77, p. 859-873.

Çiftçi, E. (2011). Sphalerite associated with pyrrhotite-chalcopyrite ore occurring in the Kotana Fe-Skarn deposit (Giresun, Ne Turkey): Exsolution or replacement. Turkish Journal of Earth Sciences. https://doi.org/10.3906/yer-1001-26

Çiftçi, E. (2019). Volcanogenic massive sulfide (VMS) deposits of Turkey. Mineral Deposit of Turkey, Modern Approaches in Solid Earth Sciences, 427–495. https://doi.org/10.1007/978-3-030-02950-0_9

Chang, Z and Meinert, L D, 2004. The magmatic-hydrothermal transition evidence from quartz phenocryst textures and endoskarn abundance in Cu-Zn skarns at the Empire mine, Idaho, USA, Chemical Geology, 210:149-171.

Chang, Z and Meinert, L D, 2008. Zonation in Skarns – Complexities and Controlling Factors, Paper presented at PACRIM Congress, 24-26 November 2008.

Chang, Z., & Meinert, L. D. (2008). The empire cu-zn mine, idaho: Exploration implications of unusual skarn features related to high fluorine activity. Economic Geology, 103(5), 909–938. https://doi.org/10.2113/gsecongeo.103.5.909

Delibaş, O., Moritz, R., Selby, D., Göç, D.,; Revan, M. K. (2019). Multiple porphyry Cu-Mo events in the Eastern pontides metallogenic belt, Turkey: From Early Cretaceous subduction to Eocene Post-collision Evolution. Economic Geology, 114(7), 1285–1300. https://doi.org/10.5382/econgeo.4663.

Demir, Y., Uysal, İ., Kandemir, R., & Jauss, A. (2017). Geochemistry, fluid inclusion and stable isotope constraints (C and O) of the sivrikaya fe-skarn mineralization (Rize, Ne Turkey). Ore Geology Reviews, 91, 153–172. https://doi.org/10.1016/j.oregeorev.2017.10.008

Einaudi, M.T., Meinert, L.D., and Newberry, R.J., 1981, Skarn deposits: Economic Geology 75th Anniversary Volume, p. 317–391.

Einaudi, M. T., & Burt, D. M., 1982. Introduction; terminology, classification, and composition of skarn deposits. Economic Geology, 77(4), 745-754. doi:10.2113/gsecongeo.77.4.745

Eyüboğlu, Y., Santosh, M., Bektas, O., and Ayhan, S., 2011. Arc magmatism as a window to plate kinematics and subduction polarity: Example from the eastern Pontides belt, NE Turkey. Geosci. Front., 2(1):49 – 56.

Giles DL., 1974 Geology and mineralization of the Ulutaş copper–molybdenum prospect, mineral exploration in two areas. UNDP Technical Report, 6, MTA, Ankara (unpublished)

Güven, İ.H., 1993. Geology of the Eastern Pontides: Compilation of the geological maps throughout the region: General Directorate of Mineral Research and Exploration (MTA), Ankara, Turkey, scale 1:250,000, 1 sheet.

Hedenquist, J., Lowenstern, J., 1994. The role of magmas in the formation of hydrothermal ore deposits. Nature 370, 519–527 (1994). https://doi.org/10.1038/370519a0

Jamtveit, B., and Andersen, T., 1993, Contact metamorphism of layered shale-carbonate sequences in the Oslo rift: III. The nature of skarn-forming fluids: Economic Geology, v. 88, p. 1830–1849.

Jiménez-Franco, A., Canet, C., Alfonso P., González- Partida, E., Rajabi, A., Escalante, E., 2020, The Velardeña Zn–(Pb–Cu) The Velardeña Zn–(Pb–Cu) skarn-epithermal deposits, central-northern Mexico: new physical-chemical constraints on ore-forming processes: Boletín de la Sociedad Geológica Mexicana, 72 (3), A270719. http://dx.doi.org/10.18268/BSGM2020v72n3a270719

Kandemir Ö, Akbayram K, Çobankaya M, Kanar F, Pehlivan Ş., et al. (2019). From arc evolution to arc-continent collision: Late Cretaceous-middle Eocene geology of the eastern Pontides, northeastern Turkey. The Geological Society of America. doi. org/10.1130/B31913.1

Karslı, O., Dokuz, A., Uysal, İ., Aydın, F., Chen, B., Kandemir, R., Wijbrans, J., 2010. Relative contributions of crust and mantle to generation of Campanian high-K calc-alkaline I-type granitoids in a subduction setting, with special reference to the Harşit Pluton, Eastern Turkey. Contributions to Mineralogy and Petrology 160, 467–487.

Karslı, O., Caran, Ş., Dokuz, A., Çoban, H., Chen, B., Kandemir, R., 2012. A-type granitoids from the Eastern Pontides, NE Turkey: records for generation of hybrid A-type rocks in a subduction-related environment. Tectonophysics 530–531, 208–224.

Kaygusuz, A., Arslan, M., Siebel, W., Sipahi, F., İlbeyli, N., Temizel, İ., 2014. LA-ICP-MS zircon dating, whole-rock and Sr–Nd–Pb–O isotope geochemistry of the Camiboğazı pluton, Eastern Pontides, NE Turkey: implications for lithospheric mantle and lower crustal sources in arc-related, I-type magmatism. Lithos 192–195, 271–290.

Kaygusuz, A., and Öztürk, M., 2015, Geochronology, geochemistry, and petrogenesis of the Eocene Bayburt intrusions, eastern Pontides, NE Turkey: Evidence for lithospheric mantle and lower crustal sources in the high-K calc-alkaline magmatism: Journal of Asian Earth Sciences, v. 108, p. 97–116.

Kaygusuz, A., Yücel, C., Arslan, M., Temizel, I., Yi, K., Jeong, Y.J, Siebel, W., 2014. Eocene I-type magmatism in the Eastern Pontides, NE Turkey: insights into magma genesis and magma-tectonic evolution from whole-rock geochemistry, geochronology and isotope systematics. International Geology Review, DOI: 10.1080/00206814.2019.1647468

Ketin, I., 1966. Tectonic units of Anatolia. MTA Bulletin 66, 23–34.

Kuşcu, İ. (2019). Skarns and skarn deposits of Turkey. Mineral Deposits of Turkey, Modern Approaches in Solid Earth Sciences, 283–336. https://doi.org/10.1007/978-3-030-02950-0_7

Kuşcu, İ., Tosdal, R. M., Gençalioğlu-Kuşcu, G. 2019. Episodic porphyry Cu (-Mo-Au) formation and associated magmatic evolution in Turkish Tethyan collage. Ore Geology Review, 119–154. https://doi.org/10.1016/j.oregeorev.2019.02.005

Konak N, Hakyemez Y, Bilgiç T, Bilgin ZR, Hepşen N et al. (2001). Kuzeydoğu Pontidlerin jeolojisi. MTA Publ. No. 10489, Ankara (in Turkish).

Meinert, L. D. 1982. Skarn, Manto, and breccia pipe formation in sedimentary rocks of the Cananea Mining District, Sonora, Mexico. Economic Geology, 77(4), 919–949. https://doi.org/10.2113/gsecongeo.77.4.919

Meinert, L.D., 1984, Mineralogy and petrology of iron skarns in western British Columbia, ECONOMIC GEOLOGY, v. 79, p. 869–882.

Meinert, L.D., 1987, Skarn zonation and fluid evolution in the Groundhog mine, Central mining district, New Mexico: ECONOMIC GEOLOGY, v. 82, p. 523–545.

Meinert, L. D. (1988). Gold skarn deposits—geology and exploration criteria. The Geology of Gold Deposits, 537–552. https://doi.org/10.5382/mono.06.41

Meinert, L.D., 1992, Skarns and skarn deposits: Geoscience Canada, v. 19, p. 145–162.

Meinert, L.D., 1997, Application of skarn deposit zonation models to mineral exploration: Exploration and Mining Geology, v. 6, p. 185–208.

Meinert, L.D., Hefton, K.K., Mayes, D., and Tasiran, I., 1997, Geology, zonation, and fluid evolution of the Big Gossan Cu-Au skarn deposit, Ertsberg district, Irian Jaya: Economic Geology, v. 92, p. 509–526.

Meinert, L D, Dipple, G M and Nicolescu, S, 2005. World skarn deposits, Economic Geology 100th Anniversary, Volume, pp 299-336.

Mrozek, S A. (2018) The giant Antamina deposit, Peru: intrusive sequence, skarn formation, and mineralisation. PhD thesis, James Cook University.

MTA., 2002. 1/500.000 ölçekli Türkiye jeoloji haritası Trabzon paftası, in: Akdeniz, N.,

Güven, İ. (Eds.), General Directorate of Mineral Research and Exploration (MTA) Publication (in Turkish).

Oğuz, E. (2010). Re-Assessment Of The Ulutaş (İspir-Erzurum) Porphyry Copper-Molybdenum System And Exploration Of Its Gold Potential MSc thesis Hacettepe University.

Okay, A.I., 2008; Geology of Turkey: A synopsis. Anschnitt, 21, 19-42.

Okay AI, Şahintürk Ö (1997) Geology of the Eastern Pontides. In: Robinson AG (ed) Regional and petroleum geology of the Black Sea and surrounding Region. Am Assoc Pet Geol Mem 68:291–310

Okay AI, Tüysüz O (1999) Tethyan sutures of northern Turkey. In: Durand B, Jolivet L, Horvath L, Serranne M (eds) The Mediterranean Basins: tertiary extension within the Alpine orogeny.Geol Soci Lond Spec Publ 156:475–515

Okay, A.I. & Nikishin, A.M., 2015, Tectonic evolution of the southern margin of Laurasia in the Black Sea region. International Geology Review, 57, 1051-1076.

Oyman, T. (2019). Epithermal deposits of Turkey. Mineral Deposits of Turkey, Modern Approaches in Solid Earth Sciences, 159–211. https://doi.org/10.1007/978-3-030-02950-0_7

Rabayrol, F., Wainwright, A. J., Lee, R. G., Hart, C. J. R., Creaser, R. A., & Camacho, A. (2022). District-scale VMS to porphyry-epithermal transitions in subduction to postcollisional Tectonic Environments: The Artvin Au-Cu district and the Hod Gold Corridor, eastern pontides belt, Turkey. Economic Geology. https://doi.org/10.5382/econgeo.4983

Revan, M. K. (2020). Review of Late Cretaceous volcanogenic massive sulfide mineralization in the Eastern Pontides, NE Turkey . Turkish Journal of Earth Sciences , 29 (7) , 1125-1153 . Retrieved from https://dergipark.org.tr/tr/pub/tbtkearth/issue/62428/942322

Richards, J. P. (2011). Magmatic to hydrothermal metal fluxes in convergent and collided margins. Ore Geology Reviews, 40(1), 1–26. https://doi.org/10.1016/j.oregeorev.2011.05.006

Richards, J. P. (2015). Tectonic, magmatic, and metallogenic evolution of the Tethyan orogen: From subduction to collision. Ore Geology Reviews, 70, 323–345. https://doi.org/10.1016/j.oregeorev.2014.11.009

Robb, L. (2005). Introduction To Ore-Forming Processes. John Wiley & Sons

Robertson, A.H.F., Dixon, J.E., 1984. Introduction: aspects of the geological evolution of the Eastern Mediterranean. In: Dixon, J.E., Robertson, A.H.F. (Eds.), The Geological Evolution of the Eastern Mediterranean. Geol. Soc., London Spec. Pub., 17, pp. 1–74.

Shelton, K.L., 1983, Composition and origin of ore-forming fluids in a carbonate-hosted porphyry copper and skarn deposit: A fluid inclusion and stable isotope study of Mines Gaspé, Quebec: Economic Geology, v. 78, p. 387–421.

Şengör AMC, Yılmaz Y (1981) Tethyan evolution of Turkey: a plate tectonic approach. Tectonophysics 75:181–241

Sillitoe, R. H. (1972). A plate tectonic model for the origin of Porphyry Copper Deposits. Economic Geology, 67(2), 184–197. https://doi.org/10.2113/gsecongeo.67.2.184

Sipahi, F., Akpınar, İ., Eker, Ç. S., Kaygusuz, A., Vural, A., & Yılmaz, M. (2017). Formation of the Eğrikar (gümüşhane) fe–cu skarn type mineralization in NE turkey: U–Pb Zircon Age, lithogeochemistry, mineral chemistry, fluid inclusion, and O-h-C-S isotopic compositions. Journal of Geochemical Exploration, 182, 32–52. https://doi.org/10.1016/j.gexplo.2017.08.006

Soylu, M., 1999. Modeling of Porphyry Copper Mineralization of the Eastern Pontides Ph.D. thesis Middle East Technical University (127 pp.).

Stampfli, G.M., Marcoux, J., Baud, A., 1991. Tethyan margins in space and time.

Palaeogeogr., Palaeoclimatol. Palaeoecol. 87, 337–409

Stampfli, G. M. (2000). Tethyan oceans. Geological society, london, special publications, 173(1), 1-23.

Stampfli, G. M., & Borel, G. D. (2002). A plate tectonic model for the Paleozoic and Mesozoic constrained by dynamic plate boundaries and restored synthetic oceanic isochrons. Earth and Planetary Science Letters, 196(1-2), 17-33.

Stampfli, G. M., & Borel, G. D. (2004). The TRANSMED transects in space and time: constraints on the paleotectonic evolution of the Mediterranean domain. In The TRANSMED Atlas. The Mediterranean region from crust to mantle (pp. 53-80). Springer, Berlin, Heidelberg.

Taner, M.F., 1977. Etudé géologique et pétrographique de la région de Güneyce-İkizdere, située au sud de Rize (Pontides orientales, Turquie) Ph.D thesis, (in French) Université de Geneve

Taylor, R.P., Fryer, B.J., 1980. Multiple-stage hydrothermal alteration in porphyry copper system in northern Turkey: the temporal interplay of potassic, propylitic and phyllic fluids. Canadian Journal of Earth Sciences 17, 901–927.

Topuz, G., Alther, R., Schwarz, W.H., Siebel, W., Satır, M., and Dokuz, A., 2005, Post-collisional plutonism with adakite-like signatures: The Eocene Saraycık granodiorite (eastern Pontides, Turkey): Contributions to Mineralogy and Petrology, v. 150, p. 441–455. doi:10.1007/s00410-005-0022-y.

Yiğit, O., 2009. Mineral deposits of Turkey in relation to Tethyan metallogeny: implications for future mineral exploration. Economic Geology 104, 19–51.

Yılmaz, M., 2016. Petrographical and geochemical investigations of the Eğrikar (Torul-Gümüşhane) Fe-Cu Skarn deposit, Gümüşhane Üniversitesi, Fen Bilimleri Enstitüsü, Master Thesis, Gümüşhane, p. 99.

Yılmaz Y, Tüysüz O, Yiğitbaş E, Genç SC, Şengör AMC (1997) Geology and tectonics of the Pontides. In: Robinson AG (eds) Regional and petroleum geology of the Black Sea and the surrounding region. Am Assoc Pet Geol Memoir 68:183–226